DETERMINATION OF DYNAMICALLY EQUIVALENT FE MODELS OF AIRCRAFT STRUCTURES BY USING MODAL TEST DATA

A THESIS SUBMITTED TO
THE GRADUATE SCHOOL OF NATURAL AND APPLIED SCIENCES
OF
MIDDLE EAST TECHNICAL UNIVERSITY

BY

TAYLAN KARAAĞAÇLI

IN PARTIAL FULFILLMENT OF THE REQUIREMENTS
FOR
THE DEGREE OF MASTER OF SCIENCE
IN
MECHANICAL ENGINEERING

SEPTEMBER 2010

Approval of the thesis:

DETERMINATION OF DYNAMICALLY EQUIVALENT FE MODELS OF AIRCRAFT STRUCTURES BY USING MODAL TEST DATA

submitted by **TAYLAN KARAAĞAÇLI** in partial fulfillment of the requirements for the degree of **Master of Science in Mechanical Engineering, Middle East Technical University** by,

Prof. Dr. Canan ÖZGEN _____
Dean, Graduate School of **Natural and Applied Sciences**

Prof. Dr. Süha ORAL _____
Head of Department, **Mechanical Engineering**

Prof. Dr. H. Nevzat ÖZGÜVEN _____
Supervisor, **Mechanical Engineering Dept., METU**

Dr. Erdinç N. YILDIZ _____
Co-Supervisor, **TÜBİTAK-SAGE**

Examining Commitee Members:

Prof Dr. Y. Samim ÜNLÜSOY _____
Mechanical Engineering Dept., METU

Prof. Dr. H. Nevzat ÖZGÜVEN _____
Mechanical Engineering Dept., METU

Dr. Erdinç N. YILDIZ _____
Chief Research Engineer, TÜBİTAK-SAGE

Asst. Prof. Dr. Yiğit YAZICIOĞLU _____
Mechanical Engineering Dept., METU

Asst. Prof. Dr. Gökhan ÖZGEN _____
Mechanical Engineering Dept., METU

Date: _____

I hereby declare that all information in this document has been obtained and presented in accordance with academic rules and ethical conduct. I also declare that, as required by these rules and conduct, I have fully cited and referenced all materials and results that are not original to this work.

Name, Last Name: Taylan KARAAĞAÇLI

Signature :

ABSTRACT

DETERMINATION OF DYNAMICALLY EQUIVALENT FE MODELS OF AIRCRAFT STRUCTURES BY USING MODAL TEST DATA

Karaağaçlı, Taylan
M.Sc., Department of Mechanical Engineering
Supervisor: Prof. Dr. H. Nevzat Özgüven
Co-Supervisor: Dr. Erdinç N. Yıldız

September 2010, 162 pages

Reliable flutter analysis of aircraft structures is a major requirement to determine safe flight envelops. Dynamically equivalent finite element model of an aircraft structure correlating well with experimental modal is a major requirement for a reliable flutter analysis. Currently available model updating techniques require enormous time and engineering work to achieve appropriate finite element models of aircraft structures. The method developed within the scope of this thesis work aims to remove important disadvantages of common model updating procedures. In doing this, the method starts with a simple finite element mesh obtained by connecting measurement points, used in the Ground Vibration Test of an aircraft structure, with 3 D Euler-Bernoulli beam elements. Initial estimates of the geometric and material properties are determined by solving structural identification equations derived from the mass and stiffness orthogonality of experimental modes. By using those initial estimates, an initial finite element model is constructed. Starting from this initial finite element model, structural identification equations are updated and solved iteratively by using experimental natural frequencies and eigenvectors of the

updated finite element model representing the same mode shapes with measured normal modes. Iterations are continued until eigen solution of the updated finite element model closely correlates with experimental modal data.

The applicability of the method is illustrated on a scaled aircraft model and a real aircraft structure. The results are quite satisfactory but the method requires further improvements to achieve a much better correlation level in case of real aircraft structures.

Keywords: Model Updating, Structural Identification, Structural Dynamics, Finite Element Method, Dynamically Equivalent Finite Element Models of Aircraft Structures.

ÖZ

MODAL TEST VERİLERİ KULLANILARAK UÇAK YAPILARININ DİNAMİK EŞDEĞER SONLU ELEMANLAR MODELİNİN BELİRLENMESİ

Karaağaçlı, Taylan
Yüksek Lisans, Makina Mühendisliği Bölümü
Tez Yöneticisi: Prof. Dr. H. Nevzat Özgüven
Ortak Tez Yöneticisi: Dr. Erdinç N. Yıldız

Eylül, 2010 162 sayfa

Uçak yapılarının güvenli uçuş zarflarının belirlenmesinde güvenilir çırpıntı analizi büyük önem taşımaktadır. Uçak yapılarının, deneysel modal veriler ile örtüşen dinamik eşdeğer sonlu elemanlar modelinin elde edilmesi güvenilir çırpıntı analizi için en temel gereksinimdir. Var olan model güncelleme teknikleri, uçak yapılarının uygun sonlu elemanlar modelinin elde edilmesi için azımsanmayacak miktarda zamana ve mühendislik çalışmasına gerek duymaktadır. Bu tez çalışması kapsamında geliştirilen yöntem, sık kullanılan model güncelleme yöntemlerinin önemli dezavantajlarını ortadan kaldırmayı amaçlamaktadır. Bunun için, geliştirilen yöntem öncellikle uçak yapılarının yer titreşim testlerinde kullanılan ölçüm noktalarını üç boyutlu Euler-Bernoulli elemanları ile birleştirerek basit bir sonlu elemanlar ağı oluşturmaktadır. Başlangıç sonlu elemanlar modelinin geometrik ve malzeme özellikleri, deneysel modal verilerin kütle ve esneklik matrislerine göre ortogonallik özelliğinden türetilen yapısal denklemlerin çözümlerinden elde edilmektedir. Elde edilen başlangıç sonlu elemanlar modelinde yer alan ve deneysel mod şekilleriyle örtüşen eigen vektörleri, deneysel olarak belirlenen doğal frekanslar

ile birlikte yapısal denklemlerin yeniden oluşturulmasında kullanılırlar. Bu yapısal denklemlerin çözümleri, güncellenmiş geometrik ve malzeme özelliklerinin belirlenmesinde ve sonlu elemanlar modelinin güncellenmesinde kullanılırlar. Model güncelleme süreci, sonlu elemanlar modeli deneysel veriler ile yeterince iyi bir şekilde örtüşene kadar sürdürülür.

Geliştirilen yöntemin uygulanabilirliği, küçük ölçekli bir uçak modeli ve gerçek bir uçak yapısı üzerinde test edilmiştir. Sonuçlar başlangıç için tatmin edici olmak ile birlikte, yöntemin gerçek uçaklara uygulanmasında daha iyi sonuçlar elde edilmesi için iyileştirmelere ihtiyaç duyulmaktadır.

Anahtar Kelimeler: Model Güncelleme, Yapısal Özelliklerin Belirlenmesi, Yapısal Dinamik, Sonlu Elemanlar Yöntemi, Uçak Yapılarının Dinamik Eşdeğer Sonlu Elemanlar Modeli.

To My Family

ACKNOWLEDGMENTS

I would like to express my sincere appreciation to my supervisor Prof. Dr. H. Nevzat ÖZGÜVEN and to my co-supervisor Dr. Erdinç N. YILDIZ for their guidance, advice, criticism, encouragements and insight throughout the research.

The work in this thesis was performed for the practical research objectives of TÜBİTAK-SAGE. I wish to thank to TÜBİTAK-SAGE administration for allowing me to make this research and TÜBİTAK-SAGE for unfolding the computational and testing capabilities.

I would like to extend my special tanks to my dear colleague M. Tuğrul KOZAK for sharing his precious knowledge throughout the research.

Enormous thanks to my grandmother Mevlüde ASMA, my mother Ceyhan KARAAĞAÇLI, my brother Timuçin KARAAĞAÇLI, my grandfather Mehmet ASMA and my father Harun Ufuk KARAAĞAÇLI for their incredible support, trust understanding to me and their precious encouragement throughout my all life and education.

Finally, I thank God for always keeping strong the flame of passion for science in my soul.

TABLE OF CONTENTS

CHAPTER 1

INTRODUCTION

1.1. OBJECTIVES OF THE THESIS

The objective of this thesis work is to develop a new method to determine dynamically equivalent finite element (FE) models of real aircraft structures directly from experimental modal data such that eigenvalues and eigenvectors of the resultant FE model correlate well with their experimental counterparts. Such an FE model is mainly used in flutter analysis to determine safe flight envelops of aircraft structures. A reliable flutter analysis is possible only with an FE model correlating well with the relevant aircraft structure in terms of its modal properties.

In literature, there are numerous techniques proposed to correct FE models of various aerospace structures by using experimental modal data, and the common name used for them is the 'Model Updating Methods'. Basically, model updating methods are classified in two groups: direct and indirect model updating techniques. Each technique brings its own advantages and drawbacks. As a result, no general method to update mathematical models of all types of structures has been developed yet.

The most important disadvantages of the common direct and indirect model updating algorithms can be stated as follows:

- Certain direct updating methods take experimental normal modes as reference to correct analytical mass and stiffness matrices of the relevant structure. Other direct methods assume that analytical mass matrix is the most accurate data and correct experimental mode shapes and stiffness matrix with respect to it. In any case, the original coordinate connectivity of the FE model is lost and

resulting mass and stiffness matrices become fully populated. When connectivity in the stiffness matrix is lost, physically meaningless off-diagonal stiffness elements appear for the degrees of freedom (dofs) among which no direct connection is present. This leads to spurious modes in the eigen solution of the FE model. Moreover, in case of an aircraft structure with free-free boundary conditions, the semi-definiteness of its stiffness matrix is degraded and rigid body modes are lost. Such an FE model may be suitable to study effects of structural modification on mode shapes and natural frequencies of a real structure but it cannot be used to carry out flutter or divergence type aeroelastic analyses.

- In case of complex aerospace structures such as aircraft structures, measurement dofs of experimental normal modes are usually at least an order of magnitude less than total dofs of the FE model. Moreover, experimental modal matrix consists of mode shapes only within the frequency range of interest. Therefore experimental modal matrix is highly truncated. As a result, direct updating methods using test data to correct mass and stiffness matrices may be satisfactory only for FE models of relatively simple structures with small number of dofs. Otherwise, experimental normal modes have to be expanded to the size of the FE model. But this is not recommended because expansion procedure adds extra error to the measured modes already degraded with experimental error. This is something that reduces success of the relevant direct updating methods.

- Methods using analytical mass matrix to correct test data and analytical stiffness matrix also bring similar challenges. First of all, the assumption of a perfectly accurate analytical mass matrix is always questionable especially for complex structures. Secondly, because of the truncated nature of the measured modes, analytical mass matrix has to be reduced to the measurement dofs to correct test data. But reduction procedures add extra error to the analytical mass matrix already ruined with simplifying engineering assumptions.

- Most common indirect model updating techniques make adjustments on individual elements of the interested FE model in an iterative and controlled way instead of unconstrained adjustments of spatial matrices as in case of direct updating techniques. This way, important drawbacks of direct methods mentioned above such as loss of coordinate connectivity are solved. But of

course, indirect algorithms bring their own challenges. Maybe the most important challenge is that FE counterparts of almost all of the measures modes must appear in the initial FE model to guarantee convergence to an FE model in good correlation with modal test data. This dictates construction of a relatively accurate initial FE model. If the model updating is accomplished by the design team of the owner company of the aircraft structure, such an accurate FE model will already be available. But if the updating procedure is carried out by a subsidiary company that makes certain modifications on the aircraft structure, the construction of an appropriate initial FE model from scratch turns into a tedious work requiring detailed studies of the blueprints and investment of considerable engineering work hour.

- An accurate initial FE model necessitated by indirect methods is usually achieved by a very detailed FE modeling procedure that duplicate morphology of the real aircraft structure as much as possible. This leads to a relatively complex FE model with enormous number of structural parameters. Determination of the FE parameters most appropriate among many others for a fast and efficient updating scheme is not easy and it is usually accomplished by a trained analyst. Although today's commercial optimization softwares such as GENESIS © simplify the job of an analyst considerable amount in updating of FE models of complex structures, the updating procedure is not fully automatic yet and still necessitates engineering judgments of an experienced analyst.

The contribution of this thesis can be summarized as follows:

- It introduces a new approach to determine dynamically equivalent FE models of real aircraft structures from experimental modal data by eliminating disadvantages of the state-of-the art model updating procedures mentioned above.

- First of all, the method starts with an FE mesh that consists of beam elements connecting measurement points used in the modal test of a real aircraft structure. In doing so it tries to find an answer to the following questions: Is it really a must to conduct the model updating with the conventional FE mesh that duplicates the morphology of a real structure as close as possible? Or can an FE mesh built up by simply connecting measurement points serve the purpose as well? If it is so, the tedious work required to develop an accurate initial FE model will be eliminated.

- Obviously, the initial FE model consists of an ‘empty’ mesh, i.e. geometric and material properties are not assigned yet. At this stage, the method converts mass and stiffness orthogonality equations of experimental normal modes into appropriate ‘Structural Identification Equations’ to determine initial estimates of geometric and material properties. Solving these equations and assigning initial estimates of the structural parameters to the FE mesh, an initial FE model is completely determined.

- Finally, eigenvectors of that initial FE model corresponding to measured normal modes are used along with experimentally obtained natural frequencies in order to reconstruct structural identification equations. Solution of those equations give updated geometric and material properties. Updated properties are used to obtain an updated FE model whose eigenvectors are to be used in the next iteration. Iterations are continued until eigen solution of the updated FE model closely correlates with experimentally measured modal data.

As explained above, in this study, a noble method of considerable mathematical elegance is developed to determine dynamically equivalent FE models of aircraft structures from modal test data by overcoming important drawbacks of existing model updating approaches.

1.2. LITERATURE SURVEY

More than 40 years has passed since the first studies related to direct updating of aerospace structures had appeared in literature. One of the important examples of early model updating procedures was proposed by Berman and Flannelly [1] under the name of the ‘Theory of Incomplete Models’. In this work, a pseudo inverse solution procedure was proposed to correct analytical mass matrix of a structure by using experimental normal modes. The corrected mass matrix was combined with measured modes to construct an incomplete stiffness matrix. By using simulated experiments, Berman and Flannelly showed that corrected mass matrix and incomplete stiffness matrix can be used to predict effects of simple structural modifications on modal properties of the relevant structure.

Later, Thoren [2] proposed a method by which spatial matrices are calculated in a manner to satisfy relevant orthogonality conditions together with measured normal modes.

On the other hand, Collins et al. [3] proposed a statistical method to modify mass and stiffness characteristics of an FE model.

In following years, Berman [4] used a modified version of his Incomplete Model Method to determine dynamic equations of motion of a helicopter transmission gearbox from shake test data.

After these preliminary studies, Baruch and Itzhack [5] published an original work that takes analytical mass matrix as reference to orthogonalize measured modes and correct the analytical stiffness matrix by using a least square solution procedure with Lagrange multipliers.

Later Berman and Nagy [6] made use of the Lagrange Multipliers Method to correct analytical mass and stiffness matrices by taking experimental mode shapes as reference. They applied this method successfully to the payload of an aerospace structure.

A year later, Sidhu and Ewins [7] proposed a method to determine error of the analytical mass and stiffness matrices using analytical and experimental modal data.

Baruch [8] proposed to take analytical stiffness matrix as reference in order to correct analytical mass matrix and experimental modal data.

Ceasar [9] made an overview of the Lagrange Multipliers Method studied by Berman and Baruch. In his work, he discussed applicability of the method to real structures and proposed some improvements.

Gypsin [10] applied the Error Matrix Method to localize FE modeling inaccuracies.

Choudhury et al. [11] published a new direct updating approach to identify spatial matrices by using frequency response function (FRF) data instead of modal data. A very similar work using FRF data was published also by Mastroddi et al. [12].

A recent contribution to direct updating methods came from Carvalho et al. [13]. This work has several advantages: Firstly, it does not need any model reduction or expansion, and secondly it is capable of preventing the appearing of spurious modes in the frequency range of interest.

Parallel to the developments of direct model updating procedures, numerous publications have been made in the area of indirect model updating techniques:

One of the early studies of indirect updating algorithms was proposed by Fox and Kapoor [14]. In this work, fist order sensitivities of modal data with respect to selected design parameters were used to correlate analytical model with experimental data. This preliminary work led a common indirect updating procedure, namely the 'Inverse Eigen Sensitivity Method'.

Lee and Parker [15] published a work studying design sensitivities to improve correlation between analytical and test modes.

Göge [16] made use of Inverse Eigen Sensitivity Method to update FE model of a commercial aircraft structure.

Kozak [17] revised and compared state-of-the art model updating techniques and applied Inverse Eigen Sensitivity Method to correct FE model of a fighter aircraft. Besides, Kozak et al. [18] proposed an indirect model updating method using miscorrelation index sensitivity.

Studies related to structural identification and model updating methods are not restricted to the publications mentioned above. In literature, there is enormous work relevant to the subject and it is practically impossible to address all of them in this thesis work. Interested readers may start to do research with afore mentioned publications and extend their knowledge with a more detailed literature survey.

1.3. SCOPE OF THE THESIS

The content of chapters and appendices are summarized below:

Chapter 2 is dedicated to explain theories of some important direct updating methods that inspired development of the structural identification approach of this thesis work.

Chapter 3 is dedicated to the explanation of the structural identification method developed during this thesis work.

In Chapter 4, the computer code based to the theory introduced in Chapter 3 and developed to determine dynamically equivalent FE models of aircraft structures is explained.

In Chapter 5, theory introduced in Chapter 3 is applied to determine FE model of a model aircraft structure designed and used by GARTEUR (Group for Aeronautical Research and Technology in Europe) and also to determine FE model of a real fighter aircraft structure.

Chapter 6 is dedicated to discussion, conclusions and recommendations for future work.

As explained in Chapter 3, FE formulations of a 3-D Euler-Bernoulli beam element play an important role in the development of the structural identification method introduced in this thesis work. But in literature, although relatively simple formulations of 2-D Euler Bernoulli beam elements are available [19-20], it is difficult to find a complete formulation of 3-D Euler-Bernoulli beam elements. For that reason, appendices A, B, C and D explain step by step how to develop FE formulations of 3 D Euler-Bernoulli beam elements from scratch.

CHAPTER 2

THEORY OF COMMONLY USED DIRECT UPDATING METHODS

2.1. METHODS OF REFERENCE BASIS IN DIRECT MODEL UPDATING

Analytical model of a real engineering structure may contain considerable error coming from different error sources [6] such as “inappropriate theoretical assumptions, inaccuracies in estimated material properties and insufficient or incorrect modeling details” etc. On the other hand, experimental natural frequencies and mode shapes also are affected by various error sources. Some of these [6] are “inexact equipment calibration, excessive noise, equipment malfunction, inappropriate transducer locations, operation in a region of nonlinearity as well as the use of inappropriate modal identification algorithms”.

Since both the mathematical model and the experimental data are erroneous, if they are combined together, they cannot comply with the basic theoretical requirements such as mass and stiffness orthogonality of normal modes. In order to satisfy those theoretical requirements in an optimum way, possibly some of the analytical data or the experimental data can be taken as ‘reference’ and can be used to correct the remaining data.

In literature, there are basically three methods of reference basis suggested and used in direct updating of analytical models of engineering structures. All these methods are studied below in detail.

2.1.1. Direct Updating Methods Using Measured Modes as Reference

Berman and Flannelly's work [1], in which the 'Theory of Incomplete Models of Dynamic Structures' is introduced, is one of the early examples of direct updating methods that make use of the measured modes to correct analytical mass matrix of a structure. In this example, correction of the mass matrix starts with the following relation:

$$\left\{ u_x^r \right\}^T \left[M_c \right] \left\{ u_x^s \right\} = 0 \quad r \neq s \tag{2.1}$$

where $\left\{ u_x^r \right\}$ are the experimental normal modes and $\left[M_c \right]$ is the unknown mass matrix reduced to the size of the experimental normal modes.

If there are N measured modes, equation (2.1) can be converted into $N(N-1)/2$ independent linear equations having the mass elements as unknowns with products of the elements of the normal modes as coefficients.

It is possible that certain mass elements may be known or assumed to be zero or to have some definite value. If they are zero, the corresponding terms are dropped from the equation. If they are to be restricted to a particular value, the corresponding terms are placed on the right hand side of the equation. If any of the generalized modal masses, m_i, are known, equation (2.1) for $r = s$ can be used and set equal to m_i. Also, the total mass of the structure may be considered to be known. With all these additional equations, equation (2.1) can be put into the following form:

$$\left[A \right] \left\{ \overline{m} \right\} = \left\{ R \right\} \tag{2.2}$$

where $\left\{ \overline{m} \right\}$ is a vector made up of the unknown elements of $\left[M_c \right]$, and $\left[A \right]$ is a matrix formed by the coefficients of equation (2.1) and of equations derived from the other conditions mentioned above.

Unfortunately, since a very limited number of normal modes can be determined from a modal test, usually the number of equations within (2.2) turns out to be less than the number unknowns. This means that there may be found infinite number of mass distributions that will make the modes orthogonal. But, in order to make physically meaningful predictions about the dynamic behavior of a structure and especially to

predict the effects of structural modification on the modal properties of that structure, it is a must to determine a mass matrix that reflects the true inertial properties of the real structure. This reveals the necessity for a relatively accurate analytical mass matrix. The analytical mass matrix cannot satisfy the orthogonality conditions of the measured normal modes but if it is used within equation (2.2), it will be possible to determine a corrected mass matrix that satisfies the mass orthogonality of the measured modes.

By defining analytical estimates of the unknown elements of the mass matrix as $\{m_A\}$, equation (2.2) can be reformulated as follows:

$$[A]\left(\{\overline{m}\}-\{m_A\}\right)=\{R\}-[A]\{m_A\} \tag{2.3}$$

At this stage a weighting matrix $[W]$ may be introduced by the analyst. Each element of $[W]$ will be a measure of the analyst's confidence in the corresponding approximation. Inserting the identity $[W]^{-1}[W]$ into equation (2.3), the following expression is obtained:

$$[A]\,[W]^{-1}\left([W]\left(\{\overline{m}\}-\{m_A\}\right)\right)=\{R\}-[A]\{m_A\} \tag{2.4}$$

Using the pseudo inverse $\left([A]\,[W]^{-1}\right)^{+}$, the solution of equation (2.4) is found as follows:

$$\{\overline{m}\}=[W]^{-1}\left([A]\,[W]^{-1}\right)^{+}\left(\{R\}-[A]\{m_A\}\right)+\{m_A\} \tag{2.5}$$

This solution is the one of the infinite number of possible solutions having the smallest weighted sum of squares of the difference between $\{\overline{m}\}$ and $\{m_A\}$.

Actually, the solution of (2.5) gives a rather general method of correcting the mass matrix; because it allows the analyst to decide which elements are to be allowed to vary and it makes it possible to introduce supplementary linear constraints. But in a subsequent study [21], Berman introduces a less general but much simpler method to correct the analytical mass matrix of a structure. The derivation of the corrected mass matrix starts with the following mass orthogonality relation.

$$[\Phi_x]^T\left([M]+[\Delta M]\right)[\Phi_x]=[I] \tag{2.6}$$

where $[M]$ is the (nxn) analytical mass matrix, $[\Phi_x]$ is the (nxm) mass normalized experimental modal matrix. Here, n represents the number of measurement dofs and m ($<$ n) represents the number of identified modes. The most important term $[\Delta M]$ indicates the mass change required to satisfy the orthogonality condition (2.6).

Equation (2.6) can be written alternatively as follows:

$$[\Phi_x]^T[\Delta M][\Phi_x] = [I] - [\Phi_x]^T[M][\Phi_x] \tag{2.7}$$

In order to obtain the optimum solution, an error function equivalent to the norm of the correction matrix $[\Delta M]$ is defined as follows:

$$\varepsilon = \left\| [N]^{-1}[\Delta M][N]^{-1} \right\| \tag{2.8}$$

where $[N] = [M]^{-1/2}$ is the weighing matrix.

Defining a Lagrange Multiplier λ_{ij} for each element in equation (2.8), the following Lagrangian function may be written:

$$\psi = \varepsilon + \sum_{i=1}^{m}\sum_{j=1}^{m}\lambda_{ij}\Big([\Phi_x]^T[\Delta M][\Phi_x] - [I] + [\Phi_x]^T[M][\Phi_x] \Big)_{ij} \tag{2.9}$$

Differentiating equation (2.9) with respect to each element of $[\Delta M]$ and equating these values to zero, the following matrix equation is obtained:

$$2[M]^{-1}[\Delta M][M]^{-1} + [\Phi_x][\Lambda]^T[\Phi_x]^T = 0 \tag{2.10}$$

Taking the correction matrix to the left hand side of the equation:

$$[\Delta M] = -1/2\ [M][\Phi_x][\Lambda]^T[\Phi_x]^T[M] \tag{2.11}$$

where $[\Lambda]$ is a (mxm) square matrix of λ_{ij}.

Substituting equation (2.11) into equation (2.7), the matrix of Lagrange multipliers is found to be:

$$[\Lambda] = -2\Big([\Phi_x]^T[M][\Phi_x] \Big)^{-1} \Big([I] - [\Phi_x]^T[M][\Phi_x] \Big) \Big([\Phi_x]^T[M][\Phi_x] \Big)^{-1} \tag{2.12}$$

Finally substituting equation (2.12) into equation (2.11) the correction matrix is obtained as below:

$$[\Delta M]=[M]\,[\Phi_x]\left([\Phi_x]^T[M]\,[\Phi_x]\right)^{-1}\left([I]-[\Phi_x]^T[M]\,[\Phi_x]\right)\left([\Phi_x]^T[M]\,[\Phi_x]\right)^{-1}[\Phi_x]^T[M] \qquad (2.13)$$

After the correction of the mass matrix, the next step is the determination of an appropriate stiffness matrix. In order to determine the stiffness matrix of the relevant structure, Berman and Flannelly [1] starts with the following eigenvalue problem:

$$\left([K]-\omega_r^2[M]\right)\{u^r\}=0 \qquad r=1,\,2\ldots P \qquad (2.14)$$

where $[K]$ is the stiffness matrix, ω_r are the natural frequencies and P is the total number of dofs of the analytical model.

Combining the eigenvalue problem given in (2.14) with the mass orthogonality relation $[U]^T[M]\,[U]=\left[\ddots\, m_r \,\ddots\right]$, it can be shown that:

$$[K]=[M]\,[U]\left[\omega_r^2/m_r\right][U]^T[M]=\sum_{r=1}^{P}\frac{\omega_r^2}{m_r}[M]\,\{u^r\}\,\{u^r\}^T[M] \qquad (2.15)$$

The expression of the stiffness matrix given in (2.15) contains summations of simple products of the individual eigenvectors of the system, $\{u^r\}\{u^r\}^T$. Each of these products is a PxP square matrix of rank 1. When P number of these matrices are summed as indicated and since $\{u^r\}$s are linearly independent, the resulting stiffness matrix will be of rank P and thus nonsingular. At this point Berman and Flannelly [1] ask the following critical question: By using the first $N(<P)$ incomplete experimental modes $\{u_x^r\}$ of the relevant structure together with the corrected mass matrix $[M_c]$, is it possible to predict effects of structural modification on the modal parameters of that structure ? To find the answer, they construct an 'incomplete' stiffness matrix by using 'incomplete' experimental modes within expression (2.15) as below:

$$[K_{inc}]=\sum_{r=1}^{N(<P)}\frac{\omega_r^2}{m_r}[M_c]\,\{u_x^r\}\,\{u_x^r\}^T\,[M_c] \qquad (2.16)$$

It must be noted that the incomplete stiffness matrix is of order P but of rank N. This means that it is a rank deficient, singular matrix and cannot be inverted.

However, this matrix can be used together with the corrected mass matrix to solve the eigenvalue problem of the relevant structure within the frequency range of interest as follows:

$$[M_c]^{-1}[K_{inc}]\left\{u_x^s\right\} = \sum_{r=1}^{N(<P)} \frac{\omega_r^2}{m_r}\left\{u_x^r\right\}\left\{u_x^r\right\}^T [M_c]\left\{u_x^s\right\} \tag{2.17}$$

$$[M_c]^{-1}[K_{inc}]\left\{u_x^s\right\} = \begin{cases} \omega_s^2\left\{u_x^s\right\} & s = 1,2,\ldots N \\ 0 & s > N \end{cases} \tag{2.18}$$

Berman and Flannelly [1] claim that the incomplete model that consists of the corrected mass matrix and the incomplete stiffness matrix is a very convenient tool to predict effects of mass and stiffness changes on the natural frequencies and mode shapes of a structure.

For example, if the mass matrix of a structure is modified by an amount $[\Delta M]$, the eigenvalue problem of the modified structure turns out to be:

$$\left([M_c]+[\Delta M]\right)^{-1}[K_{inc}]\left\{u^r\right\} = \omega_r^2\left\{u^r\right\} \tag{2.19}$$

The solution of the above eigenvalue problem gives the natural frequencies and mode shapes of the modified structure.

On the other hand, the effect of a modified stiffness matrix on the eigenvalues and eigenvectors cannot be found as straightforward as in the case of the mass matrix. If the stiffness matrix is changed by an amount $[\Delta K]$, Berman shows that it is possible to determine the corresponding incomplete version of the 'modified' stiffness matrix with the following expression:

$$\left([K]+[\Delta K]\right)_{inc} = [K_{inc}] + \sum_{r=1}^{N}\sum_{s=1}^{N} \frac{\left\{u_x^r\right\}[\Delta K]\left\{u_x^s\right\}}{m_r m_s}[M_c]\left\{u_x^r\right\}\left\{u_x^r\right\}^T[M_c] \tag{2.20}$$

By using simple case studies [1], Berman proves that the expression given in (2.20) can be used in the eigenvalue problem of a structure to obtain a good approximation of its 'new' natural frequencies and mode shapes as follows:

$$[M_c]^{-1}\left([K]+[\Delta K]\right)_{inc}\left\{u^r\right\} = \omega_r^2\left\{u^r\right\} \tag{2.21}$$

To conclude, 'The Theory of Incomplete Models' introduced by Berman and Flannelly [1] seems to be a useful tool to predict the effects of the structural modifications on the mode shapes and natural frequencies of a structure. But, the method has several disadvantages that restrict its applicability to relatively complex structures. One such disadvantage is that the size of the mass matrix cannot be more than dofs of the incomplete measured modes, because there is no complete stiffness matrix to expand measured mode shapes. Another disadvantage is that the method necessitates an accurate initial mass matrix which is not easy to determine. Moreover, the method does not provide a complete FE model that can be used in force-response analyses.

2.1.2. Direct Updating Methods Using Analytical Mass Matrix as Reference

This section is dedicated to illustrate a common direct updating method developed by Baruch and Itzhack [5]. The objective of this method is to correct experimental modal matrix and analytical stiffness matrix of a structure by taking mass matrix as reference.

Correction of the experimental normal modes to satisfy the orthogonality with respect to the analytical mass matrix starts with the definition of an error function:

$$\varepsilon = \left\| \; [N] \left(\; [\Phi_c] - [\Phi_x] \; \right) \right\| = \sum_{i=1}^{n} \sum_{k=1}^{m} \left[\sum_{j=1}^{n} n_{ij} \left(\phi_{jk}^{c} - \phi_{jk}^{x} \right)^2 \right] \tag{2.22}$$

where $[\Phi_x]_{nxm}$ and $[\Phi_c]_{nxm}$ are the mass normalized measured and corrected modal matrices respectively. Moreover, the matrix $[N]$ is a weight function determined from the analytical mass matrix $[M]$ of the relevant structure as follows:

$$[N] = [M]^{1/2} \tag{2.23}$$

The corrected modal matrix must satisfy the following orthogonality condition:

$$[\Phi_c]^T [M] \; [\Phi_c] = [I] \tag{2.24}$$

As a result, the error function given in expression (2.22) is subject to the mass orthogonality constraint by using Lagrange multipliers as below:

$$\psi = \varepsilon + \left\| \left[\Lambda_c\right] \left(\left[\Phi_c\right]^T \left[M\right] \left[\Phi_c\right] - \left[I\right] \right) \right\| \tag{2.25}$$

where $\left[\Lambda_c\right]$ is a matrix of Lagrange multipliers and

$$\left\| \left[\Lambda_c\right] \left(\left[\Phi_c\right]^T \left[M\right] \left[\Phi_c\right] - \left[I\right] \right) \right\| = \sum_{l=1}^{m} \sum_{i=1}^{m} \lambda_{li} \left(\sum_{j=1}^{n} \sum_{k=1}^{n} \phi_{ji}^{c} m_{jk} \phi_{kl}^{c} - \delta_{il} \right) \tag{2.26}$$

In equation (2.26), the term δ_{il} is the Kronecker delta function.

To minimize ψ, its partial derivatives with respect to ϕ_{ij}^{c} are equated to zero:

$$\frac{\partial \psi}{\partial \{\phi_c\}} = 2 \left[M\right] \left(\left[\Phi_c\right] - \left[\Phi_x\right] \right) + 2 \left[M\right] \left[\Phi_c\right] \left[\Lambda_T\right] = 0 \tag{2.27}$$

Rearranging the terms of equation (2.27), the following equality is obtained:

$$\left[\Phi_c\right] \left(\left[I\right] + \left[\Lambda_c\right] \right) = \left[\Phi_x\right] \tag{2.28}$$

Equation (2.28) reveals the physical significance of the Lagrange multipliers matrix $\left[\Lambda_c\right]$: It represents the difference between the measured and corrected mode shapes.

Finally, from equation (2.28) the corrected modal matrix turns out to be:

$$\left[\Phi_c\right] = \left[\Phi_x\right] \left(\left[I\right] + \left[\Lambda_c\right] \right)^{-1} \tag{2.29}$$

Substituting equation (2.29) into the mass orthogonality equation (2.24), the following equation is obtained, from which the Lagrange multipliers matrix $\left[\Lambda_c\right]$ can be solved:

$$\left[I\right] + \left[\Lambda_c\right] = \left(\left[\Phi_x\right]^T \left[M\right] \left[\Phi_x\right] \right)^{1/2} \tag{2.30}$$

Finally, solving the Lagrange multipliers matrix $\left[\Lambda_c\right]$ from equation (2.30) and substituting it into equation (2.28) the corrected modal matrix is obtained as below:

$$\left[\Phi_c\right] = \left[\Phi_x\right] \left(\left[\Phi_x\right]^T \left[M\right] \left[\Phi_x\right] \right)^{-1/2} \tag{2.31}$$

Once the experimental normal modes are corrected, Baruch and Itzhack [5] make use of them to correct the analytical stiffness matrix of the structure of interest as follows:

It is required that the corrected stiffness matrix satisfies the following equality constraints:

$$[K_c]\,[\Phi_c] = [M]\,[\Phi_c]\,\left[\ddots\ \omega_r^2\ \ddots\right] \tag{2.32}$$

$$[K_c] = [K_c]^T \tag{2.33}$$

To determine the optimum correction in which the corrected stiffness matrix deviates from the analytical stiffness matrix at a minimum level, the following error function is defined:

$$\varepsilon_K = \frac{1}{2}\left\| N^{-1}\left([K_c] - [K] \right) N^{-1} \right\| \tag{2.34}$$

where $[K]$ is the analytical stiffness matrix and $[N]$ is the same weight function given by equation (2.23).

To incorporate the equality constraints given in equations (2.32) and (2.33) into the error function, the following Lagrange function is introduced:

$$\eta = \varepsilon_K + 2\left\| [\Lambda_K]\left([K_c]\,[\Phi_c] - [M]\,[\Phi_c]\left[\ddots\ \omega_r^2\ \ddots\right] \right) \right\| + \left\| [\beta_K]\left([K_c] - [K_c]^T \right) \right\| \tag{2.35}$$

where $[\Lambda_K]$ and $[\beta_K]$ are the Lagrange multipliers matrices.

In order to determine the corrected stiffness matrix, the Lagrange function is differentiated with respect to the unknown elements of the stiffness matrix and is equated to zero. The solution of those equations gives the following stiffness matrix:

$$[K_c] = [K] - [K]\,[\Phi_c]\,[\Phi_c]^T[M] - [M]\,[\Phi_c]\,[\Phi_c]^T[K] + [M]\,[\Phi_c]\,[\Phi_c]^T[K]\,[\Phi_c]\,[\Phi_c]^T[M] +$$

$$[M]\,[\Phi_c]\left[\ddots\ \omega_r^2\ \ddots\right][\Phi_c]^T[M] \tag{2.36}$$

To conclude, the direct updating method proposed by Baruch and Itzhack [5] proves to be useful to correct experimental normal modes and analytical stiffness matrix in a manner to satisfy the orthogonality conditions and the eigenvalue problem. Of

course, the method has several drawbacks: First of all, it requires relatively accurate initial estimates of the spatial matrices. Secondly, the corrected stiffness matrix usually becomes fully populated and as a result, the connectivity characteristic of the FE model is lost.

2.1.3. Direct Updating Methods Using Analytical Stiffness Matrix as Reference

After a technical comment [22] of Berman about the mass reference based updating method of Baruch et al. [5], Baruch [8] published another work in which the stiffness matrix is taken as reference to correct experimental modes and analytical mass matrix of a structure.

In the stiffness matrix reference based updating, Baruch [8] suggests to correct the analytical stiffness matrix by using static test data. This data consists of a measured static load matrix $[F]_{gxf}$ and a measured static displacement matrix $[G]_{gxf}$. In case of an unconstrained (free-free) structure, $[G]_{gxf}$ is obtained by constraining the structure in a statically determined way.

In a real structure, all the displacements of $[G]_{gxf}$ cannot be measured. In order to supply missing displacements, Guyan's Expansion [23] is used.

Due to experimental and analytical errors, the force and displacement matrices may not be compatible. Maxwell-Betti Reciprocal Theorem requires that:

$$[F]^T[G_c] = [G_c]^T[F] \tag{2.37}$$

where $[G_c]_{gxf}$ is the corrected displacement matrix.

In order to determine the corrected displacement matrix, the following error function is defined:

$$\varepsilon_G = \frac{1}{2}\left\| [G_c] - [G] \right\| \tag{2.38}$$

Minimization of the above error function subject to the constraint given in equation (2.38) yields the corrected displacement matrix a below:

$$[G_c] = [G] + 1/2\ [F]\left([F]^T[F] \right)^{-1}\left([G]^T[F] - [F]^T[G] \right) \tag{2.39}$$

Correction of the stiffness matrix using static test data starts with the following error function:

$$\varepsilon_K = \frac{1}{2}\left\| [\bar{K}_c] - [\bar{K}] \right\| \tag{2.40}$$

where $[\bar{K}]_{gxg}$ and $[\bar{K}_c]_{gxg}$ are the analytical and corrected stiffness matrices of the physically 'constrained' structure.

The corrected matrix has to satisfy the following constraints:

$$[\bar{K}_c][G_c] = [F] \tag{2.41}$$

$$[\bar{K}_c] = [\bar{K}_c]^T \tag{2.42}$$

By using Lagrange multipliers to incorporate the constraints into the error function, a new Lagrange function is obtained. Minimization of this function with respect to $[K_c]_{gxg}$ yields [8]:

$$[\bar{K}_c] = [\bar{K}] - [G_c]\left([G_c]^T[G_c] \right)^{-1}\left([G_c]^T[\bar{K}] - [F]^T \right)\left([I] - 1/2[G_c]\left([G_c]^T[G_c] \right)^{-1}[G_c]^T \right) + \\ -\left([I] - 1/2[G_c]\left([G_c]^T[G_c] \right)^{-1}[G_c]^T \right)\left([\bar{K}][G_c] - [F] \right)\left([G_c]^T[G_c] \right)^{-1}[G_c]^T \tag{2.43}$$

The corrected stiffness matrix of the physically unconstrained (free-free) structure is determined as follows:

$$[K_c]_{nxn} = [\beta]_{nxg}\ [\bar{K}_c]_{gxg}\ [\beta]^T_{gxn} \tag{2.44}$$

where $[\beta]_{nxg}$ is the equilibrium matrix in which the vectors include a unit load in any one of the degrees of freedom of the constrained structure and the reactions of the constrained structure caused by unit load.

If the measurement dofs are less than the analytical dofs, the experimental mode shapes have to be expanded to the size of the spatial matrices. This can be

accomplished by using analytical stiffness matrix of the relevant structure in Guyan's Expansion.

Corrected normal modes must fulfill the following requirement:

$$[\Phi_c]^T [K_c] [\Phi_c] = \left[\ddots \omega_r^2 \ddots\right] \tag{2.45}$$

Similar to the procedure followed in previously studied direct updating methods, an error function is defined as follows:

$$[\varepsilon] = \left\| [L] \left([\Phi_c] - [\Phi_x] \right) \right\| \tag{2.46}$$

where $[L] = [K_c]^{1/2}$ is the weight function.

Minimization of the error function with respect to $[\Phi_c]$ with the constraint equation (2.45) yields:

$$[\Phi_c] = [\Phi_x] \left[\ddots \omega_r^2 \ddots\right] \left(\left[\ddots \omega_r^2 \ddots\right] [\Phi_x]^T [K_c] [\Phi_x] \left[\ddots \omega_r^2 \ddots\right] \right)^{-1/2} \left[\ddots \omega_r^2 \ddots\right] \tag{2.47}$$

The corrected mass matrix must fulfill the following requirements:

$$[M_c] [\Phi_c] \left[\ddots \omega_r^2 \ddots\right] = [K_c] [\Phi_c] \tag{2.48}$$

$$[M_c]^T = [M_c] \tag{2.49}$$

In order that the corrected mass matrix gets as close as possible to the given analytical mass matrix, the following error function is introduced:

$$\varepsilon_M = \frac{1}{2} \left\| [L]^{-1} \left([M_c] - [M] \right) [L]^{-1} \right\| \tag{2.50}$$

By substituting constraints equations (2.48) and (2.49) into the error function with Lagrange multipliers and minimizing that new error function with respect to $[M_c]$, the corrected mass matrix is obtained as:

$$[M_c] = [M] - [M] [\Phi_c] \left[\ddots \omega_r^2 \ddots\right]^{-2} [\Phi_c]^T [K_c] - [K_c] [M] \left[\ddots \omega_r^2 \ddots\right]^{-2} [\Phi_c]^T [M] +$$

$$[K_c][\Phi_c] \left[\ddots \omega_r^2 \ddots\right]^{-4} [\Phi_c]^T [K_c] + [K_c] [\Phi_c] \left[\ddots \omega_r^2 \ddots\right]^{-2} [\Phi_c]^T [M] [\Phi_c] \left[\ddots \omega_r^2 \ddots\right]^{-2} [\Phi_c]^T [K_c] \tag{2.51}$$

Similar to other reference based updating algorithms, stiffness matrix reference based method also requires relatively accurate initial estimates of the analytical mass and stiffness matrices. As a result, it is concluded that a mathematical model updated by using methods of reference basis is only suitable to study the effect of small structural modifications on the mode shapes and natural frequencies of a real structure.

2.2. FREQUENCY RESPONSE FUNCTION BASED METHODS IN DIRECT MODEL UPDATING

Experimental data used in modal updating usually consists of mode shapes and natural frequencies. Actually, those parameters are extracted from the measured frequency response functions (FRFs) throughout a modal analysis. So, using FRFs directly (without extracting modal data) in a modal updating process seems to be a promising approach to correct analytical model of a real structure.

Choudhury et al. [11] propose such a method that makes use of measured FRFs to determine mass and stiffness matrices of a structure. This method starts with the governing equations of motion of an N dofs undamped structure in frequency domain as follows:

$$\left([K] - \omega^2 [M] \right) \{X(\omega)\} = \{F(\omega)\} \tag{2.52}$$

where $[M]$ and $[K]$ are the unknown mass and stiffness matrices, respectively, and $\{F(\omega)\}$ and $\{X(\omega)\}$ are the force and displacement terms, respectively.

By the way, FRF matrix of a structure relates the applied forces to the dynamic response as follows:

$$\{X(\omega)\} = [\alpha(\omega)] \{F(\omega)\} \tag{2.53}$$

where $[\alpha(\omega)]$ is the receptance (FRF) matrix.

Combination of equations (2.52) and (2.53) gives rise to the following relation:

$$[\alpha(\omega)] = \left([K] - \omega^2 [M] \right)^{-1} \tag{2.54}$$

Considering only one column of the receptance matrix equation (2.54) can be written a follows:

$$\left([K] - \omega^2 [M] \right) \{\alpha(\omega)\}_m = \{\delta_m\} \tag{2.55}$$

where $\{\delta_m\}$ is a null vector except the m^{th} element which is unity. Here m corresponds to the column number of $[\alpha(\omega)]$ used in equation (2.55).

Let us evaluate equation (2.56) at 2 different frequencies ω_1 and ω_2:

$$[K] \{\alpha(\omega_1)\}_m = \{\delta_m\} + \omega_1^2 [M] \{\alpha(\omega_1)\}_m \tag{2.56}$$

$$[K] \{\alpha(\omega_2)\}_m = \{\delta_m\} + \omega_2^2 [M] \{\alpha(\omega_2)\}_m \tag{2.57}$$

Taking the transpose of equation (2.56):

$$\{\alpha(\omega_1)\}_m^T [K] = \{\delta_m\}^T + \omega_1^2 \{\alpha(\omega_1)\}_m^T [M] \tag{2.58}$$

Post multiplying both sides of equation (2.58) by $\{\alpha(\omega_2)\}_m$:

$$\{\alpha(\omega_1)\}_m^T [K] \{\alpha(\omega_2)\}_m = \{\delta_m\}^T \{\alpha(\omega_2)\}_m + \omega_1^2 \{\alpha(\omega_1)\}_m^T [M] \{\alpha(\omega_2)\}_m \tag{2.59}$$

Also premultiplying both sides of equation (2.57) by $\{\alpha(\omega_1)\}_m^T$:

$$\{\alpha(\omega_1)\}_m^T [K] \{\alpha(\omega_2)\}_m = \{\alpha(\omega_2)\}_m^T \{\delta_m\} + \omega_2^2 \{\alpha(\omega_1)\}_m^T [M] \{\alpha(\omega_2)\}_m \tag{2.60}$$

Subtracting equation (2.60) from (2.59):

$$\{\alpha(\omega_1)\}_m^T [M] \{\alpha(\omega_2)\}_m = \left(\alpha_{mm}(\omega_1) - \alpha_{mm}(\omega_2)\right) / \left(\omega_1^2 - \omega_2^2\right) \tag{2.61}$$

Substituting equation (2.61) into equation (2.59) the following expression is obtained:

$$\{\alpha(\omega_1)\}_m^T [K] \{\alpha(\omega_2)\}_m = \left(\omega_1^2 \alpha_{mm}(\omega_1) - \omega_2^2 \alpha_{mm}(\omega_2)\right) / \left(\omega_1^2 - \omega_2^2\right) \tag{2.62}$$

Theoretically, by using experimentally obtained receptance data in equations (2.61) and (2.62) it is possible to determine unknown stiffness and mass matrices of a structure. But the applicability of the method to complex engineering structure is questionable for several reasons: First of all, the mass and stiffness matrices are

restricted to the measurement dofs. Secondly, inappropriate choices of frequency points and excessive experimental error may result ill conditioned equations which will lead to erroneous mass and stiffness matrices.

CHAPTER 3

THEORY

3.1. INTRODUCTION

The theory introduced herein is developed to achieve dynamically equivalent finite element (FE) models of real aircraft structures. Here, the challenging part is that the eigenvalues and eigenvectors of the FE model must correlate well with their experimental counterparts, i.e. natural frequencies and mode shapes of the interested aircraft.

Dynamically equivalent FE model of an aircraft structure has a crucial role in various aeroelastic problems such as the flutter phenomenon. Flutter is “a self-exciting and destructive vibration where aerodynamic forces on an object couple with the structure’s natural mode of vibration to produce rapidly increasing periodic motion” [25]. A new aircraft design or a modified aircraft structure have to be processed with an appropriate flutter analysis to determine the safe flight envelops within which no flutter phenomenon will occur.

The ‘reliability’ of the flutter analysis is highly dependent on the degree of correlation between the modal properties of the FE model and their experimental counterparts. In order to achieve a good correlation between the mathematical model and the experimental data, different techniques have been developed within the last 40 years and they created a specific branch of the vibration discipline, namely the ‘Model Updating’.

In TÜBİTAK-SAGE, a recent work accomplished by Kozak [17] has investigated the most common model updating techniques and applied one of them, namely the ‘Inverse Eigen Sensitivity Method’, to update the FE model of a real aircraft

structure. But Kozak's research has shown that currently available model updating methods demand considerable time and effort. Challenges encountered at different levels of a model updating procedure led TÜBİTAK-SAGE to look for alternative approaches in determining the FE model of a real aircraft structure.

The theory developed herein has evolved with the motivation to obtain a superior technique purified from the weak sides of the currently used model updating techniques. Of course in doing so, the theory brings its own challenges and constraints. Consequently, this theory is not a final speech but rather an introductory work that collates finite element and modal analysis backgrounds within a different perspective to obtain the dynamically equivalent FE model of a real aircraft structure.

3.2. CONSTRUCTION OF THE FINITE ELEMENT MESH

Widely used indirect model updating methods such as the 'Inverse Eigen Sensitivity Method' are iterative procedures that necessitate the construction of an initial FE model. In order to guarantee convergence, the FE counterparts of the experimental mode shapes must already appear in that initial model with a sufficient correlation. With this requirement, the determination of an appropriate initial FE model becomes a challenge. If the model updating is accomplished by the design team of the owner company of the aircraft structure, such a detailed FE model will be already available. But if the updating procedure is carried out by a subsidiary company that makes certain modification on the aircraft structure, the construction of an appropriate initial FE model from scratch turns out to be a tedious work requiring detailed studies of the blueprints and investment of considerable engineering work. In order to eliminate this difficulty, the theory starts with an FE mesh constructed by connecting measurement points of the aircraft structure of interest with beam elements without assignment of any geometric or material properties. Measurement points are nothing but the acceleration locations used in the 'Ground Vibration Test' (GVT) carried out to extract the modal properties of the relevant aircraft.

In the usual way of meshing an aircraft structure, beam elements are laid along the physical load paths, i.e. spars and ribs of the wing. Moreover, the skin of the aircraft is modeled by shell elements. Geometric properties of beam and shell elements such as beam cross sections, shell thicknesses imitate the properties of the spars,

ribs and the skin of the real structure as much as possible. Although the initial FE model obtained with this approach is more likely to correlate with the experimental modal data, it requires detailed investigation of the blueprints followed by considerable FE modeling effort. On the other hand, an FE mesh built by connecting GVT measurement points with beam elements is very straightforward. With this approach, measurement points turn out to be the nodes of the FE mesh. The resulting FE model includes much less degrees of freedom (dofs) than an FE model obtained from the conventional procedure explained above.

As a result, the theory developed herein aims to find an answer to the following questions: Is it really a must to conduct the model updating with the conventional FE mesh that duplicates the morphology of the real structure? Or can an FE mesh built up by simply connecting GVT measurement points serve the purpose as well?

The theory has suggested a simple FE mesh but it did not explain yet how to obtain initial estimates of the geometric and material properties that will be assigned to each finite element. As explained in detail in the subsequent sections, the initial estimates of the geometric and material properties are going to be determined from the mass and stiffness orthogonality equations of the experimental mode shapes.

3.3. DETERMINATION OF THE MASS NORMALIZED EXPERIMENTAL NORMAL MODES

In the determination of the mode shapes and natural frequencies of a real aircraft structure, the first step is the ‘Ground Vibration Test’ (GVT). In a GVT, an aircraft structure is suspended on soft supports to achieve free-free boundary conditions. Then, several electrodynamic shakers are attached to critical points to be able to excite all of the modes within the frequency range of interest. Vibration measurement is usually accomplished by accelerometers placed on the wing, vertical and horizontal stabilizers, fuselage, pylons and external stores of the aircraft structure. In a GVT test, depending on the size of the aircraft structures, number of accelerometers used varies between 100 and 200 for fighter aircrafts and increases up to 1000 for civil aircrafts. After the experimental setup is constructed, the aircraft structure is excited within the frequency range of interest by using one of the numerous excitation signals such as stepped sine, pseudo-random, true random etc., each having its own particular advantages and drawbacks. In phase separation

technique an appropriate signal analyzer is used to determine the discrete Fourier transforms of the input and output signals (i.e. force and acceleration) and the ratio of these transforms gives the 'Frequency Response Functions' (FRFs) of the aircraft structure during test. FRFs obtained from the modal test are processed by one of the appropriate modal analysis techniques such as the 'Least-Squares Method', 'Rational Fraction Polynomials Method' etc. to extract the mode shapes and natural frequencies of the aircraft structure. Another technique is the phase resonance, which is also called normal modes, where only one mode is excited at a time and modal parameters are extracted directly during testing.

Modal analysis methods are classified under two main categories: time domain and frequency domain modal analysis methods. Frequency domain modal analysis techniques are basically curve fitting techniques that fit a predefined mathematical model to the experimentally obtained FRFs of a structure.

For structurally damped linear elastic systems, the analytical expression of a receptance FRF can be stated as follows:

$$H_{ik} = \sum_{r=1}^{n} \frac{A_{ik}^{r}}{\omega_r^2 - \omega^2 + \omega_r^2 \eta_r j} \tag{3.1}$$

where H_{ik} is the receptance FRF between the measurement points i and k, ω_r is the natural frequency of the r^{th} mode, η_r is the r^{th} modal damping and A_{ik}^{r} is the modal constant of the r^{th} mode.

A real structure has infinitely many dofs and vibration modes. But practically, only a limited number of modes within a frequency range of interest can be determined. To be able to determine relevant vibration modes accurately, the effects of the out of range modes on the FRFs have to be represented by appropriate residual terms in the analytical model as follows:

$$H_{ik}(\omega) = \sum_{r=m_1}^{m_2} \frac{A_{ik}^{r}}{\omega_r^2 - \omega^2 + \omega_r^2 \eta_r j} + \frac{1}{K_{ik}^{R}} - \frac{1}{\omega^2 M_{ik}^{R}} \tag{3.2}$$

where M_{ik}^{R} and K_{ik}^{R} are the mass and stiffness residuals that represent the cumulative effects of the lower and higher out of range modes, respectively.

The objective of the modal analysis techniques is to calculate the modal constants A_{ik}^{r}, the natural frequencies ω_r, the damping coefficients η_r and the residual terms M_{ik}^{R} and K_{ik}^{R} of each FRF by minimizing the following error function defined between the measured and analytical FRFs:

$$E_{ik}(\omega) = \tilde{H}_{ik}(\omega) - H_{ik}(\omega) \tag{3.3}$$

where $\tilde{H}_{ik}$ are the measured FRFs.

Theoretically, the FRF matrix of n dof FE model of a structure is expressed in terms of its eigenvectors and eigenvalues as follows:

$$\left[H(\omega)\right]_{nxn} = \left[\Phi\right]_{nxn}\left[\begin{array}{ccc} \ddots & & \\ & \left(\lambda_r^2 - \omega^2\right) & \\ & & \ddots \end{array}\right]_{nxn}^{-1}\left[\Phi\right]_{nxn}^{T} \tag{3.4}$$

where $\left[\Phi\right]$ is the mass normalized modal matrix, and $\lambda_r^2 = \omega_r^2\left(1 + \eta_r j\right)$.

Unfortunately, the size of the experimental FRF matrix cannot be nxn due to practical reasons. In order that the experimental FRF matrix has n columns, the structure must be excited at each measurement point separately. This is practically impossible. Moreover in order that the experimental FRF matrix includes n rows, all of the dofs corresponding to the FE model of the real structure have to be measured. This is not feasible as well. So the experimental FRF matrix of a real structure turns out to be truncated as below:

$$\left[H(\omega)\right]_{pxm} = \begin{bmatrix} H_{11} & H_{12} & \cdots & H_{1m} \\ \vdots & \ddots & & \vdots \\ H_{p1} & \cdots & & H_{pm} \end{bmatrix} \tag{3.5}$$

where $m\,(<n)$ is the number of excitation points and $p\,(<n)$ is the number of measurement dofs.

The s^{th} column of the experimental FRF matrix can be expressed as follows:

$$\{H(\omega)\}_s = \begin{Bmatrix} H(\omega)_{1s} \\ H(\omega)_{2s} \\ \vdots \\ H(\omega)_{ps} \end{Bmatrix} = [A_s]_{pxN} \left\{ \frac{1}{\lambda_r^2 - \omega^2} \right\} \tag{3.6}$$

where

$$[A_s]_{pxN} = \begin{bmatrix} A_{1s}^1 & A_{1s}^2 & \cdots & A_{1s}^N \\ A_{2s}^1 & A_{2s}^2 & \cdots & A_{1s}^N \\ \vdots & \vdots & \ddots & \vdots \\ A_{ps}^1 & A_{ps}^2 & \cdots & A_{ps}^N \end{bmatrix} \tag{3.7}$$

$[A_s]$ is the experimentally obtained modal constant matrix of a real structure and it is obtained from a single column (s^{th} column) of the FRF matrix given in equation (3.5).

According to equation (3.4), the s^{th} column of the experimental FRF matrix can also be written as follows:

$$\{H(\omega)\}_s = [\Phi_s] \left\{ \frac{1}{\lambda_r^2 - \omega^2} \right\} \tag{3.8}$$

where

$$\left[\Phi_s\right]_{pxN} = \begin{bmatrix} \phi_s^1\phi_1^1 & \phi_s^2\phi_1^2 & \cdots & \phi_s^N\phi_1^N \\ \phi_s^1\phi_2^1 & \phi_s^2\phi_2^2 & \cdots & \phi_s^N\phi_2^N \\ \vdots & \vdots & \ddots & \vdots \\ \phi_s^1\phi_p^1 & \phi_s^2\phi_p^2 & \cdots & \phi_s^N\phi_p^N \end{bmatrix} \tag{3.9}$$

Here ϕ_i^r is the i^{th} element of the r^{th} mode shape vector.

Comparing equations (3.7) and (3.9), the following equality holds:

$$\begin{bmatrix} A_{1s}^1 & A_{1s}^2 & \cdots & A_{1s}^N \\ A_{2s}^1 & A_{2s}^2 & \cdots & A_{1s}^N \\ \vdots & \vdots & \ddots & \vdots \\ A_{ps}^1 & A_{ps}^2 & \cdots & A_{ps}^N \end{bmatrix}_{pxN} = \begin{bmatrix} \phi_s^1\phi_1^1 & \phi_s^2\phi_1^2 & \cdots & \phi_s^N\phi_1^N \\ \phi_s^1\phi_2^1 & \phi_s^2\phi_2^2 & \cdots & \phi_s^N\phi_2^N \\ \vdots & \vdots & \ddots & \vdots \\ \phi_s^1\phi_p^1 & \phi_s^2\phi_p^2 & \cdots & \phi_s^N\phi_p^N \end{bmatrix}_{pxN} \tag{3.10}$$

Consider the first column of the right hand side matrix in equation (3.10). It is nothing but the first mode shape vector of the real structure. In order to obtain the mass normalized mode shape, the column must be divided by ϕ_s^1. But ϕ_s^1 is not a directly available experimental data. Only the left hand side matrix of equation (3.10) is directly available. The key parameters that are used to extract the mass normalized mode shapes lay in the s^{th} row of the modal constant matrix as follows:

$$\left\{A_{ss}^1 \;\; A_{ss}^2 \;\; \cdots \;\; A_{ss}^N\right\} = \left\{\phi_s^1\phi_s^1 \;\; \phi_s^2\phi_s^2 \;\; \cdots \;\; \phi_s^N\phi_s^N\right\} \tag{3.11}$$

Modal constants given in equation (3.11) are the parameters of the point FRF $H_{ss}(\omega)$ and ϕ_s^1, ϕ_s^2 etc. can be calculated by simply taking the square root of those parameters as follows:

$$\left\{\phi_s^1 \;\; \phi_s^1 \;\; \cdots \;\; \phi_s^N\right\} = \left\{\sqrt{A_{ss}^1} \;\; \sqrt{A_{ss}^2} \;\; \cdots \;\; \sqrt{A_{ss}^N}\right\} \tag{3.12}$$

The mass normalized modes are simply calculated by dividing each column of the right hand side matrix of equation (3.9) with the relevant parameter from the equation (3.12). As a result, the following expression is obtained:

$$\left[\Phi_x^t\right]_{pxN} = \begin{bmatrix} \phi_1^1 & \phi_1^2 & \cdots & \phi_1^N \\ \phi_2^1 & \phi_2^2 & \cdots & \phi_2^N \\ \vdots & \vdots & \ddots & \vdots \\ \phi_p^1 & \phi_p^2 & \cdots & \phi_p^N \end{bmatrix}_{pxN} \tag{3.13}$$

Although the size of the theoretical modal matrix corresponding to the FE model is nxn, the experimental modal matrix is highly truncated. The number of rows, p, of the experimental modal matrix corresponds to the number of measurement dofs. Measurement dofs are less than the actual dofs of the FE model, because rotational dofs cannot be measured. It is also not practical to take measurement along all of the translational dofs that appear in an FE model. The number of columns, N, of the experimental modal matrix corresponds to the number of the modes that appear in the frequency range of interest and it is much less than the total number of modes of an n dofs FE model.

The theory developed herein aims to use experimental modal matrix to derive the necessary equations to obtain the initial estimates of geometric and material properties mentioned in section 3.2. In order to use in the mass and stiffness orthogonality equations of the FE model of an aircraft structure, truncated experimental modes have to be expanded to the size of the FE model. This is the subject of the next section.

3.4. EXPANSION OF THE EXPERIMENTALLY MEASURED NORMAL MODES TO THE SIZE OF THE FE MODEL

In section 3.2, an FE mesh obtained by connecting GVT measurement points with beam elements is suggested for aircraft structures. However the geometric and material properties need to be determined. The necessary equations to obtain the

initial estimates for properties can be derived from the mass and stiffness orthogonality relations of the experimental normal modes.

Consider the following mass and stiffness orthogonality equations:

$$[\Phi]^T [M] [\Phi] = [I] \tag{3.14}$$

$$[\Phi]^T [K] [\Phi] = \begin{bmatrix} \ddots & & \\ & \omega_r^2 & \\ & & \ddots \end{bmatrix} \tag{3.15}$$

where $[M]$ and $[K]$ are the global mass and stiffness matrices, $[I]$ is the identity matrix and $\begin{bmatrix} \ddots & & \\ & \omega_r^2 & \\ & & \ddots \end{bmatrix}$ is the diagonal matrix including squares of the natural frequencies.

For an n dof FE model, the mass normalized modal matrix $[\Phi]$ will be an nxn square matrix. However, the experimental modal matrix corresponding to that FE model will be highly incomplete as explained in the previous section. In order to use them in equations (3.14) and (3.15), experimental normal modes have to be expanded to the size of the eigenvectors of the FE model.

The *'Guyan's Expansion'* [23] is a simple and reliable technique to be used for the expansion of the experimental normal modes. This method predicts the unmeasured (slave) dofs of the experimental normal modes by using the force-displacement and connectivity relations between the primary (measurement) and slave coordinates. Mathematically, these relations are expressed in terms of a transformation matrix, between the primary and slave coordinates, determined from the stiffness matrix of the FE model. Unfortunately, the theory developed herein starts with an 'empty' mesh and seemingly there is no stiffness matrix to be used. In order to overcome this dilemma in which an unknown (stiffness matrix) is required in its own solution procedure, the following critical question is asked: to obtain the transformation matrix, is it really necessary to use the stiffness matrix of the true FE model or a stiffness matrix of some other FE model with the same mesh can be used? This idea will be clarified by the following example:

Consider the FE model of a wing like structure with free-free boundary conditions as shown in Figure 3.1. The FE model consists of 16 nodes and 24 Euler-Bernoulli beam elements resulting 96 dofs. Moreover, the beam elements are divided into three groups of geometric properties as given in Table 3.1.

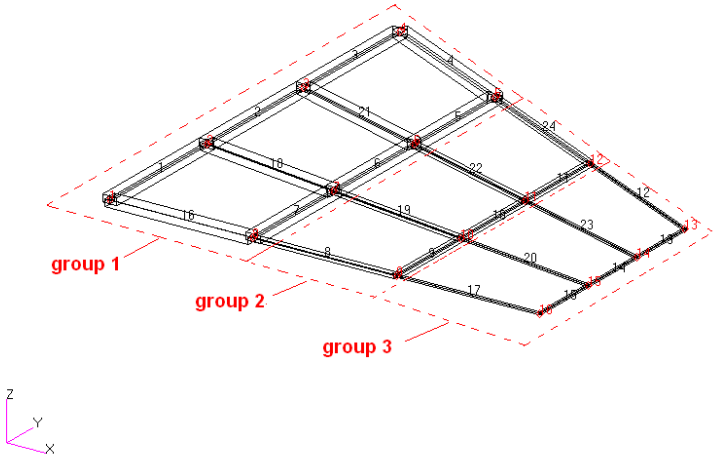

Figure 3.1. FE model of a wing like structure

In the modal test of the wing like structure illustrated in Figure 3.1, reliable measurements can only be taken along the z-axis of its global coordinate frame. Accordingly, in order to examine the idea of using an FE model with the same mesh but arbitrary geometric and material properties in Guyan's expansion of the experimental normal modes, the first 10 eigenvectors of the FE model are truncated by extracting their components along the z direction. Those truncated eigenvectors are called simulated-experimental normal modes because they simulate the incompleteness of the real experimental normal modes but they are free from experimental errors.

Similar to the case of a real aircraft wing, it is assumed that geometric and material properties are not known for the wing like structure studied herein. And its FE mesh is constructed by connecting measurement points with beam elements. In order to construct a stiffness matrix to be used in Guyan's expansion of the simulated-experimental normal modes, two arbitrary case studies of the geometric properties are proposed in Table 3.2. The first case study assumes that all beam elements have square cross sections of unit area which leads to a relatively flexible structure.

And the second case is obtained by scaling the unit area of the previous case study one million times that leads to a very stiff structure.

Table 3.1. Beam element properties of the wing like structure

GROUP NO	GEOMETRIC PROPERTIES						MATERIAL PROPERTIES		
	A (mm^2)	I_x (mm^2)	I_1 (mm^4)	I_2 (mm^4)	I_{12} (mm^4)	J_e (mm^4)	E (MPa)	ρ (ton/mm^3)	ν
1	50.0	10.4	104.2	416.7	0.0	286.1	7.0E+04	2.8E-09	0.3
2	10.0	2.4	3.3	20.8	0.0	10.0	7.0E+04	2.8E-09	0.3
3	2.0	0.4	0.2	0.7	0.0	0.5	7.0E+04	2.8E-09	0.3

Table 3.2. Properties of arbitrary stiffness matrices used in Guyan's expansion

CASE STUDY	GEOMETRIC PROPERTIES					
	A (mm^2)	I_x (mm^2)	I_1 (mm^4)	I_2 (mm^4)	I_{12} (mm^4)	J_e (mm^4)
Flexible	1.0E+00	1.7E-01	8.3E-02	8.3E-02	0.0E+00	1.4E-01
Stiff	1.0E+06	1.7E+05	8.3E+10	8.3E+10	0.0E+00	1.4E+11

According to the Guyan's Expansion Method, a global stiffness matrix is partitioned to separate elements corresponding to the primary and slave coordinates as follows:

$$[K] = \begin{bmatrix} K_{ss} & K_{sp} \\ K_{ps} & K_{pp} \end{bmatrix} \tag{3.16}$$

Then a transformation matrix is obtained as below:

$$[T] = \begin{bmatrix} -[K_{ss}]^{-1}[K_{sp}] \\ [I] \end{bmatrix} \tag{3.17}$$

Finally, experimentally measured mass normalized normal modes can be expanded into the FE model size by using the transformation matrix given in equation (3.17) as follows:

$$\left[\Phi_x\right]_{nxN} = \left[T\right]_{nxp} \left[\Phi_x^t\right]_{pxN} \tag{3.18}$$

where $\left[\Phi_x^t\right]_{pxN}$ is the truncated experimental mass normalized modal matrix and p is the number of primary (measurement) coordinates.

Consequently, the simulated-experimental normal modes of the wing like structure described in Figure 3.1 are expanded to the size of the FE model by using two different arbitrary stiffness matrices whose geometric properties are introduced in Table 3.2. The estimated components of the first five eigenvectors corresponding to α and θ dofs (rotational dofs about the global x and y axes respectively) are compared to their true values appearing in the original FE model in Figures 3.2 to 3.6. Within the frequency range of interest, the eigenvector components related to the remaining slave coordinates are all zero and so are their estimates. For that reason, they are not shown here to avoid redundant graphics.

One of the interesting observations related to Figures 3.2 to 3.6 is that α components of the eigenvectors are estimated much better than θ components. Actually, α corresponds to the deflection slope of the 'constant' cross section beams lying along the y axis as shown in Figure 3.1, and θ corresponds to the deflection slope of the variable cross section beams. But the arbitrary stiffness matrices proposed to expand the simulated-experimental modes are derived by assuming uniform cross section for the entire FE mesh. This assumption that does not overlap with reality for the beams lying along x axis degrades the θ estimates of the experimental normal modes. Of course, this fact will affect the quality of the rotational dof estimates, when the method is applied to real aircraft structures.

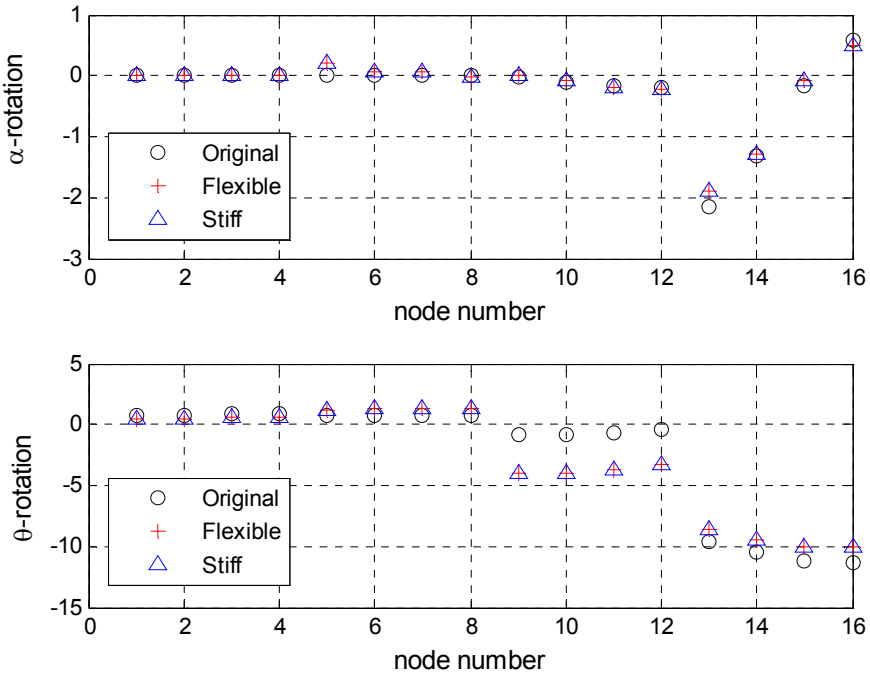

Figure 3.2. Estimates of the rotational components of the 1st elastic mode of the wing like structure

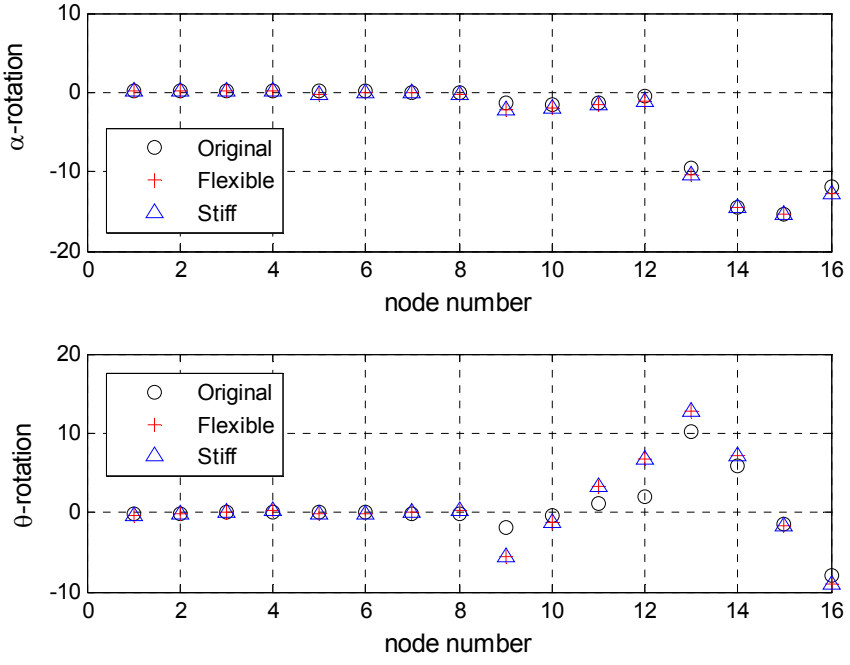

Figure 3.3. Estimates of the rotational components of the 2nd elastic mode of the wing like structure

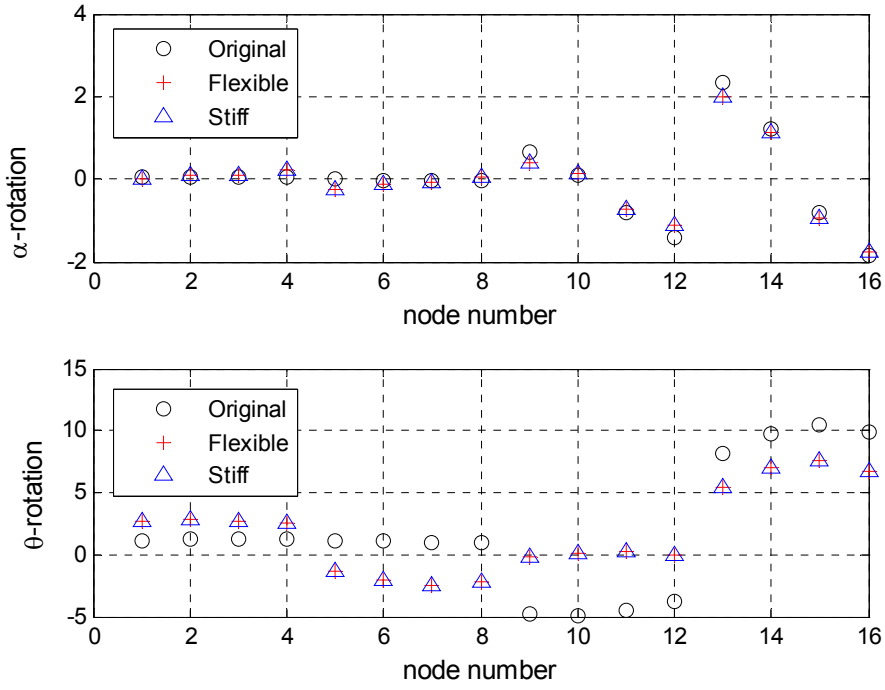

Figure 3.4. Estimates of the rotational components of the 3rd elastic mode of the wing like structure

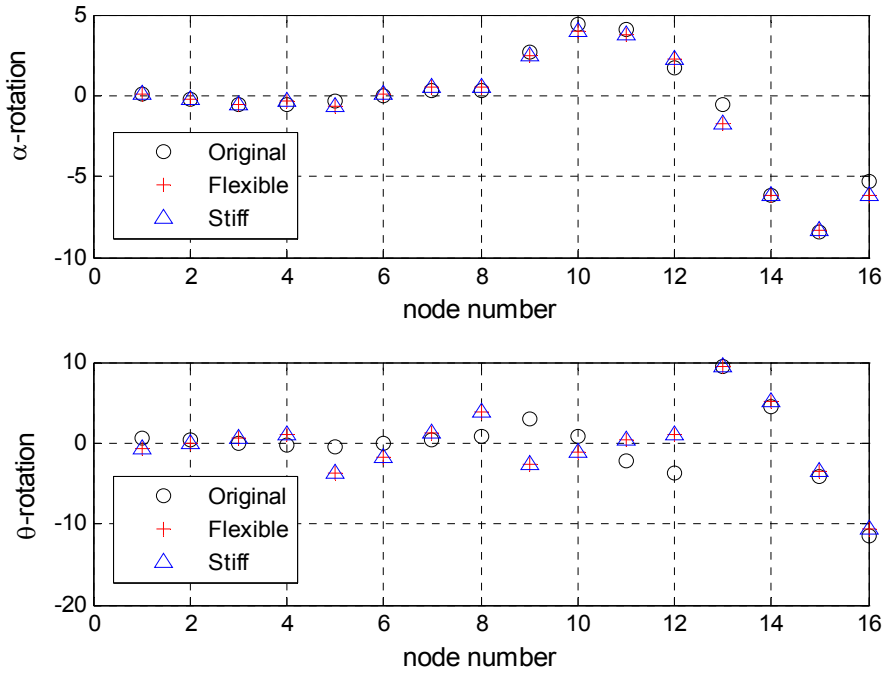

Figure 3.5. Estimates of the rotational components of the 4th elastic mode of the wing like structure

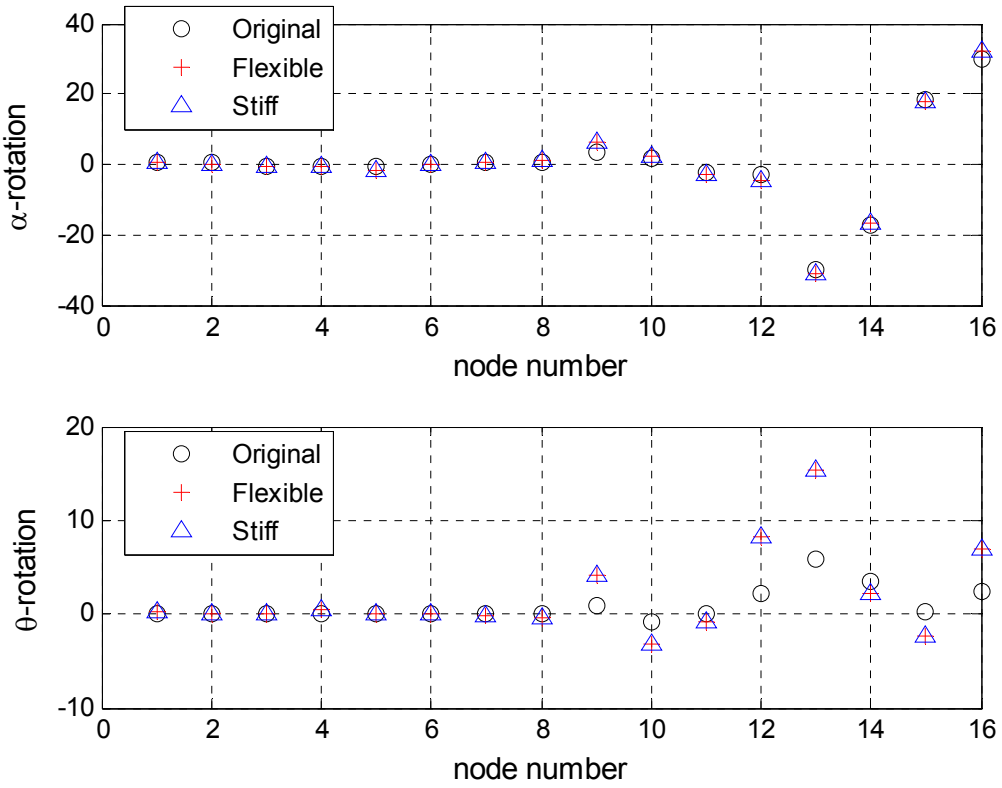

Figure 3.6. Estimates of the rotational components of the 5th elastic mode of the wing like structure

Another observation related to Figures 3.2 to 3.6 is that changing the order of magnitude of the geometric properties the same amount, as in the case of flexible and stiff FE models of Table 3.2, does not affect the estimates of the slave eigenvector components. Of course, if all of the geometric properties of beam elements of the flexible FE model would not be scaled the same amount to obtain the stiff FE model, estimates of the slave components would be somewhat different.

Another factor that will degrade estimates of the slave dofs is the experimental error. In literature, it is claimed that 15 % error [24] in each measured modal displacement is quite usual. Hence, in order to simulate this amount of error, truncated normal modes are polluted within a ± 7.5 % error band. Estimates of the slave dofs obtained from pure and erroneous truncated normal modes using the arbitrary stiffness matrix of the flexible FE model of Table 3.2 are compared in Figures 3.7 to 3.11. Obviously, there is not a dramatic deviation within the predictions of the rotational components of the normal modes.

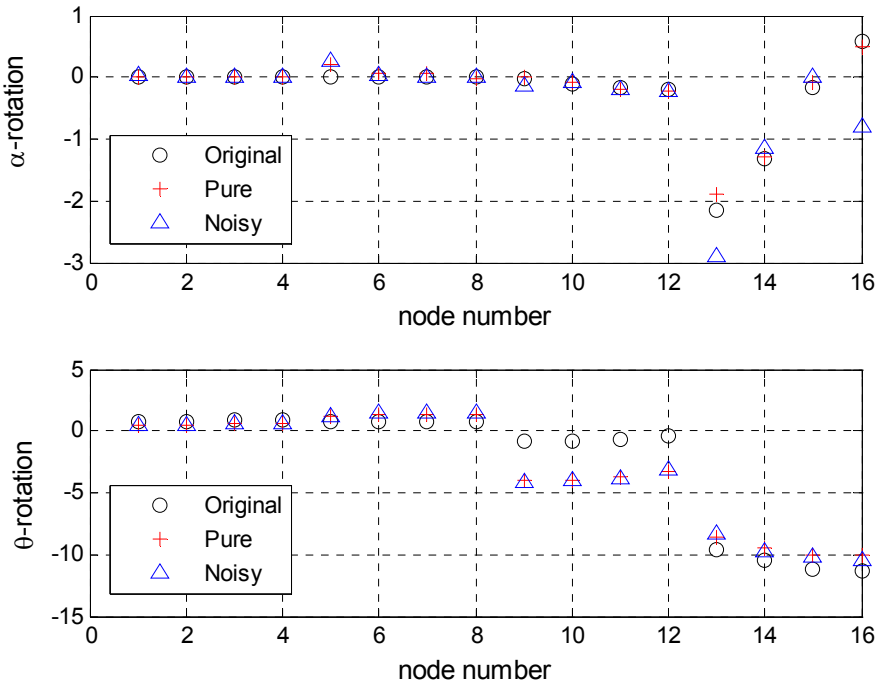

Figure 3.7. Slave dofs determined from pure and noisy truncated normal modes (1st elastic mode)

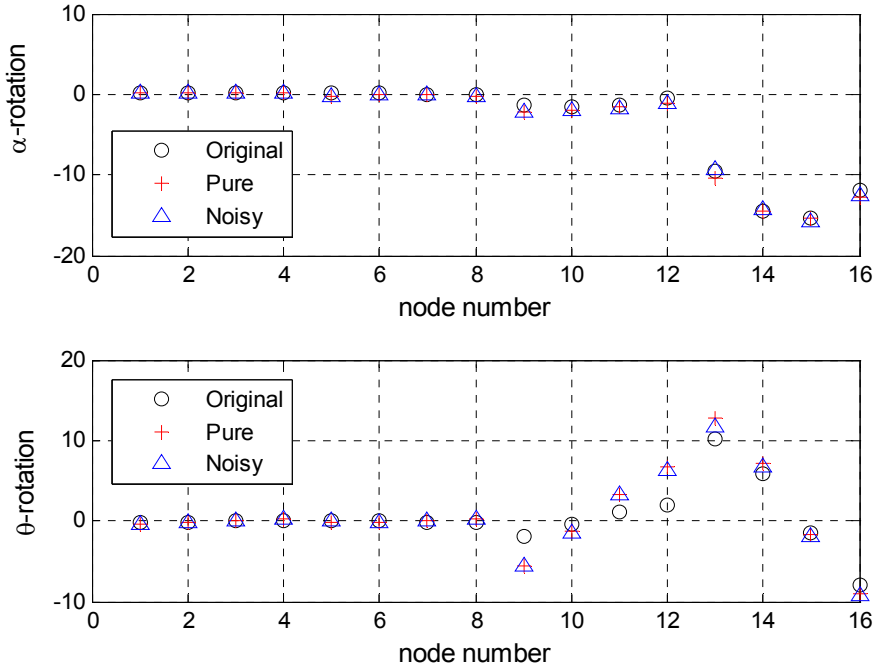

Figure 3.8. Slave dofs determined from pure and noisy truncated normal modes (2nd elastic mode)

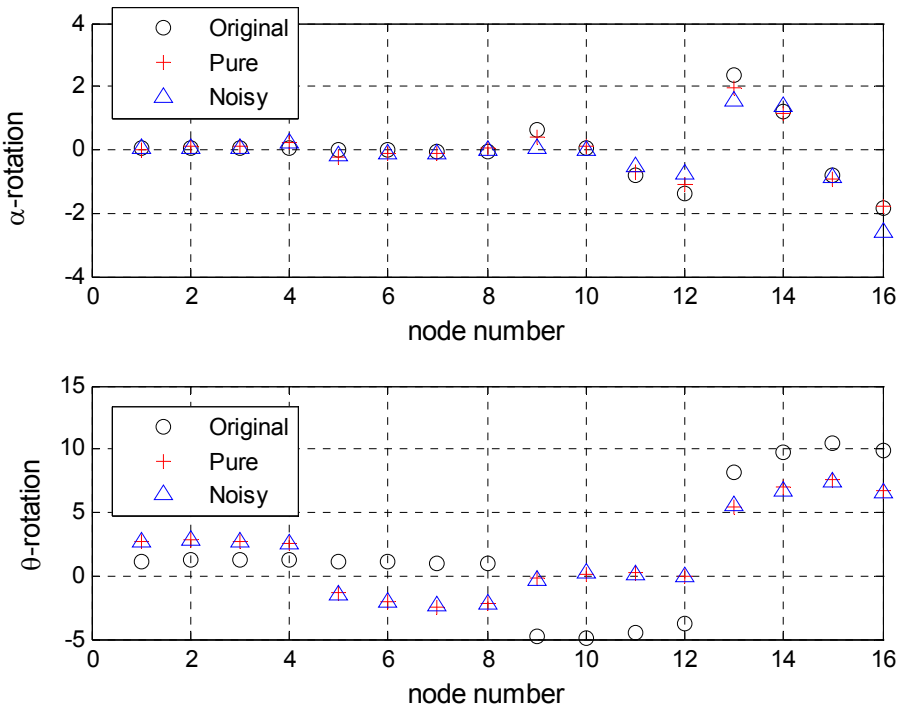

Figure 3.9. Slave dofs determined from pure and noisy truncated normal modes (3th elastic mode)

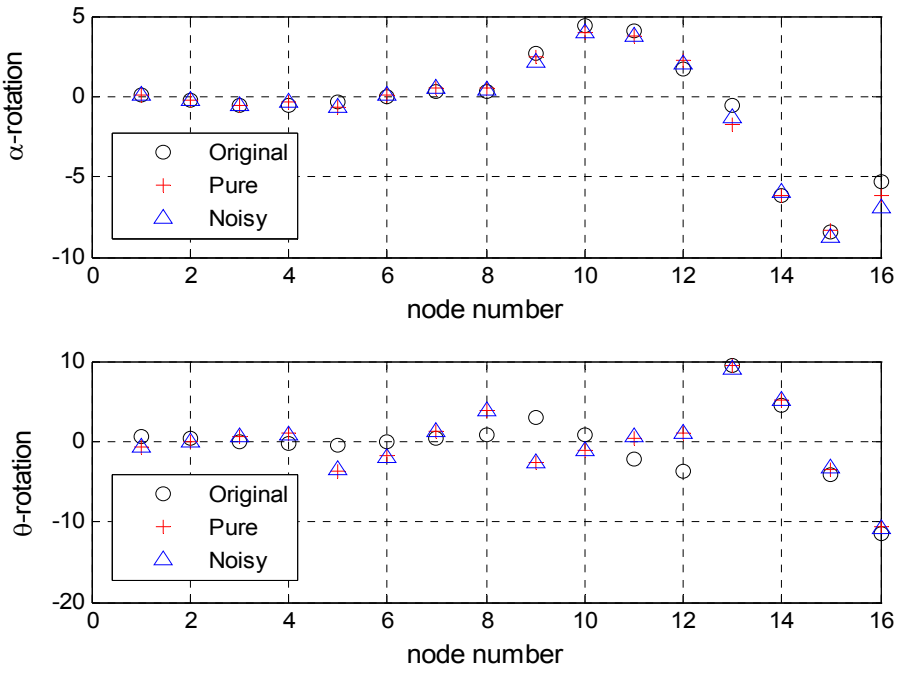

Figure 3.10. Slave dofs determined from pure and noisy truncated normal modes (4th elastic mode)

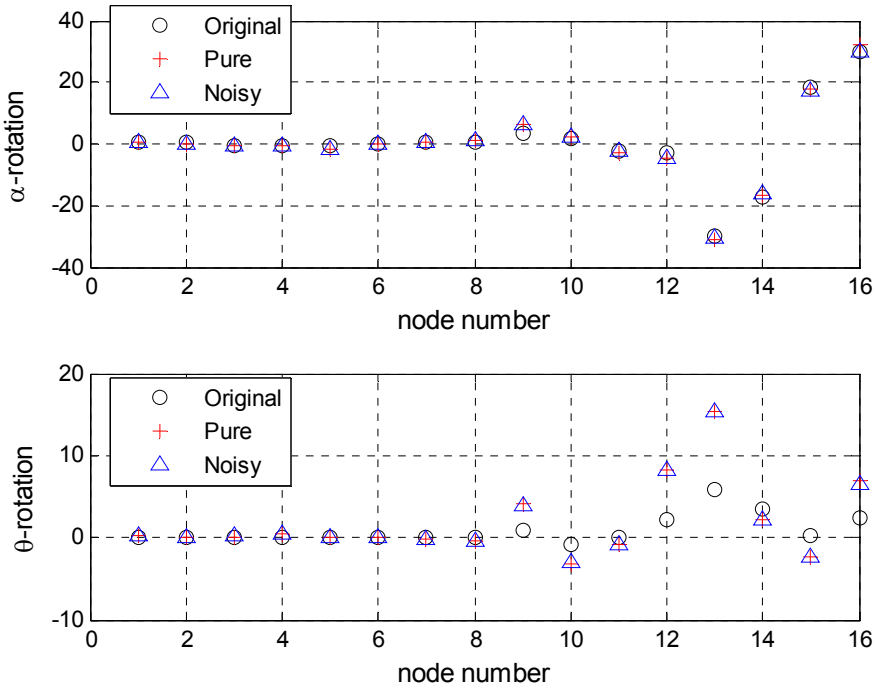

Figure 3.11. Slave dofs determined from pure and noisy truncated normal modes (5^{th} elastic mode)

At this stage of the theory, an empty FE mesh and a useful approach to expand experimental normal modes to the size of the FE model are available. The next step is the derivation of the necessary equations to determine the geometric and material properties of the FE model.

3.5. DERIVATION OF THE STRUCTURAL IDENTIFICATION EQUATIONS FROM MASS AND STIFFNESS ORTHOGONALITY OF EXPERIMENTAL NORMAL MODES

Once the experimental normal modes are expanded to the size of the FE model, the next step is the derivation of the 'structural identification equations' from mass and stiffness orthogonality relations of normal modes.

Consider an n dofs FE model with k elements. The global mass and stiffness matrices can be expressed in terms of the element mass and stiffness matrices as follows:

$$[K]_{nxn} = \sum_{e=1}^{k} [k_e]_{nxn} \tag{3.19}$$

$$[M]_{nxn} = \sum_{e=1}^{k} [m_e]_{nxn} \tag{3.20}$$

where $[k_e]$ and $[m_e]$ are the element stiffness and mass matrices respectively.

The actual size of each element matrix is mxm, m being the dof of an element. On the other hand, the size of the global mass and stiffness matrices is nxn and $n > m$ because the global matrices encompass the physical information of the entire FE model.

During the assembly process described in equations (3.19) and (3.20), relevant cells of a null stiffness matrix of size nxn are filled with none zero terms of a specific element stiffness matrix. This way, an element stiffness matrix is augmented to the size of the global stiffness matrix. The same thing is valid for each element mass matrix.

Substituting the right hand sides of equations (3.19) and (3.20) into equations (3.14) and (3.15) yields:

$$[\Phi]^T \sum_{e=1}^{k} [m_e] [\Phi] = [I] \tag{3.21}$$

$$[\Phi]^T \sum_{e=1}^{k} [k_e] [\Phi] = \begin{bmatrix} \ddots & & \\ & \omega_r^2 & \\ & & \ddots \end{bmatrix} \tag{3.22}$$

Equations (3.21) and (3.22) can be further expanded as follows:

$$\{\phi^r\}^T \{ [m_1] + [m_2] + \ldots + [m_k] \} \{\phi^s\} = \delta_{rs} \quad (3.23)$$

$$\{\phi^r\}^T \{ [k_1] + [k_2] + \ldots + [k_k] \} \{\phi^s\} = \omega_r^2 \, \delta_{rs} \quad (3.24)$$

where δ_{rs} is the Kronecker delta function.

Expanding equations (3.23) and (3.24), it is possible to write

$$\{\phi^r\}^T [m_1] \{\phi^s\} + \{\phi^r\}^T [m_2] \{\phi^s\} + \ldots + \{\phi^r\}^T [m_k] \{\phi^s\} = \delta_{rs} \quad (3.25)$$

$$\{\phi^r\}^T [k_1] \{\phi^s\} + \{\phi^r\}^T [k_2] \{\phi^s\} + \ldots + \{\phi^r\}^T [k_k] \{\phi^s\} = \omega_r^2 \, \delta_{rs} \quad (3.26)$$

Since the individual element matrices in equations (3.25) and (3.26) are sparse, i.e. augmented to the size nxn , they can be condensed as follows:

$$\{\phi^r\}_{1xn}^T [m_e]_{nxn} \{\phi^s\}_{nx1} = \{\bar{\phi}_e^r\}_{1xm}^T [\bar{m}_e]_{mxm} \{\bar{\phi}_e^s\}_{mx1} \quad (3.27)$$

$$\{\phi^r\}_{1xn}^T [k_e]_{nxn} \{\phi^s\}_{nx1} = \{\bar{\phi}_e^r\}_{1xm}^T [\bar{k}_e]_{mxm} \{\bar{\phi}_e^s\}_{mx1} \quad (3.28)$$

where $[\bar{m}_e]_{mxm}$ and $[\bar{k}_e]_{mxm}$ are the element matrices expressed in the global coordinate frame. $\{\phi_e^r\}_{mx1}$ represents the part of the r^{th} eigenvector $\{\phi^r\}_{nx1}$ corresponding to the dofs of the element of interest.

$[\bar{m}_e]_{mxm}$ and $[\bar{k}_e]_{mxm}$ are obtained by transforming element matrices from the local coordinate frame of an element to the global coordinate frame as described below:

$$\left[\overline{m}_e\right]_{mxm} = \left[T_e\right]^T \left[\overline{m}_e^l\right] \left[T_e\right] \tag{3.29}$$

$$\left[\overline{k}_e\right]_{mxm} = \left[T_e\right]^T \left[\overline{k}_e^l\right] \left[T_e\right] \tag{3.30}$$

where $\left[\overline{m}_e^l\right]_{mxm}$ and $\left[\overline{k}_e^l\right]_{mxm}$ are the element matrices in the local coordinate frame of an element, and $\left[T_e\right]$ is the transformation matrix of a specific element that transforms matrices from the local (element) coordinates to the global coordinates.

Substituting equations (3.29) and (3.30) into equations (3.27) and (3.28) yields following expressions:

$$\left\{\overline{\phi}_e^r\right\}^T \left[\overline{m}_e\right] \left\{\overline{\phi}_e^s\right\} = \left\{\overline{\phi}_e^r\right\}^T \left(\left[T_e\right]^T \left[\overline{m}_e^l\right] \left[T_e\right] \right) \left\{\overline{\phi}_e^s\right\} \tag{3.31}$$

$$\left\{\overline{\phi}_e^r\right\}^T \left[\overline{k}_e\right] \left\{\overline{\phi}_e^s\right\} = \left\{\overline{\phi}_e^r\right\}^T \left(\left[T_e\right]^T \left[\overline{k}_e^l\right] \left[T_e\right] \right) \left\{\overline{\phi}_e^s\right\} \tag{3.32}$$

Before substituting equations (3.31) and (3.32) into equations (3.23) and (3.24) one last arrangement is necessary as shown below:

$$\left\{\overline{\phi}_e^r\right\}^T \left(\left[T_e\right]^T \left[\overline{m}_e^l\right] \left[T_e\right] \right) \left\{\overline{\phi}_e^s\right\} = \left(\left[T_e\right] \left\{\overline{\phi}_e^r\right\} \right)^T \left[\overline{m}_e^l\right] \left(\left[T_e\right] \left\{\overline{\phi}_e^s\right\} \right) \tag{3.33}$$

$$\left\{\overline{\phi}_e^r\right\}^T \left(\left[T_e\right]^T \left[\overline{k}_e^l\right] \left[T_e\right] \right) \left\{\overline{\phi}_e^s\right\} = \left(\left[T_e\right] \left\{\overline{\phi}_e^r\right\} \right)^T \left[\overline{k}_e^l\right] \left(\left[T_e\right] \left\{\overline{\phi}_e^s\right\} \right) \tag{3.34}$$

Right hand sides of equations (3.33) and (3.34) can be put in more compact forms with the following definition:

$$\{\bar{\phi}_e^{rl}\} = [T_e]\ \{\bar{\phi}_e^{r}\} \tag{3.35}$$

By using the above definition in equations (3.33) and (3.34), and substituting them into equations (3.23) and (3.24), the following equations are obtained:

$$\{\bar{\phi}_1^{rl}\}^T [\bar{m}_1^l]\ \{\bar{\phi}_1^{sl}\} + \{\bar{\phi}_2^{rl}\}^T [\bar{m}_2^l]\ \{\bar{\phi}_2^{sl}\} + \ldots + \{\bar{\phi}_k^{rl}\}^T [\bar{m}_k^l]\ \{\bar{\phi}_k^{sl}\} = \delta_{rs} \tag{3.36}$$

$$\{\bar{\phi}_1^{rl}\}^T [\bar{k}_1^l]\ \{\bar{\phi}_1^{sl}\} + \{\bar{\phi}_2^{rl}\}^T [\bar{k}_2^l]\ \{\bar{\phi}_2^{sl}\} + \ldots + \{\bar{\phi}_k^{rl}\}^T [\bar{k}_k^l]\ \{\bar{\phi}_k^{sl}\} = \omega_r^2\ \delta_{rs} \tag{3.37}$$

For a 3 D Euler-Bernoulli beam element, the size of the element matrices $[\bar{m}_e^l]$ and $[\bar{k}_e^l]$ is 12x12 and their complete parametric representations are given in the Appendix D. For the sake of simplicity, the element matrices of a 2 D Euler-Bernoulli beam model without axial dof (see Figure 3.12) are given here just to explain the derivation of the structural identification equations. However, the original formulation is obtained for 3 D Euler-Bernoulli beam elements, and this formulation is used in the case studies presented in this thesis.

Two-noded beam element shown in Figure 12 has 4 dofs and its element matrices are given as follows:

$$[\bar{k}_e^l] = \frac{EI}{L^3}\begin{bmatrix} 12 & 6L & -12 & 6L \\ 6L & 4L^2 & -6L & 2L^2 \\ -12 & -6L & 12 & -6L \\ 6L & 2L^2 & -6L & 4L^2 \end{bmatrix} \tag{3.38}$$

$$\left[\overline{m}_e^l\right] = \frac{\rho AL}{420}\begin{bmatrix} 156 & 22L & 54 & -13L \\ 22L & 4L^2 & 13L & -3L^2 \\ 54 & 13L & 156 & -22L \\ -13L & -3L^2 & -22L & 4L^2 \end{bmatrix} \tag{3.39}$$

On the other hand $\left\{\overline{\phi}_e^{rl}\right\}$ vector given in equations (3.36) and (3.37) is given below:

$$\left\{\overline{\phi}_e^{rl}\right\} = \left\{v_1 \;\; \theta_1 \;\; v_2 \;\; \theta_2\right\}^T \tag{3.40}$$

where v and θ represent the translational and rotational dofs at the element nodes, respectively.

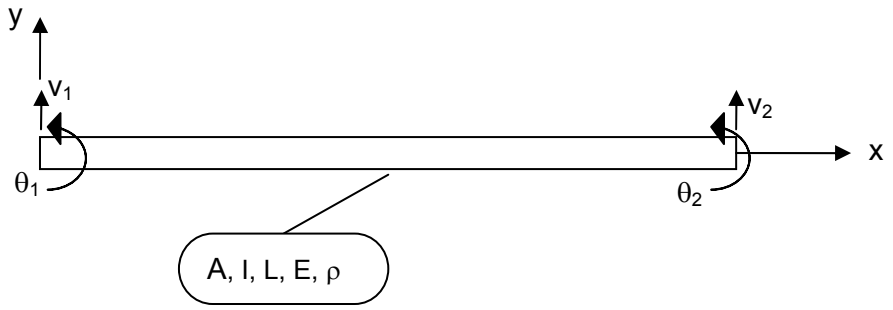

Figure 3.12. 2 D Euler-Bernoulli beam model without the axial dof

Substituting expressions (3.38), (3.39) and (3.40) into equations (2.36) and (2.37) the following equations are obtained:

$$a_1^{rs}(\rho A)_1 + a_2^{rs}(\rho A)_2 + \ldots + a_k^{rs}(\rho A)_k = \delta_{rs} \tag{3.41}$$

$$b_1^{rs}(EI)_1 + b_2^{rs}(EI)_2 + \ldots + b_k^{rs}(EI)_k = \omega_r^2\ \delta_{rs} \tag{3.42}$$

where a_e^{rs} and b_e^{rs} are the coefficients from the mesh properties and the experimental mode shapes.

It can easily be seen that the coefficients a_e^{rs} and b_e^{rs} can be calculated by using the experimental mass normalized modes expanded to the size of the FE model as shown in equation (3.18) and the element matrices given in expressions (3.38) and (3.39).

In case of 3 D Euler-Bernoulli beam elements, equations (3.41) and (3.42) take the following forms:

$$\underbrace{a_1^{rs}(\rho A)_1 + b_1^{rs}(\rho A I_x)_1}_{\text{element 1}} + \underbrace{a_2^{rs}(\rho A)_2 + b_2^{rs}(\rho A I_x)_2}_{\text{element 2}} + \ldots + \underbrace{a_k^{rs}(\rho A)_k + b_k^{rs}(\rho A I_x)_k}_{\text{element k}} = \delta_{rs} \tag{3.43}$$

$$\underbrace{c_1^{rs}(EA)_1 + d_1^{rs}(EI_1)_1 + e_1^{rs}(EI_2)_1 + f_1^{rs}(EI_{12})_1 + g_1^{rs}(GJ_e)_1}_{\text{element 1}} + \underbrace{c_2^{rs}(EA)_2 + \ldots + g_2^{rs}(GJ_e)_2}_{\text{element 2}} +$$

$$\ldots + \underbrace{c_k^{rs}(EA)_k + \ldots + g_k^{rs}(GJ_e)_k}_{\text{element k}} = \omega_r^2\ \delta_{rs} \tag{3.44}$$

Equations (3.43) and (3.44) can be put into the following compact forms:

$$[A_m]\{x_m\} = \{b_m\} \tag{3.45}$$

$$[A_k]\{x_k\} = \{b_k\} \tag{3.46}$$

where $[A_m]$ and $[A_k]$ are the coefficient matrices that consist of a_e^{rs}, b_e^{rs} and $c_e^{rs} \ldots g_e^{rs}$ terms, respectively. $\{x_m\}$ and $\{x_k\}$ are the unknown vectors which consist of the product of the geometric and material properties as illustrated in equations (3.43) and (3.44).

Equations (3.43) and (3.44) are called the 'Structural Identification Equations' within the context of this thesis study.

The number of equations within (3.45) and (3.46) is determined by the number of the experimentally determined normal modes. If N experimental modes have been extracted in the frequency range of interest, $N(N+1)/2$ number of independent equations can be written for each set of equations (3.45) and (3.46).

In case of the complex structures such as a real aircraft structure, the number of equations turns out to be much less than the number of unknowns due to the limited number of experimentally obtained mode shapes in the frequency range of interest. In this case, the number of unknowns can be reduced by grouping similar beam elements with the assumption that elements within the same group have the same geometric and material properties.

Reducing the number of unknowns below the number of equations, initial estimates for the unknown system parameters can 'theoretically' be calculated as follows:

$$\{x_m\} = [A_m]^+ \{b_m\} \tag{3.47}$$

$$\{x_k\} = [A_k]^+ \{b_k\} \tag{3.48}$$

where $[A_m]^+$ and $[A_k]^+$ are the pseudo inverses of $[A_m]$ and $[A_k]$ respectively.

Studies have shown that experimental errors and errors introduced during the expansion of the experimental modes may give rise to ill conditioned coefficient matrices $[A_m]$ and $[A_k]$. Another source of ill conditioning is the order of magnitude difference between the values of unknown parameters. The way of manipulating coefficient matrices to be able to derive relatively accurate initial estimates of the structural parameters will be studied in Chapter 5.

3.6. ITERATIVE SOLUTION PROCEDURE

After determining the initial estimates of the products of geometric and material properties by solving equations (3.45) and (3.46), mesh only FE model of the aircraft structure is completed by using the elastic and inertial estimates obtained. Due to ill conditioned feature of the structural identification equations, eigen solution of the initial FE model will not perfectly correlate with the experimental modes. To improve correlation, the following algorithm is applied:

Step 1:

Solve the eigenvalues and eigenvectors of the initial FE model.

Step 2:

By using the 'Modal Assurance Criterion' (MAC) [24] which gives degree of proportionality between analytical and measured normal modes, extract eigenvectors of the FE model corresponding to the measured mode shapes and reconstruct coefficient matrix of equation (3.46) by using those eigenvectors to reduce ill conditioning.

Step 3:

Solve for $\{x_k\}$ from the reconstructed versions of equations (3.46), by using a non-linear least square solver with lower and upper bounds to avoid the divergence problem.

Step 4:

After obtaining the updated parameters in Step 3, update the FE model stiffness matrix and go to Step 2. Use the previous solutions as initial guess for the non-linear

least square solver. Continue until eigenvalues and eigenvectors converge to their experimental counterparts.

The stiffness orthogonality equations of the initial FE model are not perfectly satisfied with the initial FE parameters because the right hand side vector consists of the experimental natural frequencies. This makes it possible to use an iterative algorithm. But in case of the mass orthogonality equations, the right hand side vector consists of zeros and ones. Consequently, mass orthogonality equations derived from the eigenvectors of the initial FE model are perfectly satisfied with the initial FE properties and cannot be subjected to an iterative solution procedure.

This completes the theoretical part of the thesis study. Of course application of the technique suggested herein is not straight forward when it is applied to real complex aircraft structures. The obstacles that arise during the application of the theory to real structures and experiences gained in the way of eliminating those obstacles will be studied in detail in Chapter 5.

CHAPTER 4

IMPLEMENTED SOFTWARE

4.1. INTRODUCTION

The theory introduced in Chapter 3 can be converted to a useful engineering tool by an appropriate software design. Actually, this is the most efficient way of testing and improving the theory by means of various case studies. With this motivation, a detailed code has been developed in MATLAB© (R2007a) which is a very suitable programming tool for preliminary software design. One of the reasons of choosing MATLAB is that it provides lots of built in functions that implement various mathematical tools. Least square equation solver, matrix inversion function, eigenvalue problem solver etc. are several examples of MATLAB's functions that have been used to develop the computer code of this thesis work. Another reason of using MATLAB is that it provides a variety of graphical post processing tools for the visualization of the software outputs.

The computer algorithm is summarized below:

1. Read experimental mode shapes from an input file.
2. Read the FE mesh information of the relevant aircraft structure from another input file.
3. Construct an arbitrary stiffness matrix by assigning arbitrary geometric and material properties to the empty FE mesh.
4. Expand the experimental normal modes to the size of the FE model by using the arbitrary stiffness matrix in Guyan's Expansion.

5. Combine the expanded experimental modes together with the experimental natural frequencies and element group information to construct the structural identification equations.

6. Determine the initial estimates of the geometric and material properties from the structural identification equations.

7. Obtain an initial FE model by assigning initial estimates of the structural properties to the finite elements.

8. Compare the experimental mode shapes with their FE counterparts by using 'Modal Assurance Criterion' (MAC) [24]. Compare also experimental natural frequencies with the corresponding eigenvalues of the FE model.

9. If the correlation is not good enough, reconstruct the stiffness orthogonality equations by using FE counterparts of the experimental mode shapes.

10. Determine the updated FE parameters from the solution of the updated equations.

11. Update the FE model and compare the measured and analytical modes once again. If the correlation is sufficient stop the analysis. Otherwise return to step 9.

The subsequent sections of this chapter are dedicated to the detailed explanations of the input files and important subroutines of the implemented software.

4.2. INPUT FILES

The software developed within the scope of this thesis work makes use of 3 fundamental input files. The function of each input file is explained below in detail:

- **fem_input_unit_***structure_name***.txt** : One of the main purposes of this input file is to supply the FE mesh information to the software. The other purpose is to provide 'arbitrary' geometric and material properties to the Euler-Bernoulli beam elements of the FE mesh. Consequently, it becomes possible to construct an arbitrary stiffness matrix that shall be used in the Guyan's Expansion of the experimental normal modes as previously explained in section 3.4 of Chapter 3.

  In case studies of this thesis work, arbitrary geometric properties are generated by assuming that each beam element of the FE mesh has a square cross

section of unit area. The term ‘unit’ that appears in the name of the input file stands for the ‘unit area’. Of course, some other users may come up with a much better definition to generate arbitrary FE properties.

In the first case study of Chapter 5, a scaled aircraft model designed and used by GARTEUR (Group for Aeronautical Research and Technology in Europe) is investigated in details. For this case study, the input file explained above takes the following name: ‘**fem_input_unit_garteur.txt’**. A portion of that input file is illustrated in Figure 4.1.

- **freqs_n_groups_***structure_name***.txt** : This input file supplies the numerical values of the experimental natural frequencies and the number of experimental mode shapes that will be used in the derivation of the structural identification equations. Moreover, it indicates which beam element belongs to which ‘element group’.

  Element group concept is based on the assumption that elements within the same group have the same geometric and material properties. If FE properties of each element are assumed to be different from the properties of other finite elements, the number of unknowns within the structural identification equations (3.43) and (3.44) may exceed the number of equations. On the other hand, assuming that elements within a neighborhood have identical FE properties helps to reduce the number of unknowns below the number of equations and this makes it possible to obtain a unique solution from the structural identification equations.

  A portion of the input file used in the first case study of Chapter 5 is shown in Figure 4.2.

- **real_test_modes_***structure_name***.txt** : This input file simply consists of the mass normalized experimental mode shapes.

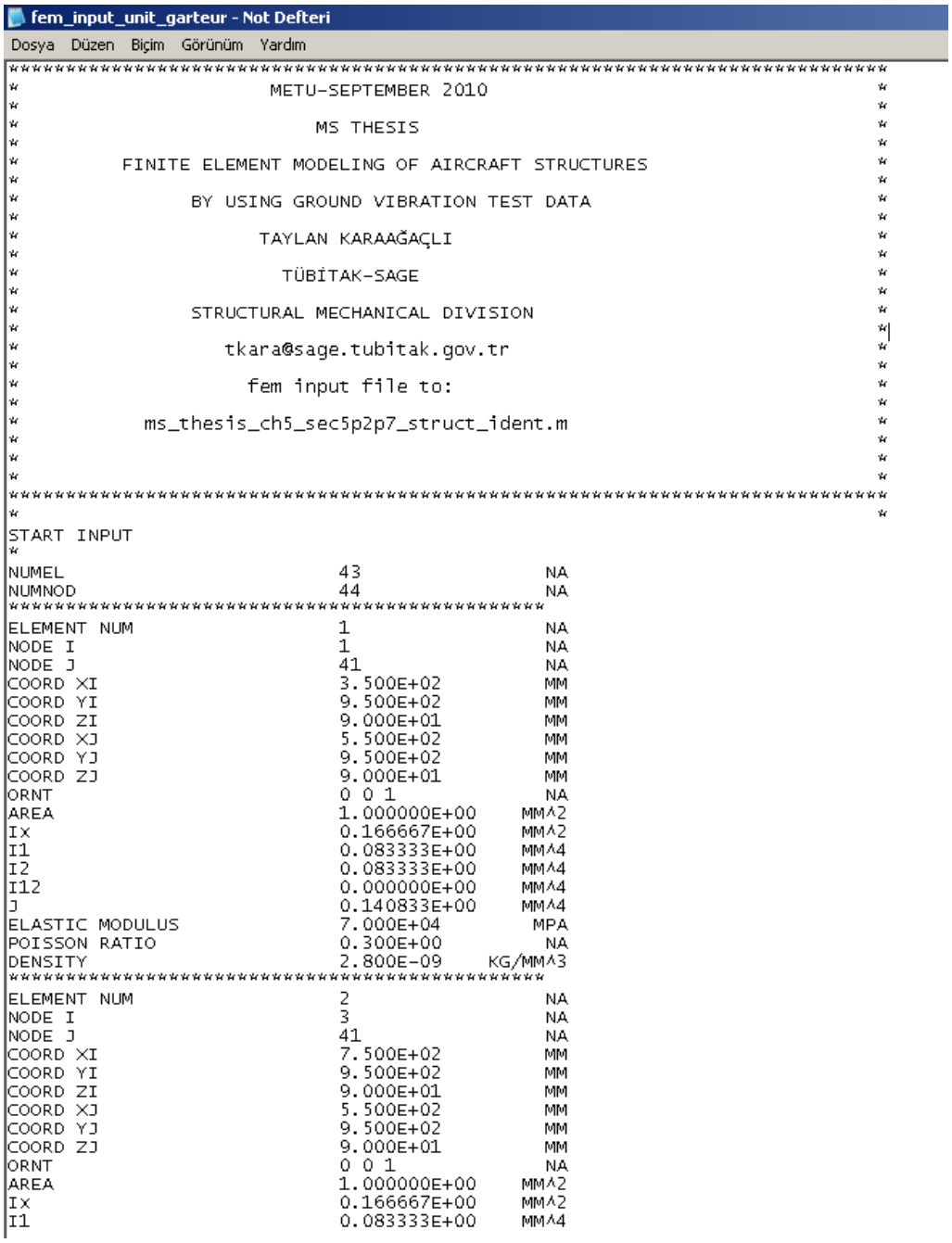

fem_input_unit_garteur - Not Defteri

Dosya Düzen Biçim Görünüm Yardım

```
**************************************************************************************
*                        METU-SEPTEMBER 2010                                         *
*                                                                                    *
*                             MS THESIS                                              *
*                                                                                    *
*          FINITE ELEMENT MODELING OF AIRCRAFT STRUCTURES                            *
*                                                                                    *
*                BY USING GROUND VIBRATION TEST DATA                                 *
*                                                                                    *
*                      TAYLAN KARAAĞAÇLI                                             *
*                                                                                    *
*                       TÜBİTAK-SAGE                                                 *
*                                                                                    *
*                STRUCTURAL MECHANICAL DIVISION                                      *
*                                                                                    *
*                   tkara@sage.tubitak.gov.tr                                        *
*                                                                                    *
*                     fem input file to:                                             *
*                                                                                    *
*           ms_thesis_ch5_sec5p2p7_struct_ident.m                                    *
*                                                                                    *
*                                                                                    *
*                                                                                    *
**************************************************************************************
*                                                                                    *
START INPUT
*
NUMEL                          43                NA
NUMNOD                         44                NA
*****************************************************
ELEMENT NUM                    1                 NA
NODE I                         1                 NA
NODE J                         41                NA
COORD XI                       3.500E+02         MM
COORD YI                       9.500E+02         MM
COORD ZI                       9.000E+01         MM
COORD XJ                       5.500E+02         MM
COORD YJ                       9.500E+02         MM
COORD ZJ                       9.000E+01         MM
ORNT                           0 0 1             NA
AREA                           1.000000E+00    MM^2
Ix                             0.166667E+00    MM^2
I1                             0.083333E+00    MM^4
I2                             0.083333E+00    MM^4
I12                            0.000000E+00    MM^4
J                              0.140833E+00    MM^4
ELASTIC MODULUS                7.000E+04         MPA
POISSON RATIO                  0.300E+00         NA
DENSITY                        2.800E-09    KG/MM^3
*****************************************************
ELEMENT NUM                    2                 NA
NODE I                         3                 NA
NODE J                         41                NA
COORD XI                       7.500E+02         MM
COORD YI                       9.500E+02         MM
COORD ZI                       9.000E+01         MM
COORD XJ                       5.500E+02         MM
COORD YJ                       9.500E+02         MM
COORD ZJ                       9.000E+01         MM
ORNT                           0 0 1             NA
AREA                           1.000000E+00    MM^2
Ix                             0.166667E+00    MM^2
I1                             0.083333E+00    MM^4
```

Figure 4.1. fem_input_unit_garteur.txt input file used in the structural identification of the GARTEUR structure

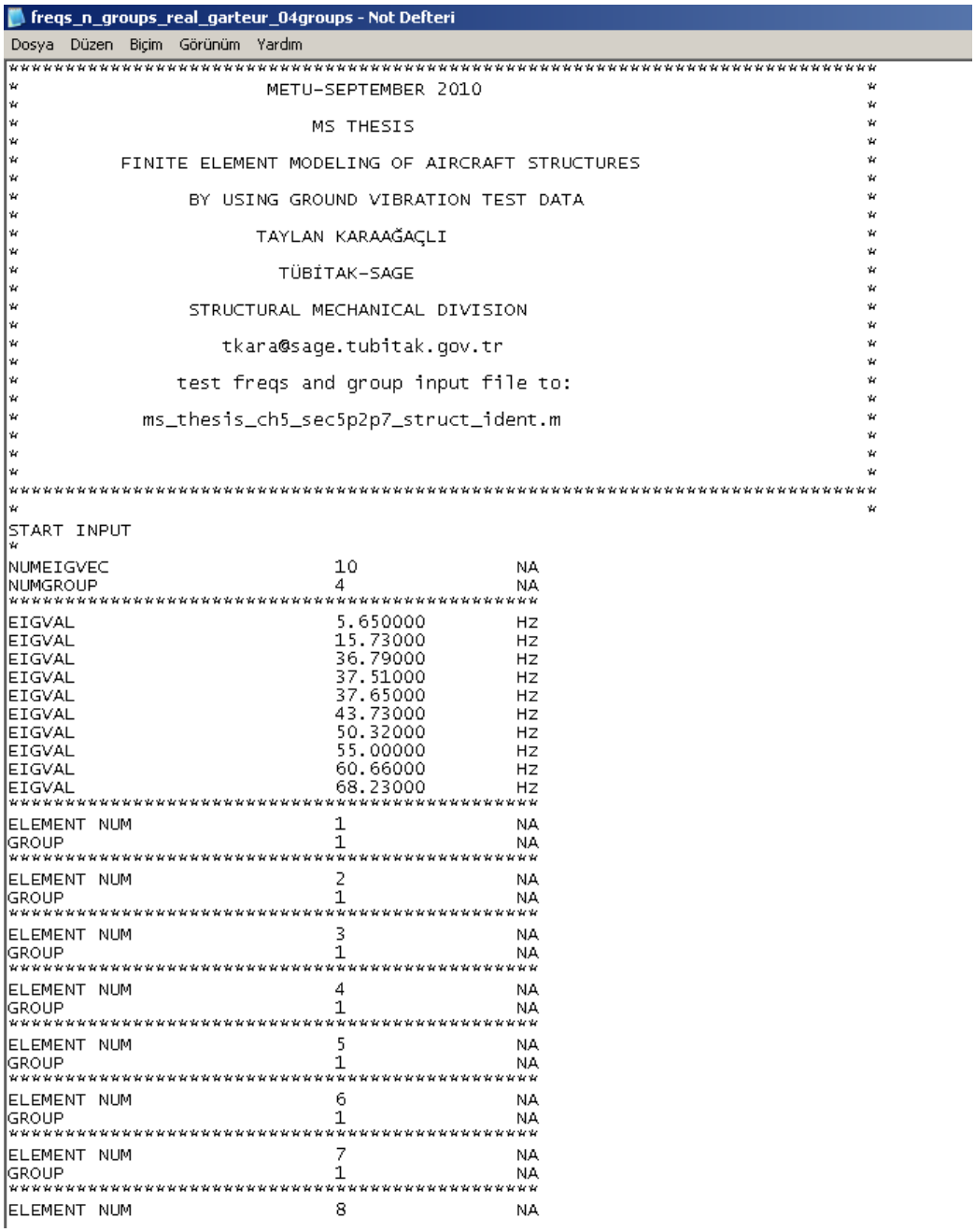

freqs_n_groups_real_garteur_04groups - Not Defteri

Dosya Düzen Biçim Görünüm Yardım

```
*****************************************************************************************
*                        METU-SEPTEMBER 2010                                            *
*                                                                                       *
*                            MS THESIS                                                  *
*                                                                                       *
*          FINITE ELEMENT MODELING OF AIRCRAFT STRUCTURES                               *
*                                                                                       *
*                BY USING GROUND VIBRATION TEST DATA                                    *
*                                                                                       *
*                      TAYLAN KARAAĞAÇLI                                                *
*                                                                                       *
*                        TÜBİTAK-SAGE                                                   *
*                                                                                       *
*                STRUCTURAL MECHANICAL DIVISION                                         *
*                                                                                       *
*                   tkara@sage.tubitak.gov.tr                                           *
*                                                                                       *
*               test freqs and group input file to:                                     *
*                                                                                       *
*           ms_thesis_ch5_sec5p2p7_struct_ident.m                                       *
*                                                                                       *
*                                                                                       *
*                                                                                       *
*****************************************************************************************
*                                                                                       *
START INPUT
*
NUMEIGVEC                      10              NA
NUMGROUP                       4               NA
*****************************************************
EIGVAL                         5.650000        Hz
EIGVAL                         15.73000        Hz
EIGVAL                         36.79000        Hz
EIGVAL                         37.51000        Hz
EIGVAL                         37.65000        Hz
EIGVAL                         43.73000        Hz
EIGVAL                         50.32000        Hz
EIGVAL                         55.00000        Hz
EIGVAL                         60.66000        Hz
EIGVAL                         68.23000        Hz
*****************************************************
ELEMENT NUM                    1               NA
GROUP                          1               NA
*****************************************************
ELEMENT NUM                    2               NA
GROUP                          1               NA
*****************************************************
ELEMENT NUM                    3               NA
GROUP                          1               NA
*****************************************************
ELEMENT NUM                    4               NA
GROUP                          1               NA
*****************************************************
ELEMENT NUM                    5               NA
GROUP                          1               NA
*****************************************************
ELEMENT NUM                    6               NA
GROUP                          1               NA
*****************************************************
ELEMENT NUM                    7               NA
GROUP                          1               NA
*****************************************************
ELEMENT NUM                    8               NA
```

Figure 4. 2. freqs_n_groups_real_garteur_04groups.txt input file used in the structural identification of the GARTEUR structure

4.3. FLOW CHART OF THE SOFTWARE DEVELOPED

The flowchart of the software developed is shown in Figure 4.3. The function of each subroutine appearing in the flowchart is explained below:

- **test_modes_read.m** - This is a preprocessor subroutine that reads experimental mode shapes from an input file in .txt format.
- **test_freq_n_group_read.m -** This is another preprocessor subroutine that reads and stores experimental natural frequencies and group information of each element from an input file in .txt format.
- **fem_prop_read.m** - This subroutine reads all necessary information (geometric, material etc…) to create global mass and stiffness matrices of an FE model.
- **fem.m** - This subroutine determines the global mass and stiffness matrix as well as the eigenvalues and eigenvectors of an FE model.
- **expand.m** - This subroutine is used to expand experimental normal modes to the size of the FE model of the relevant structure.
- **struct_ident_eqns_gen.m -** The main purpose of this subroutine is to generate structural identification equations by using the experimental normal modes (or the FE counterparts of the experimental modes) expanded to the size of the FE model and the experimental natural frequencies.
- **model_update.m -** This subroutine runs an iterative algorithm until the updated FE model correlates well with the experimental data. The flow chart of this subroutine is illustrated in Figure 4.4.

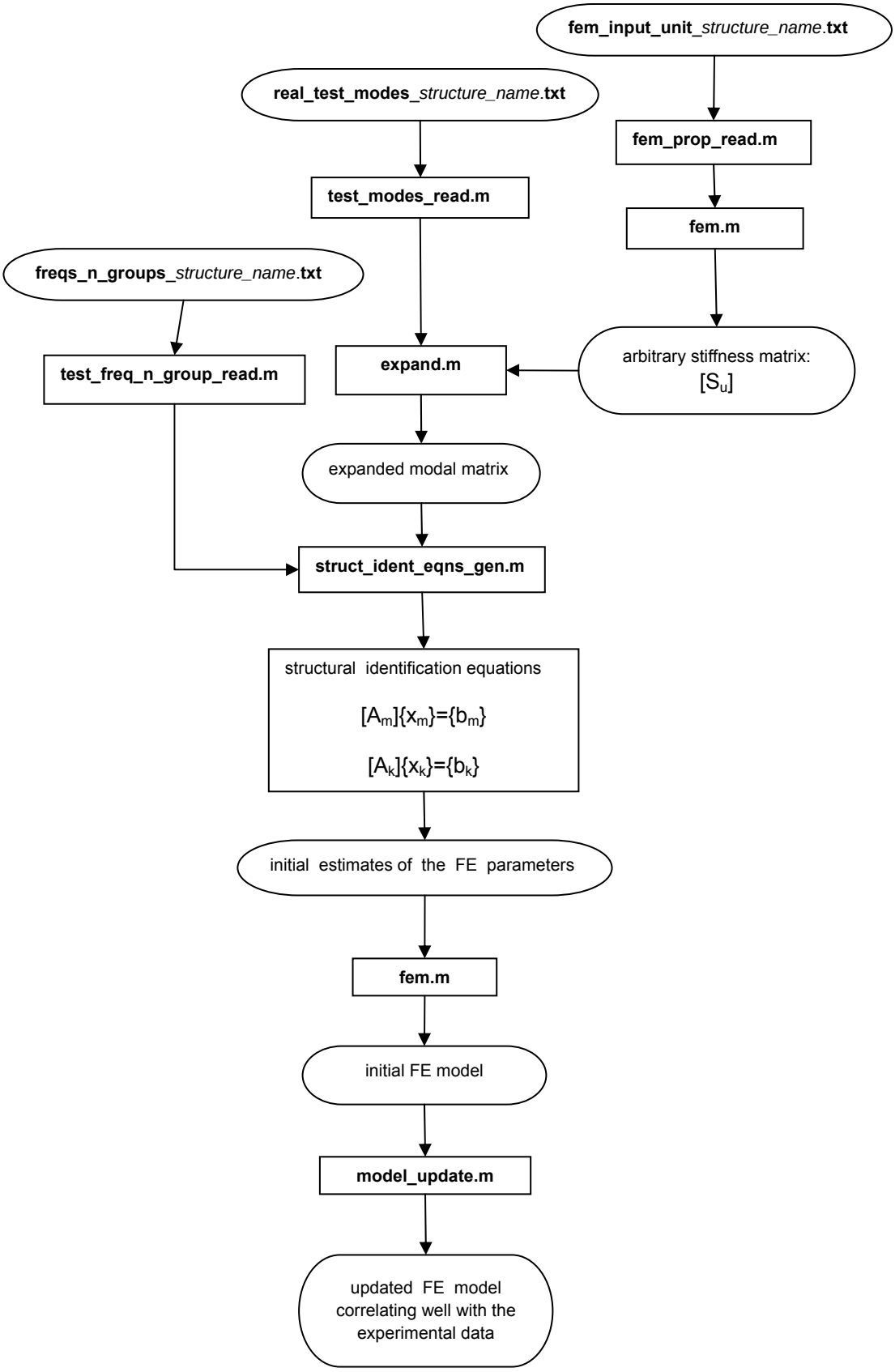

Figure 4.3. Flow chart of the software developed

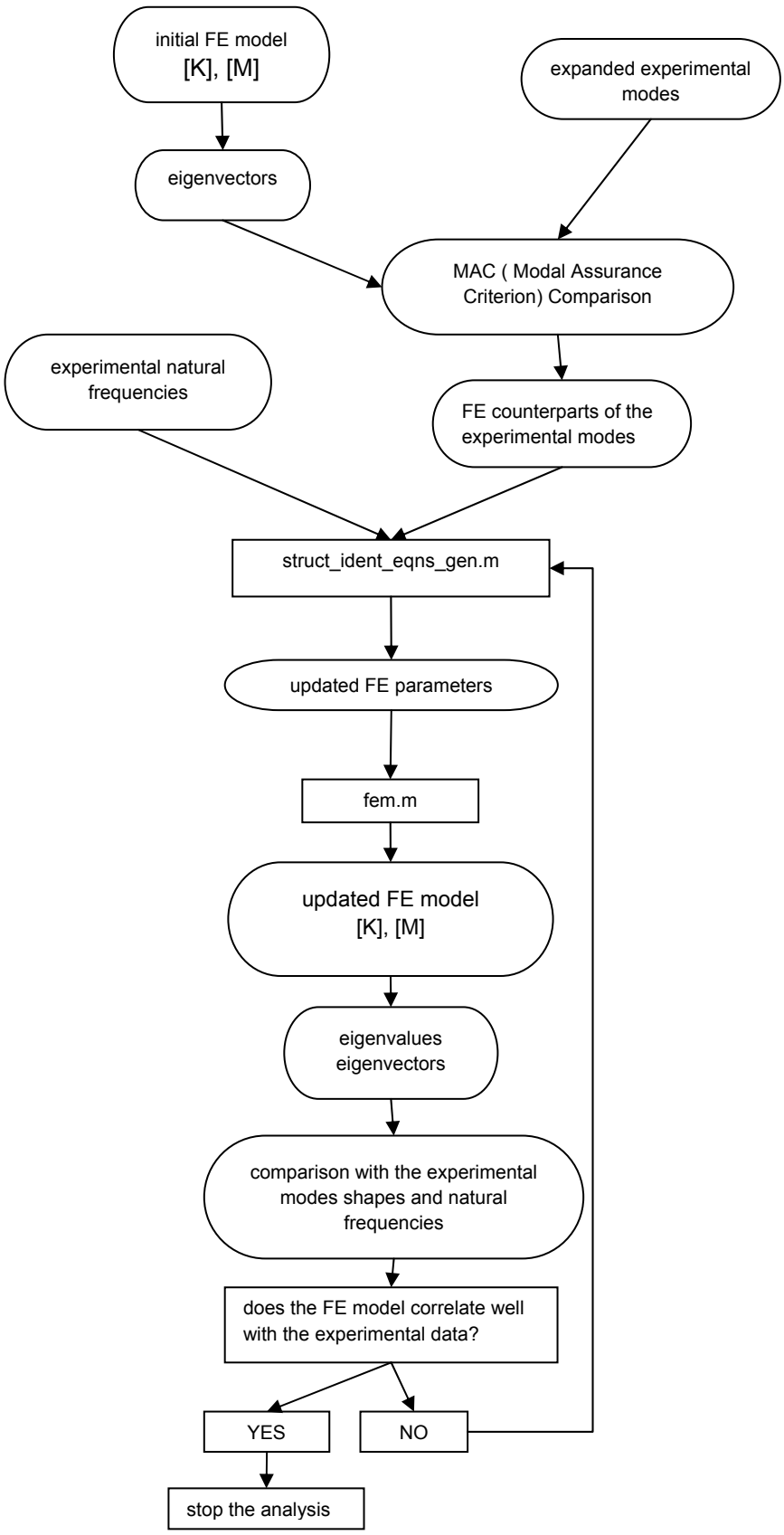

Figure 4.4. Flow chart of the model_update.m subroutine

CHAPTER 5

CASE STUDIES

5.1. INTRODUCTION

The theory developed herein has been applied to the experimental data used in Kozak's thesis study [17], in order to show the structural identification and model updating skills obtained by the method developed in this thesis.

In this chapter, the theory introduced in Chapter 3 is challenged by the following two case studies:

In the first case study, the method is applied to a scaled aircraft model designed and used by GARTEUR (Group for Aeronautical Research and Technology in Europe). The case study starts with the definition of the 'ideal GARTEUR structure'. This ideal structure is simply the FE model of the GARTEUR's scaled aircraft constructed by Euler-Bernoulli beam elements. The first 10 elastic modes of this ideal structure are treated as the experimental mode shapes extracted from a fictitious ideal modal test (simulated experiment) and they are free from any experimental error. This way, first of all, the effect of the modal truncation on the method developed in this study is investigated in detail. Then the modal data is further truncated in terms of the rotational dofs and some of the translational dofs. As a result, the combined effects of the modal truncation and the lack of measurement capabilities on the applicability of the method are discussed in detail. Finally, the method is applied to the real experimental data of the GARTEUR structure.

In the second case study, under the light of the experiences obtained from the case study of the GARTEUR structure, the method is applied to derive the FE model of a real aircraft structure from its experimental data.

5.2. SCALED AIRCRAFT MODEL

5.2.1. Description of the Experimental Setup

The outline of the experimental setup is summarized below, yet the reader is referred to Kozak [17] for more detailed information about the modal test and analysis procedures.

The test structure studied herein is the duplicate in dimensions of the 'SM-AG 19 Test-Bed' designed by GARTEUR. But there are some differences between the structure manufactured at TÜBİTAK-SAGE and the original test bed: Firstly, in the TÜBİTAK-SAGE's version of the test bed, the wing-fuselage, fuselage-vertical stabilizer, vertical-stabilizer and horizontal-stabilizer are joined by welding although bolted joints are used in the original structure. Secondly, the viscoleastic tape covering the surface of the wing in the original test bed does not appear in the TÜBİTAK-SAGE's test structure.

The test bed manufactured by TÜBİTAK-SAGE is shown in Figure 5.1. The dimensions of the test bed are also illustrated in Figure 5.2.

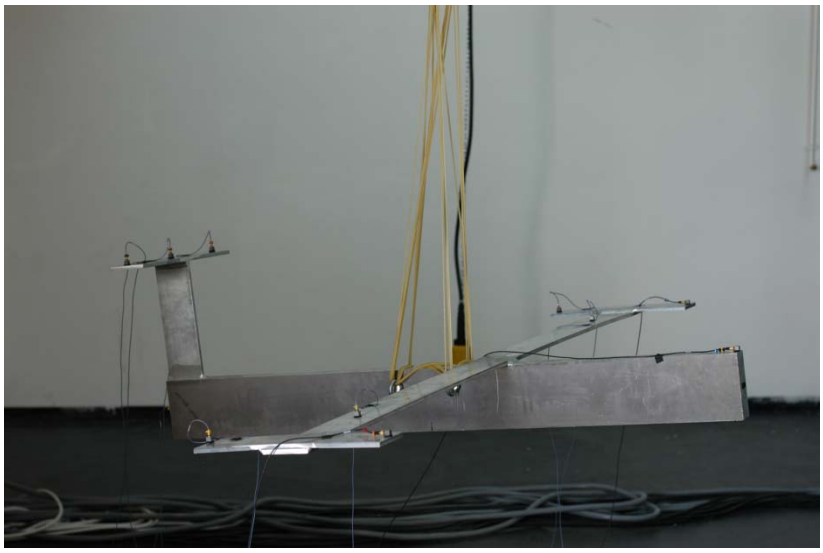

Figure 5.1. Scaled aircraft model tested at TÜBİTAK-SAGE

The GARTEUR test structure has been hanged with elastic cords to simulate free-free boundary conditions. Its modal test has been carried out by using piezoelectric type accelerometers (see Figure 5.1) and a modal impact hammer. A total of 12

accelerometers, 36 impact points and 66 measurement dofs have been used throughout the tests [17]. The excitation and measurement points as well as the global coordinate system are shown in Figure 5.3.

Data acquisition details of the modal test are given in Table 5.1.

In order to extract the experimental normal modes and natural frequencies, POLYMAX modal analysis software of LMS has been used. As a result, the first 10 mass normalized elastic mode shapes with 66 measurement dofs and corresponding 10 natural frequencies have been obtained from the modal analysis software. This is the experimental data to which the method developed in Chapter 3 will be applied in the subsequent sections in order to derive the FE model of the GARTEUR test structure.

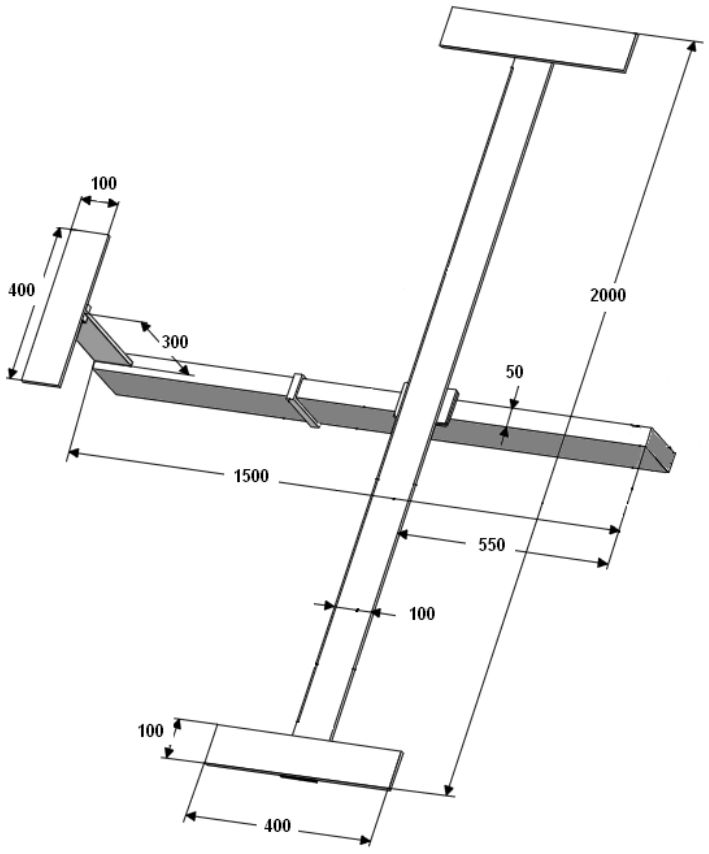

Figure 5.2. The dimensions of the SM-AG 19 test bed (all dimensions are in mm)

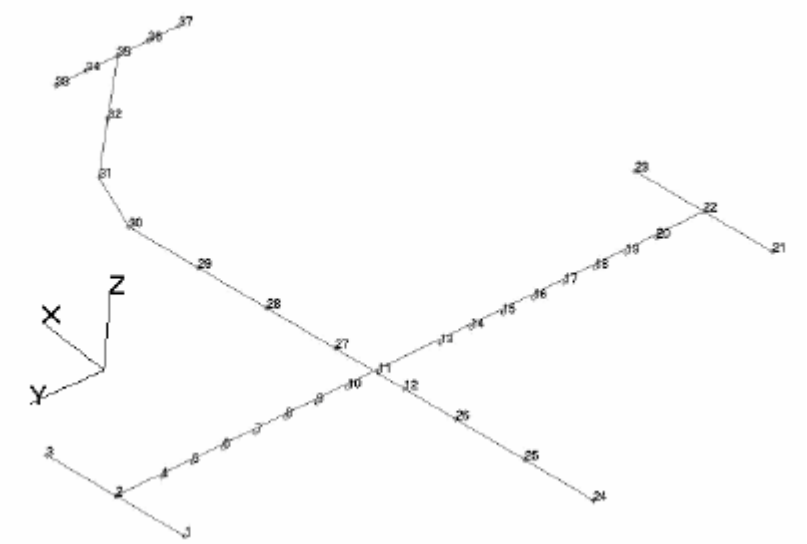

Figure 5.3. Measurement and excitation points of the SM-AG 19 test bed

Table 5.1. Data acquisition details of the modal test carried the for SM-AG 19 test bed

Data Acquisition Frontend	LMS SCADAS III
Max. Capacity of the Accelerometers (g)	50
Max. Capacity of the Modal Hammer (N)	240
Accelerometer Saturation Potential (V)	5
Modal Hammer Saturation Potential (V)	2
Windowing Type	Force-Exponential
Frequency Resolution (Hz)	1/1024
Data Acquisition Time per Hit (s)	10.24
Number of Samples per Degree of Freedom	5
Modal Analysis Software	LMS POLYMAX

5.2.2. Definition of the Ideal GARTEUR Structure

The ideal GARTEUR structure is a hypothetical test structure used to study different aspects of the structural identification method developed in this thesis work. This ideal structure is basically an FE model constructed by connecting the measurement points of the SM-AG 19 test bed, introduced in the previous section, with Euler-Bernoulli beam elements. It consists of 43 beam elements, 44 nodes and 264 dofs. Its FE mesh is illustrated in Figure 5.4.

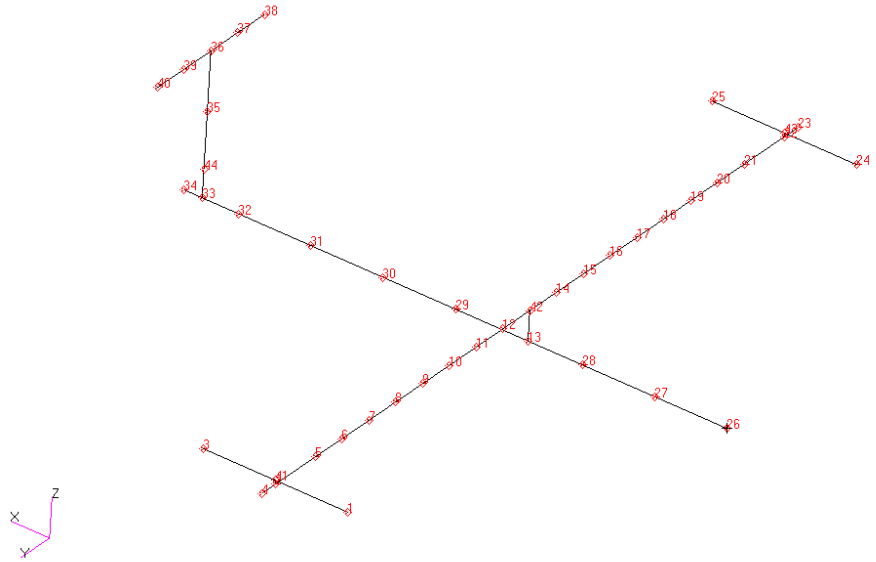

Figure 5.4. FE mesh of the ideal GARTEUR structure

The geometric properties of the FE model are calculated from the dimensions of the real SM-AG 19 test bed shown in Figure 5.2 and they are tabulated in Table 5.2.

The material properties are given in Table 5.3.

The first 10 elastic modes of the ideal GARTEUR structure are treated as the '*experimental data'* obtained from a '*fictitious*' modal test free from any experimental error. These simulated-experimental mode shapes include also the rotational dofs although in a real modal test, only some of the translational dofs can be measured. It is assumed that the 10 simulated-experimental mode shapes mentioned above and corresponding natural frequencies are the only experimental information

available to obtain the FE model of the ideal GARTEUR structure. Using the mass and stiffness orthogonality of that truncated modal data, it is possible to derive the structural identification equations to determine initial estimates of the geometric and material properties of the FE model.

Table 5.2. Geometric properties of the ideal GARTEUR structure

SUBSTRUCTURE	GEOMETRIC PROPERTIES					
	A (mm^2)	I_x (mm^2)	I_1 (mm^4)	I_2 (mm^4)	I_{12} (mm^4)	J_e (mm^4)
WING	1.00E+03	8.42E+02	8.33E+03	8.33E+05	0.00E+00	3.12E+04
FUSELAGE	7.50E+03	2.08E+03	1.41E+07	1.56E+06	0.00E+00	4.94E+06
VERTICAL STABILIZER	1.00E+03	8.42E+02	8.33E+03	8.33E+05	0.00E+00	3.12E+04
HORIZONTAL STABILIZER	1.00E+03	8.42E+02	8.33E+03	8.33E+05	0.00E+00	3.12E+04

Table 5.3. Material properties of the ideal GARTEUR structure

MATERIAL PROPERTIES*		
E (MPa)	ρ (ton/mm^3)	ν
7.0E+04	2.8E-09	0.3

The reason of starting the case study with such a simulated test data instead of a real test data can be explained as follows: Manipulating an ideal test data to make it look like a real test data in a step by step fashion offers the opportunity of developing a deeper understanding of the relative effects of the truncation and experimental errors on the structural identification equations. For example, studying

* In FE analysis, lengths are usually expressed in mm. As a result, in order to obtain eigenvalues in rad/s and eigenvectors in appropriate units, material properties have to be expressed in units other than SI units.

the sole effect of modal truncation reveals important features of the structural identification equations that are impossible to determine when the experimental error is introduced. This makes it possible to take precautions against experimental error by reformulating coefficient matrices of the equations. As a result, a more robust technique is obtained. This will be illustrated in detail in the subsequent sections.

5.2.3. Investigation of the Structural Identification Equations Derived from the Simulated-Experimental Data of the Ideal GARTEUR Structure

According to a simulated modal test scenario, it is assumed that the first 10 elastic modes of the ideal GARTEUR structure with 264 'measurement' dofs including 'rotational' dofs is the only experimental data to determine the FE model of that structure. It is also assumed that the determination of the geometric and material properties of the different components such as the wing, the vertical stabilizer etc. from the blueprints requires enormous time and effort as in the case of the real aircraft structures and it has to be avoided. This makes it impossible to obtain an initial FE model required by a standard model updating procedure. As a result, all these circumstances constitute an appropriate basis to make use of the method developed in Chapter 3 to derive an accurate FE model of the ideal GARTEUR structure correlating well with the experimental data.

Following the theory introduced in Chapter 3, first of all, an empty FE mesh is constructed by connecting the measurement points of the ideal GARTEUR structure as shown in Figure 5.4. The FE mesh consists of 43 beam elements, 44 nodes and 264 dofs. Each element having 7 unknown parameters in terms of the product of the geometric and material properties such as $\rho A, \rho AI_x, EI_1$ etc., 43 elements will introduce 301 unknowns to be determined in order to obtain the complete mass and stiffness matrices of the FE model. Unfortunately, using only the first 10 elastic modes of the ideal GARTEUR structure, it is possible to determine 10(11)/2 = 55 structural identification equations from the stiffness orthogonality and another 55 equations from the mass orthogonality. To be able to solve the problem, the number of unknown terms must be reduced below the total number of equations. This is accomplished by grouping similar elements together with the assumption that elements within the same group have the same geometric and material properties. For this initial case study, only 4 element groups shall be used as shown in Table

5.4. Consequently, the number of unknowns shall be reduced to 28 and the structural identifications equations (3.43) and (3.44) shall be transformed into the following forms:

$$\underbrace{a_1^{rs}(\rho A)_1 + b_1^{rs}(\rho AI_x)_1}_{\text{group 1}} + \underbrace{a_2^{rs}(\rho A)_2 + b_2^{rs}(\rho AI_x)_2}_{\text{group 2}} + \ldots + \underbrace{a_4^{rs}(\rho A)_4 + b_4^{rs}(\rho AI_x)_4}_{\text{group 4}} = \delta_{rs} \quad (5.1)$$

$$\underbrace{c_1^{rs}(EA)_1 + d_1^{rs}(EI_1)_1 + e_1^{rs}(EI_2)_1 + f_1^{rs}(EI_{12})_1 + g_1^{rs}(GJ_e)_1}_{\text{group 1}} + \underbrace{c_2^{rs}(EA)_2 + \ldots + g_2^{rs}(GJ_e)_2}_{\text{group 2}} +$$

$$\ldots + \underbrace{c_4^{rs}(EA)_4 + \ldots + g_4^{rs}(GJ_e)_4}_{\text{group 4}} = \omega_r^2 \, \delta_{rs} \quad (5.2)$$

Table 5.4. Element groups of the ideal GARTEUR structure

GROUP NO	STRUCTURAL COMPONENT
1	WING
2	FUSELAGE
3	VERTICAL STABILIZER
4	HORIZONTAL STABILIZER

It must be noticed that even if the assumption of the identical element properties may be tolerable for this relatively simple GARTEUR problem, it may cause convergence problems of the FE model of a real aircraft structure. This will be studied later in this Chapter.

The stiffness orthogonality equations are naturally decoupled from the mass orthogonality equations and they must be solved separately. As seen in equation (5.1), the mass orthogonality equations possess the following two unknowns per element group: ρA and ρAI_x. Similarly, the stiffness orthogonality equations given

in (5.2) possess the following 5 unknowns per element group: EI_1, EI_2, EI_{12}, GJ_e and EA.

45 out of 55 stiffness orthogonality equations are obtained from the 'cross orthogonality' of the 10 elastic modes of the ideal GARTEUR structure as shown in equation (5.3). The remaining 10 equations are obtained from the 'self orthogonality' of the individual normal modes (see equation 5.4). The same thing is valid also for the mass orthogonality equations.

$$\underbrace{c_1^{rs}(EA)_1 + d_1^{rs}(EI_1)_1 + e_1^{rs}(EI_2)_1 + f_1^{rs}(EI_{12})_1 + g_1^{rs}(GJ_e)_1}_{\text{group 1}} + \underbrace{c_2^{rs}(EA)_2 + \ldots + g_2^{rs}(GJ_e)_2}_{\text{group 2}} +$$

$$\ldots + \underbrace{c_4^{rs}(EA)_4 + \ldots + g_4^{rs}(GJ_e)_4}_{\text{group 4}} = 0 \qquad (r \neq s) \tag{5.3}$$

$$\underbrace{c_1^{rs}(EA)_1 + d_1^{rs}(EI_1)_1 + e_1^{rs}(EI_2)_1 + f_1^{rs}(EI_{12})_1 + g_1^{rs}(GJ_e)_1}_{\text{group 1}} + \underbrace{c_2^{rs}(EA)_2 + \ldots + g_2^{rs}(GJ_e)_2}_{\text{group 2}} +$$

$$\ldots + \underbrace{c_4^{rs}(EA)_4 + \ldots + g_4^{rs}(GJ_e)_4}_{\text{group 4}} = \omega_r^2 \qquad (r = s) \tag{5.4}$$

From a detailed investigation of the 'cross' and 'self' orthogonality equations, several important conclusions are obtained as follows:

A linear least square solution of 45 'cross orthogonality' equations out of 55 stiffness orthogonality equations for 4 x 5 = 20 unknown parameters gives the 'trivial' (zero) solution. The same thing is valid also for the mass orthogonality equations. So, it is deduced that only the 'cross orthogonality' equations are not sufficient to determine the geometric and material properties of the ideal GARTEUR structure.

If the cross orthogonality equations given in (5.3) are accompanied by anyone of the 10 self orthogonality equations given in (5.4), the products of the structural parameters are 'exactly' determined. Exact solutions are special only to the case study of the ideal GARTEUR structure for the following reasons:

- Elements within the same group given in Table 5.4 have exactly the same geometric and material properties. This will never happen in case of a real aircraft structure.

- Structural identification equations have been derived directly from the eigen solution of the ideal GARTEUR structure. The eigen solution is free from any experimental error and the eigenvectors are not truncated in terms of the rotational dofs. In a real problem, experimental error and the truncated nature of the experimental normal modes will degrade the structural identification equations. All these problems will be studied in this Chapter.

Obviously, the self orthogonality equations play the key role in the solution of the FE parameters of the ideal GARTEUR structure and they will be investigated in a more detailed way below:

The coefficient matrix of the 10 self orthogonality equations related with the stiffness orthogonality of the ideal GARTEUR structure is shown in Tables 5.5 and 5.6. The most prominent feature of the coefficient matrix is that coefficients of certain structural parameters are extremely large and coefficients of some other parameters are extremely small. The physical interpretation of this phenomenon is based on the two useful definitions: 'active' and 'passive' parameters as explained below:

Self orthogonality equations related to the stiffness orthogonality are derived from the following relations:

$$\{\phi^r\}^T [K] \{\phi^r\} = \omega_r^2 \qquad r = 1\ldots10 \tag{5.5}$$

This expression is very similar to the general potential energy expression written for discrete systems as below:

$$PE = \frac{1}{2}\{q\}^T [K]\{q\} \tag{5.6}$$

where $\{q\}$ are the generalized coordinates of the relevant structure.

Comparing equations (5.5) and (5.6), it is deduced that $\{\phi^r\}^T [K] \{\phi^r\}$ term derived from the r^{th} mode of the ideal GARTEUR structure is proportional to its r^{th} modal strain energy. Accordingly, coefficients of the self orthogonality equations given in

(5.4) show the degree of contribution of a structural parameter to the strain energy of the relevant mode of vibration.

Table 5.5. Columns 1 to 10 of the coefficient matrix* of the self orthogonality equations derived from the stiffness orthogonality of the ideal GARTEUR structure

EQUATION NO	WING					FUSELAGE				
	c_1^{rs}	d_1^{rs}	e_1^{rs}	f_1^{rs}	g_1^{rs}	c_2^{rs}	d_2^{rs}	e_2^{rs}	f_2^{rs}	g_2^{rs}
1	0	21335	0	3	0	0	0	0	0	0
2	11	142098	2	-775	1	0	0	2	0	3
3	237	294062	290	9069	69450	0	0	179	0	30
4	2	28110	48	-111	237450	1	0	7	0	0
5	58	163123	10	935	166639	0	0	18	0	9
6	41	1262941	1	-432	182	16	0	0	0	0
7	1222	101001	6338	-7641	3803	0	0	2668	0	262
8	408	1760	20169	610	2803	358	1	8	0	0
9	10288	1489382	285	-3677	48	0	0	112	0	18
10	9	452	245	-86	12	0	0	156	0	18

Table 5.6. Columns 10 to 20 of the coefficient matrix of the self orthogonality equations derived from the stiffness orthogonality of the ideal GARTEUR structure

EQUATION NO	VERTICAL STABILIZER					HORIZONTAL STABILIZER				
	c_3^{rs}	d_3^{rs}	e_3^{rs}	f_3^{rs}	g_3^{rs}	c_4^{rs}	d_4^{rs}	e_4^{rs}	f_4^{rs}	g_4^{rs}
1	0	0	0	0	0	0	0	0	0	0
2	0	24932	0	0	0	3	66	0	0	0
3	0	265363	0	0	14	22	2005	0	0	0
4	1	0	0	0	0	0	6	0	0	0
5	0	132216	0	0	0	11	1153	0	0	0
6	0	0	0	0	0	0	2	0	0	0
7	0	29550	0	0	1674	1	1623	0	0	0
8	2	0	4	0	0	0	12	0	0	0
9	0	917887	0	0	898	17	44327	0	0	0
10	0	1630	0	0	792830	0	193	31	0	0

*Coefficient matrix given in Tables 5.5 and 5.6 has been obtained by scaling up the actual coefficient matrix with 10^7 to clearly compare order of magnitude of coefficients.

To get a better understanding, the coefficients of the first self orthogonality equation illustrated at Tables 5.5 and 5.6 may be observed. The largest coefficient of the first equation belongs to the EI_1 parameter of the FE elements of the wing and the coefficients of all other structural parameters are nearly zero. This indicates that EI_1 is the only 'active' parameter that contributes to the strain energy of the first mode and all other FE parameters remain 'passive'.

Of course, all of the structural parameters do not have the same order of magnitude. For example, EI_1 of the fuselage is 10^3 times larger than EI_1 parameter of the wing. The above interpretation of the structural identification equations can be questioned as follows: The coefficients of the fuselage parameters given in Tables 5.5 and 5.6 may be smaller than the wing parameters, but if those coefficients are multiplied with their corresponding structural parameters, it may be revealed that the fuselage and the wing both contribute an equal amount to the stain energy of the first mode. Actually, this is not true, because if the structural parameters of a component such as the fuselage get larger, the component becomes stiffer and coefficients of those parameters get smaller such that in ***the limit,*** the product of the parameters with their own coefficients become zero. To demonstrate this, all the coefficients given in Tables 5.5 and 5.6 are multiplied with their corresponding structural parameters shown in Table 5.2 and results are illustrated in Tables 5.7 and 5.8.

The most active parameters contributing to the strain energies of the first 10 elastic modes of the ideal GARTEUR structure are determined from Tables 5.5 and 5.6, and the results are shown in Table 5.9.

Observation of the Table 5.9 shows that EI_1, GJ_e parameters of the wing and of the vertical stabilizer are the most important parameters governing the modal strain energies of the ideal GARTEUR structure for the first 10 elastic modes.

Although the coefficients of the passive FE parameters appearing in the self orthogonality equations are nearly zero, when those equations are solved together with the cross orthogonality equations, nearly all of the unknown parameters of the FE model are determined accurately. Unfortunately, good estimates of the passive parameters that do not appear in Table 5.9 are possible only for the ideal GARTEUR structure because the structural identification equations are derived from the pure and complete eigenvectors of the FE model.

Table 5.7. Products of the FE parameters of the wing and fuselage with their coefficients appearing in the self orthogonality equations related to the stiffness orthogonality

EQN NO	WING					FUSELAGE				
	$c_1^{rs}\ EA$	$d_1^{rs}\ EI_1$	$e_1^{rs}\ EI_2$	$f_1^{rs}\ EI_{12}$	$g_1^{rs}\ GJ_e$	$c_2^{rs}\ EA$	$d_2^{rs}\ EI_1$	$e_2^{rs}\ EI_2$	$f_2^{rs}\ EI_{12}$	$g_2^{rs}\ GJ_e$
1	0	1245	0	0	0	0	0	0	0	0
2	0	8289	12	0	0	0	2	24	0	97
3	2	17154	1693	0	15184	0	11	1956	0	1025
4	0	1640	281	0	51914	0	20	76	0	0
5	0	9515	59	0	36433	0	5	200	0	302
6	0	73672	4	0	40	1	38	0	0	0
7	9	5892	36970	0	832	0	1	29182	0	9053
8	3	103	117654	0	613	19	93	86	0	0
9	72	86881	1663	0	10	0	30	1226	0	606
10	0	26	1427	0	3	0	0	1702	0	605

Table 5.8. Products of the FE parameters of the vertical and horizontal stabilizers with their coefficients appearing in the self orthogonality equations related to the stiffness orthogonality

EQN NO	VERTICAL STABILIZER					HORIZONTAL STABILIZER				
	$c_3^{rs}\ EA$	$d_3^{rs}\ EI_1$	$e_3^{rs}\ EI_2$	$f_3^{rs}\ EI_{12}$	$g_3^{rs}\ GJ_e$	$c_4^{rs}\ EA$	$d_4^{rs}\ EI_1$	$e_4^{rs}\ EI_2$	$f_4^{rs}\ EI_{12}$	$g_4^{rs}\ GJ_e$
1	0	0	0	0	0	0	0	0	0	0
2	0	1454	0	0	0	0	4	0	0	0
3	0	15480	0	0	3	0	117	0	0	0
4	0	0	0	0	0	0	0	0	0	0
5	0	7713	0	0	0	0	67	0	0	0
6	0	0	0	0	0	0	0	0	0	0
7	0	1724	0	0	366	0	95	0	0	0
8	0	0	21	0	0	0	1	0	0	0
9	0	53543	0	0	196	0	2586	0	0	0
10	0	95	0	0	173339	0	11	184	0	0

In reality, coefficient matrix will be degraded by the experimental error and the truncated nature of the experimental normal modes. As a matter of fact, coefficients of the passive parameters shall be more error prone than coefficients of the active parameters and no valuable information will be determined for the passive terms of the structural identification equations from the real experimental data. But this is not

a very important problem because the correlation between the FE model and the experimental data of an aircraft structure is highly dependent on the accurate estimates of the active parameters.

Table 5.9. Active parameters of the structural identification equations

MODE NO	ACTIVE PARAMETERS			
	WING	FUSELAGE	VERTICAL STABILIZER	HORIZONTAL STABILIZER
1	EI_1	-	-	-
2	EI_1	-	EI_1	-
3	EI_1, GJ_e	-	EI_1	-
4	EI_1, GJ_e	-	-	-
5	EI_1, GJ_e	-	EI_1	-
6	EI_1	-	-	-
7	EI_1, EI_2, GJ_e	EI_2	EI_1	-
8	EI_2	-	-	-
9	EI_1	-	EI_1	EI_1
10	-	-	GJ_e	-

Since in reality, the coefficient matrix of the cross orthogonality equations are more error sensitive than the coefficient matrix of the self orthogonality equations, it would be useful to be able to extract accurate estimates of the active parameters given in Table 5.9 directly from the self orthogonality equations. Although there are less self orthogonality equations than unknowns, by using the pseudo inverse of the coefficient matrix, it is possible to obtain a unique solution as explained below:

Consider the following linear matrix equation in which the number of equations m is less than the number of unknowns n:

$$[A]_{mxn}\{x\} = \{b\}_{mx1} \tag{5.7}$$

Multiplying both sides of the equation (5.7) by the transpose of the coefficient matrix $[A]$ the following expression is obtained:

$$[A]^T_{nxm}[A]_{mxn}\{x\} = [A]^T_{nxm}\{b\}_{mx1} \tag{5.8}$$

Then taking the inverse of the matrix product at the left hand side of the equation (5.8), a unique solution for the unknown terms $\{x\}$ is obtained as follows:

$$\{x\} = \left([A]^T [A] \right)^{-1} [A]^T \{b\}_{mx1} \tag{5.9}$$

The pseudo inverse of the coefficient matrix $[A]$ is then defined as:

$$[A]^+ = \left([A]^T [A] \right)^{-1} [A]^T \tag{5.10}$$

When the number of equations is greater than the number of unknowns, pseudo inverse is equivalent to the least square solution procedure. But in the reverse case, the interpretation of the pseudo inverse also changes as follows:

Consider the first self orthogonality equation derived from the first elastic mode of the ideal GARTEUR structure as below:

$$\left\{ c_1^{11} \;\; d_1^{11} \;\; e_1^{11} \;\; f_1^{11} \;\; g_1^{11} \;\; \ldots c_4^{11} \;\; \ldots g_4^{11} \right\} \{x\} = \omega_1^2 \tag{5.11}$$

The pseudo inverse solution of equation (5.11) is given below:

$$\{x\} = \frac{\omega_1^2}{\left(\left(c_1^{11}\right)^2 + \left(d_1^{11}\right)^2 + \ldots + \left(g_1^{11}\right)^2 \right)} \left\{ c_1^{11} \;\; d_1^{11} \;\; e_1^{11} \;\; f_1^{11} \;\; g_1^{11} \;\; \ldots c_4^{11} \;\; \ldots g_4^{11} \right\}^T \tag{5.12}$$

Expression given in (5.12) indicates that the solution corresponding to each unknown term is weighted by the coefficient of that unknown given in equation (5.11). As a result, while an ‘active’ parameter with a greater coefficient is getting a higher credit, the solution turns out to be trivial for a ‘passive’ parameter with zero coefficient.

As shown in Tables 5.5 and 5.6, the only active parameter in the first equation is EI_1 parameter of the wing elements and this is the only non-zero solution predicted by the pseudo inverse solution mentioned above. The estimates of all other parameters turn out to be zero.

Pseudo inverse solution of the self orthogonality equations related to the stiffness orthogonality of the ideal GARTEUR structure is very interesting: All of the active parameters given in Table 5.9, except EI_1 of the horizontal stabilizer, are very accurately estimated. On the other hand, either poor estimates or the trivial solution is obtained for the passive FE parameters.

By using the pseudo-inverse solution of the active parameters (see Table 5.9) obtained from the 10 self orthogonality equations and by assigning large arbitrary values for the passive FE parameters (except EI_{12} parameters that must be taken zero with the assumption of symmetric beam element cross sections), it is possible to derive a stiffness matrix for the FE model of the ideal GARTEUR structure. Since the 10 self orthogonality equations related to the 'mass orthogonality' still gives exact solution for the ρA and ρAI_x parameters, the mass matrix of the FE model is perfectly determined. The comparison of the eigenvectors of the resultant FE model with the simulated-experimental modal data via 'Modal Assurance Criterion' (MAC) is given in Figure 5.5. The natural frequencies of the FE model are compared with the simulated-experimental natural frequencies in Table 5.10.

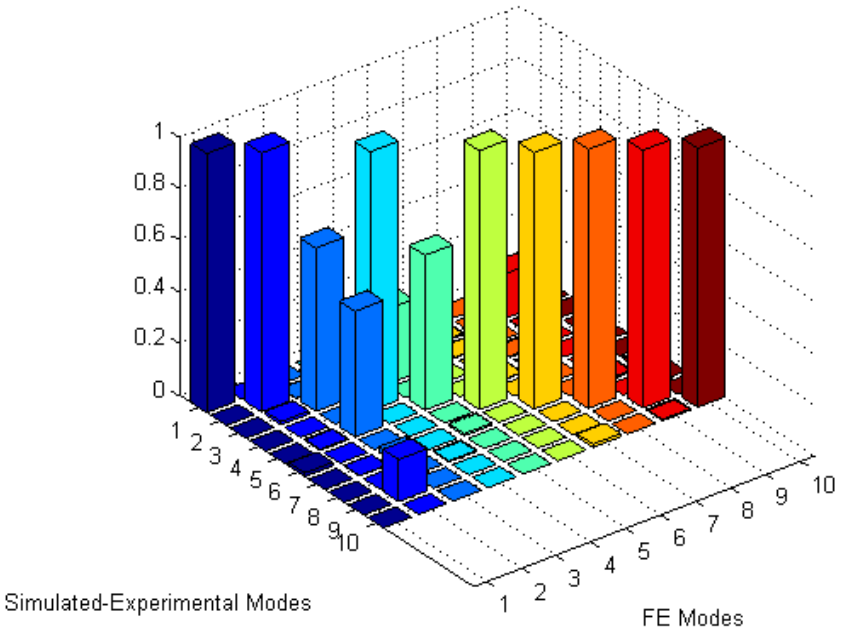

Figure 5.5. MAC matrix between the simulated-experimental modes and eigenvectors of the FE model of the ideal GARTEUR structure identified from the self orthogonality equations in case of the 4 element groups

Table 5.10. Comparison of the simulated-experimental natural frequencies and natural frequencies of the FE model of the ideal GARTEUR structure identified from the self orthogonality equations in case of the 4 element groups

Simulated-Experimental Modes	Simulated-Experimental Natural Frequencies (Hz)	Corresponding Modes of the Identified FE Model	Natural Frequencies of the Identified FE Model (Hz)	Difference in the Natural Frequencies (%)
1	5.61	1	5.61	0.00
2	15.82	2	15.93	0.67
3	36.51	3	36.86	0.95
4	36.96	4	36.96	0.01
5	37.09	5	37.61	1.41
6	43.22	6	43.22	-0.01
7	46.16	7	49.61	7.46
8	54.81	8	54.75	-0.10
9	60.98	9	62.29	2.14
10	67.03	10	67.26	0.33

Obviously, the FE model derived from the solution of the self orthogonality equations is in good correlation with the simulated-experimental modes of the ideal GARTEUR structure except modes 3 and 5. However, by using the iterative procedure mentioned in Chapter 3, it is possible to achieve a much better FE model.

Two important notices to avoid misinterpretation of the results obtained in this subsection are given below:

- In the subsequent sections, it will be shown that pseudo-inverse solution of the self orthogonality equations does not give good estimates of all active FE parameters in the case of real test data as in the case of ideal GARTEUR structure. As a result, in a real problem, self orthogonality equations must be solved together with cross orthogonality equations.

- In case of a real test data, accurate estimates of the active FE parameters may be obtained, but estimates of passive parameters are usually very poor. In such a case, the general approach (introduced first time in this section) to construct a FE model is to assign arbitrary large values (several orders of magnitude 'larger' than values of the active parameters) to the passive parameters. Since the modes of interest are insensitive to the values of passive structural well with the experimental data.

5.2.4. Solutions of the Structural Identification Equations in Case of Large Number of Element Groups

So far, the structural identification equations have been derived by dividing elements of the FE model of the ideal GARTEUR structure into 4 groups. This is not a realistic assumption in case of a real aircraft structure. For that reason, the performance of the structural identification equations reconstructed for different group numbers is studied below:

By using 10 simulated-experimental normal modes, it is possible to derive 55 structural identification equations from the stiffness orthogonality and another 55 equations from the mass orthogonality as mentioned previously. In case of the stiffness orthogonality equations, each element group brings 5 unknown parameters, and so the ideal GARTEUR structure can be divided into maximum 11 element groups in order to keep the number of unknowns below the number of equations.

By dividing the wing of the ideal GRTEUR structure into more and more groups, structural identification equations have been reconstructed for 5, 6, 7, 8 and 9 groups cases. As a result, up to the 6 element groups, FE parameters are nearly perfectly determined. MAC comparison of the eigenvectors of the identified FE model with the simulated-experimental normal modes for the 6 element groups is shown in Figure 5.6. Moreover, natural frequencies of the FE model compared to the corresponding simulated-experimental natural frequencies are illustrated in Table 5.11.

On the other hand, starting from the 7 element groups, solution of the 55 structural identification equations related to the stiffness orthogonality does not give sufficiently accurate estimates of certain critical FE parameters such as GJ_e of the wing elements and it becomes impossible to determine an initial FE model accurate enough to converge to a much better FE model by using the iterative solution procedure explained in Chapter 3.

For element groups greater than 4, pseudo-inverse solution of the self orthogonality equations does not give accurate results and determination of an initial FE model becomes impossible once again.

It is concluded that constructing and solving structural identification equations for different group definitions may be a good practice to check reliability of the initial FE

parameter estimates. But one must be careful in increasing number of element groups because it may degrade initial estimates of certain active structural parameters.

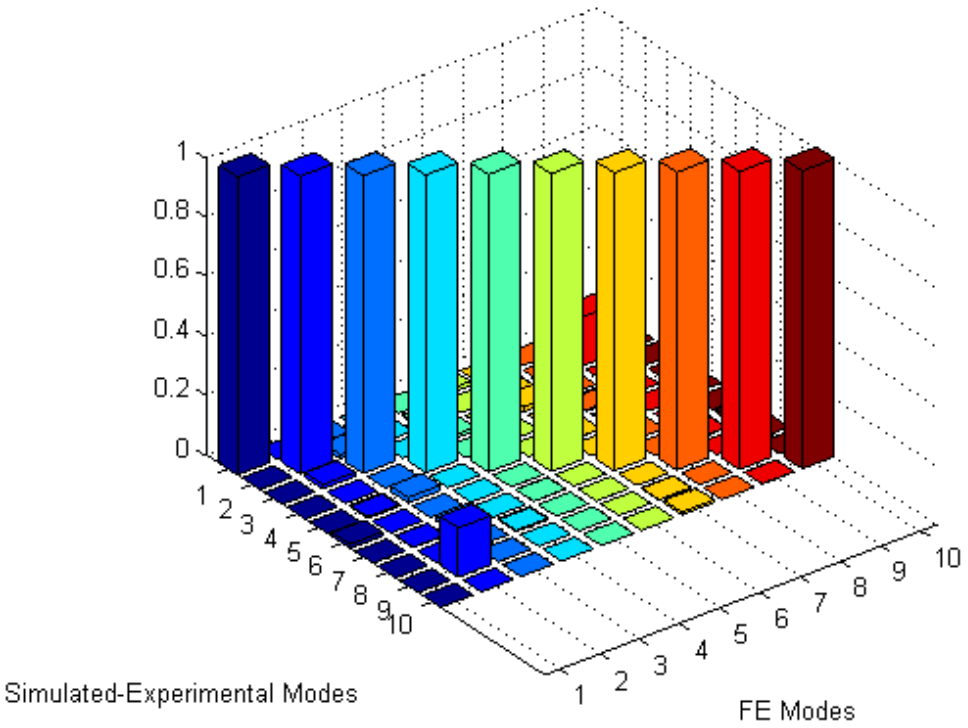

Figure 5.6. MAC matrix between the simulated-experimental modes and eigenvectors of the identified FE model of the ideal GARTEUR structure in case of the 6 element groups

Table 5.11. Comparison of the natural frequencies of the FE model with the simulated-experimental natural frequencies of the ideal GARTEUR structure in case of the 6 element groups

Simulated-Experimental Modes	Simulated-Experimental Natural Frequencies (Hz)	Corresponding Modes of the Identified FE Model	Natural Frequencies of the Identified FE Model (Hz)	Difference in the Natural Frequencies (%)
1	5.61	1	5.61	0.00
2	15.82	2	15.83	0.02
3	36.51	3	36.54	0.08
4	36.96	4	36.94	-0.05
5	37.09	5	37.10	0.03
6	43.22	6	43.22	0.00
7	46.16	7	46.12	-0.08
8	54.81	8	54.62	-0.34
9	60.98	9	61.49	0.83
10	67.03	10	67.03	0.00

5.2.5. Reduction of the Coefficient Matrix of the Stiffness Orthogonality Equations

Up to this point, the structural identification equations related to the stiffness orthogonality have been derived by introducing 5 unknown terms per element group as shown in equation (4.2). But, definitions of the ‘active’ and ‘passive’ parameters introduced early in this section have shown that experimental normal modes and natural frequencies of a structure within the frequency range of interest are more sensitive to certain parameters than others. Accordingly, for the ideal GARTEUR structure, it has been shown that using relatively accurate estimates for the active parameters and arbitrary values for the passive parameters several order of magnitude larger than values of active parameters, it is possible to construct a quite ‘good’ initial FE model that can be updated to converge to a much better FE model correlating well with the experimental data. All these observations eventually raised the following critical question: Is it possible to reformulate the structural identification equations related to the stiffness orthogonality in a manner to reduce the number of unknowns down to the number of the active parameters? This reduction is important for the following reason: When the structural identification equations are derived from the real experimental data, coefficients of the passive structural parameters are degraded in a manner to frustrate solutions of the active parameters. Solutions of

the reduced structural identification equations of the ideal GARTEUR structure are studied below:

In case of the 4 element groups, mass orthogonality equations does not necessitate any reduction because there are 55 equations to solve only for 8 unknowns and solutions are very accurate. On the other hand, the coefficient matrix of the stiffness orthogonality equations are reduced by removing all the columns that belong to the finite elements of the fuselage and horizontal stabilizer, and also the coefficients of the EA and EI_{12} terms that belong to the finite elements of the wing and vertical stabilizer. As a result, the number of unknowns is reduced from 20 to 6. Solutions of the reduced structural identification equations give very accurate estimates of the 6 active parameters. By using the active parameter estimates and arbitrary large numbers for the passive parameters, an initial FE model is constructed. The MAC comparison of that initial FE model with the simulated-experimental modes is given in Figure 5.7. Moreover, natural frequencies of the FE model compared to the corresponding simulated-experimental natural frequencies are illustrated in Table 5.12.

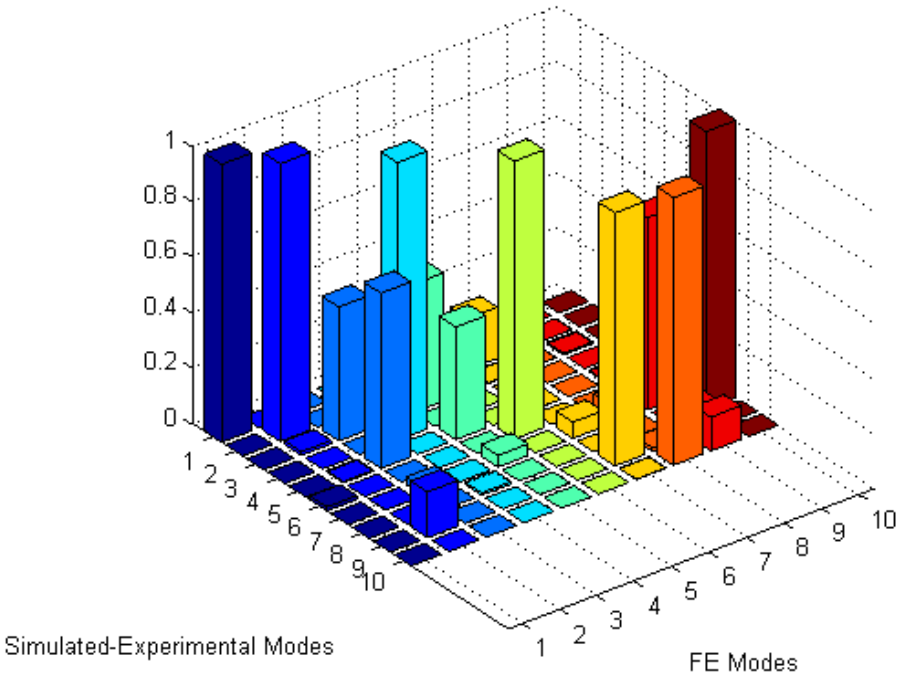

Figure 5.7. MAC comparison of the simulated-experimental modes with the eigenvectors of the initial FE model derived from the reduced stiffness orthogonality equations of the ideal GARTEUR structure in case of the 4 element groups

Table 5.12. Comparison of the simulated-experimental natural frequencies with the natural frequencies of the initial FE model derived from the reduced stiffness orthogonality equations of the ideal GARTEUR structure in case of the 4 element groups

Simulated-Experimental Modes	Simulated-Experimental Natural Frequencies (Hz)	Corresponding Modes of the Initial FE Model	Natural Frequencies of the Initial FE Model (Hz)	Difference in the Natural Frequencies (%)
1	5.61	1	5.67	0.98
2	15.82	2	16.05	1.44
3	36.51	3	37.05	1.48
4	36.96	4	37.11	0.40
5	37.09	3	37.05	-0.09
6	43.22	6	43.63	0.94
7	46.16	9	73.42	59.05
8	54.81	10	74.69	36.27
9	60.98	7	61.96	1.60
10	67.03	8	67.31	0.41

Obviously, the initial FE model does not correlate well with the simulated-experimental data of the ideal GARTEUER structure. But, by using the iterative procedure explained in Chapter 3 it is possible to force that initial model to converge to an FE model that correlates perfectly with the simulated-experimental data. The history plots of the wing and vertical stabilizers are shown in Figures 5.8 and 5.9. The MAC comparison of the eigenvectors of the converged FE model with the simulated-experimental modes is given in Figure 5.10. Moreover, natural frequencies of the converged FE model are compared with the corresponding simulated-experimental natural frequencies in Table 5.13. It must be noticed that to improve readability of the history plots, structural parameters shown in Figures 5.8 and 5.9 have been normalized with the parameters calculated in the last iteration. The superscript ' * ' in EI_1^*, EI_2^* and GJ_e^* parameters indicates that they have been subjected to the afore mentioned normalization.

Comparison of Figures 5.7 and 5.10 as well as Tables 5.12 and 5.13 shows that the iterative solution procedure explained in Chapter 3 proves to be very successful.

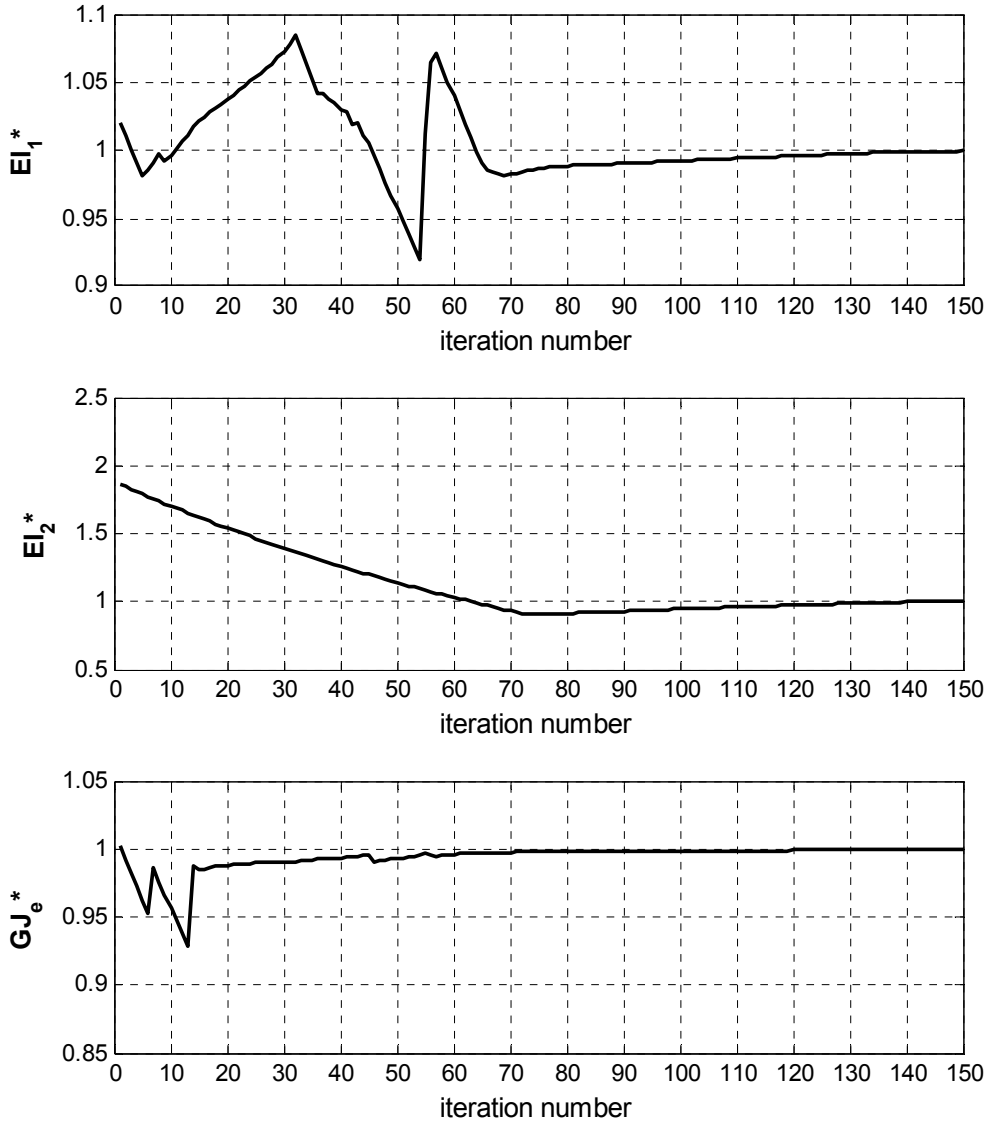

Figure 5.8. History plots of the structural parameters that belong to the wing elements of the FE model of the ideal GARTEUR structure in case of the 4 element groups

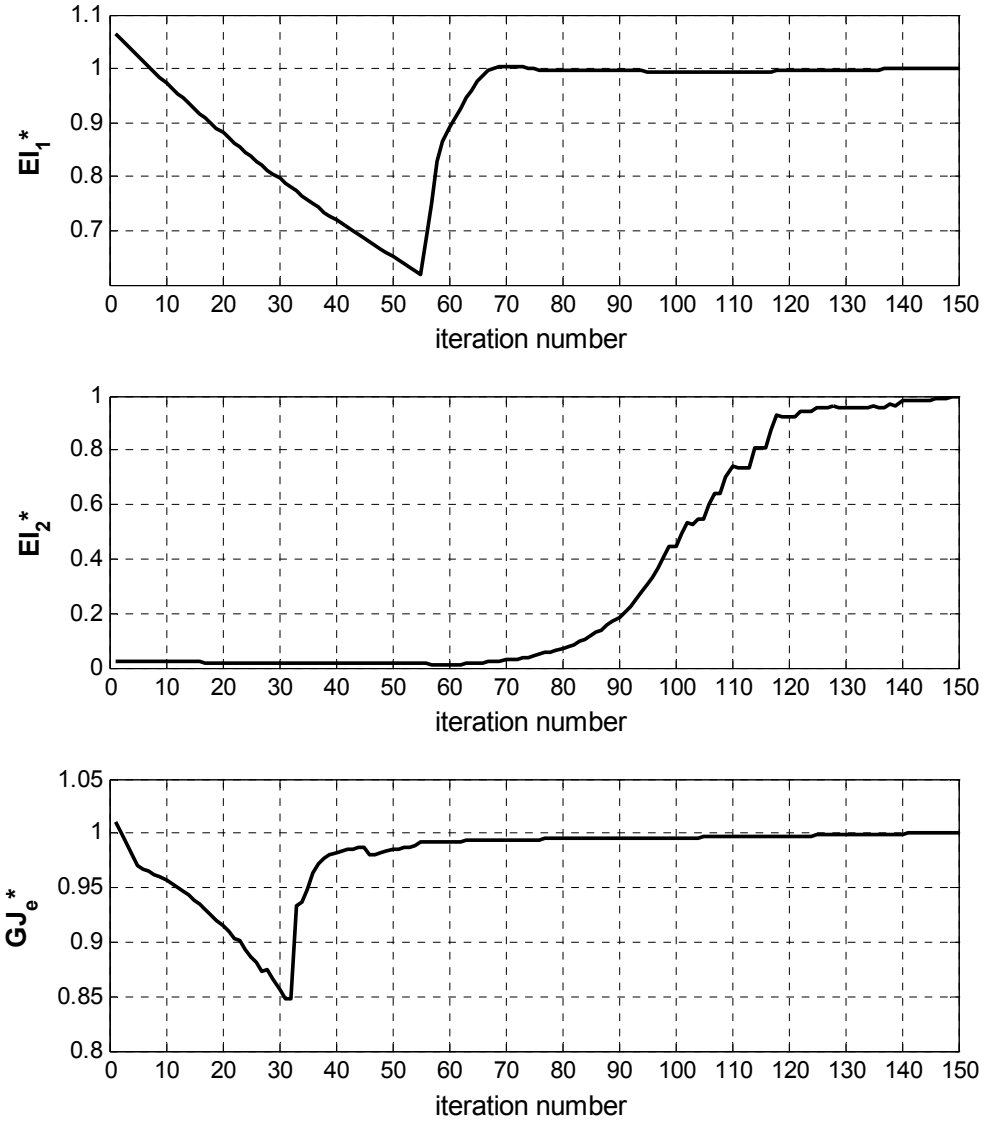

Figure 5.9. History plots of the structural parameters that belong to the vertical stabilizer elements of the FE model of the ideal GARTEUR structure in case of the 4 element groups

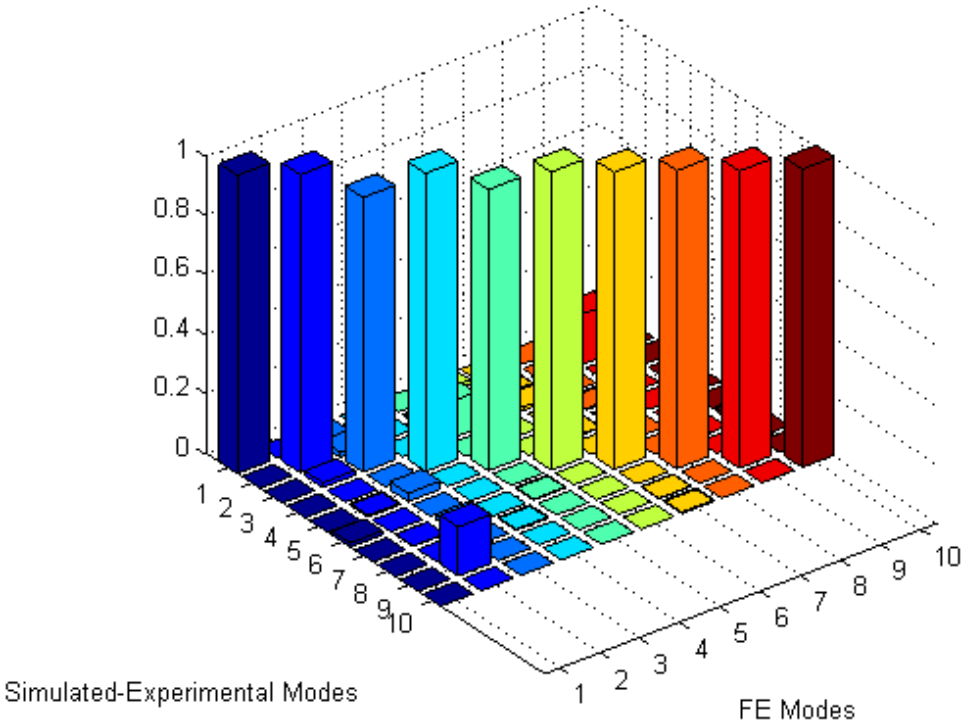

Figure 5.10. MAC comparison of the simulated-experimental modes with the eigenvectors of the updated FE model of the ideal GARTEUR structure in case of the 4 element groups

Table 5.13. Comparison of the simulated-experimental natural frequencies with the natural frequencies of the updated FE model of the ideal GARTEUR structure in case of the 4 element groups

Simulated-Experimental Modes	Simulated-Experimental Natural Frequencies (Hz)	Corresponding Modes of the Updated FE Model	Natural Frequencies of the Updated FE Model (Hz)	Difference in the Natural Frequencies (%)
1	5.61	1	5.61	-0.11
2	15.82	2	15.71	-0.70
3	36.51	3	36.21	-0.82
4	36.96	4	37.03	0.18
5	37.09	5	37.04	-0.12
6	43.22	6	43.19	-0.09
7	46.16	7	46.18	0.04
8	54.81	8	54.81	0.00
9	60.98	9	61.07	0.14
10	67.03	10	67.03	0.00

The solution of the reduced stiffness orthogonality equations in case of 5 and higher element groups does not give accurate estimates for all of the active parameters as in the case of the 4 element groups. Especially, for GJ_e parameters of the wing elements very poor estimates are obtained. As a result, an initial FE model derived from the structural identification equations of element groups greater than 4 cannot converge to an FE model correlating well with the experimental data.

5.2.6. Determination of the FE Model of the Ideal GARTEUR Structure from the Simulated-Experimental Normal Modes Truncated in Terms of the Measurement Dofs

The ideal GARTEUR structure concept was very useful in developing a deep understanding of the structural identification and model updating theory developed within the scope of this thesis study. But, the eigenvectors used in the derivation of the structural identification equations were including all of the 264 dofs of the ideal GARTEUR structure and they were free from any experimental error. However, the real test data brings extra challenges to the theory developed herein, for the following reasons:

- A real structure has infinitely many dofs and a very limited number of them can be measured during a modal test. For example, the experimental mode shapes determined from the modal test of the SM-AG 19 test bed described in section 5.2.1 consist of 66 measurement dofs.
- In a real modal test, rotational dofs cannot be measured. The 66 measurement dofs mentioned above are only composed of the translational dofs.
- Real modal test data includes experimental error.

Before applying the theory to a real test data, the effect of the truncated nature of the experimental modes on the solutions of the structural identification equations will be studied as follows:

The ideal GARTEUR structure is an FE model that consists of 43 elements, 44 nodes and 264 dofs as mentioned previously in this chapter. The FE mesh has been constructed by connecting measurement points of the real test setup introduced in section 5.2.1 with Euler-Bernoulli beam elements. Accordingly, nodal points of the

FE model coincide with the measurement points of the real test setup. As a result, in order to simulate the truncation of the real mode shapes in terms of measurement dofs, it is sufficient to truncate the simulated-experimental modes of the ideal GARTEUR structure in terms of rotational dofs and some of the translational dofs that could not been measured in the real modal test. This way, the dofs of the simulated-experimental modes are reduced from 264 to 66. Finally, the new modal test scenario is obtained as follows:

The first 10 elastic modes of the ideal GARTEUR structure that consist of 66 measurement dofs and corresponding natural frequencies are the only experimental data available to derive the FE model of the ideal GARTEUR structure.

As explained in Chapter 3, the first step of the structural identification is the construction of an FE mesh by connecting measurement points with Euler-Bernoulli beam elements as given in Figure 5.4. The resultant FE mesh consists of 264 dofs. In order to derive the structural identification equations, the simulated-experimental modes have to be expanded from 66 to 264 dofs. This can be accomplished by using the Guyan's Expansion. But the Guyan's Expansion requires the global stiffness matrix of the FE model. This means that the stiffness matrix is required to be used by its own solution procedure. In order to solve this dilemma, an arbitrary stiffness matrix sharing the same connectivity as the actual stiffness matrix will be used. This brings the definition of the 'unit GARTEUR structure'. Unit GARTEUR structure is an FE model having the same mesh as the actual FE model but the entire beam elements consist of square cross sections of unit area. Using the stiffness matrix of the unit GARTEUR structure, it is possible to derive the transformation matrix dictated by the Guyan's Expansion method. The 66 measurement dofs of the pseudo-experimental modes are then expanded to the size of the FE model.

The rotational dofs of the wing elements calculated from the Guyan's Expansion of the truncated simulated-experimental modes are compared to the original rotational dofs of the ideal GARTEUR structure for the first 6 elastic modes in Figures 5.11 to 5.13. Observation of Figures 5.11 to 5.13 shows that slave coordinates cannot be determined exactly by using the Guyan's Expansion even if the simulated-experimental modes are free from any experimental error. Errors appearing in the estimates of the slave coordinates will also affect the accuracy of the structural identification equations in a negative sense as discussed below:

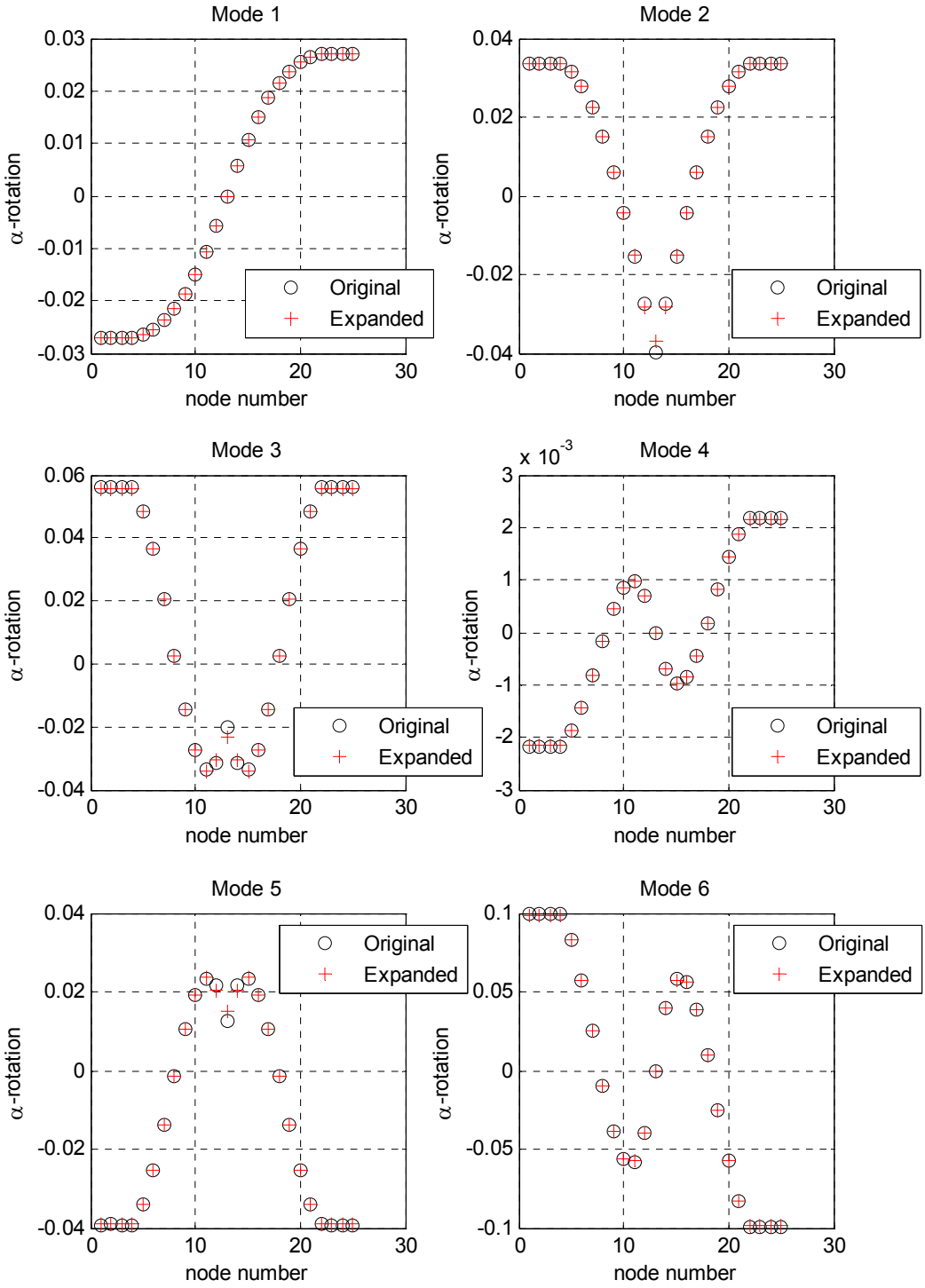

Figure 5.11. Comparison of the rotational dofs of the wing elements calculated from the Guyan's Expansion with the original rotational dofs about the global x-axis of the ideal GARTEUR structure

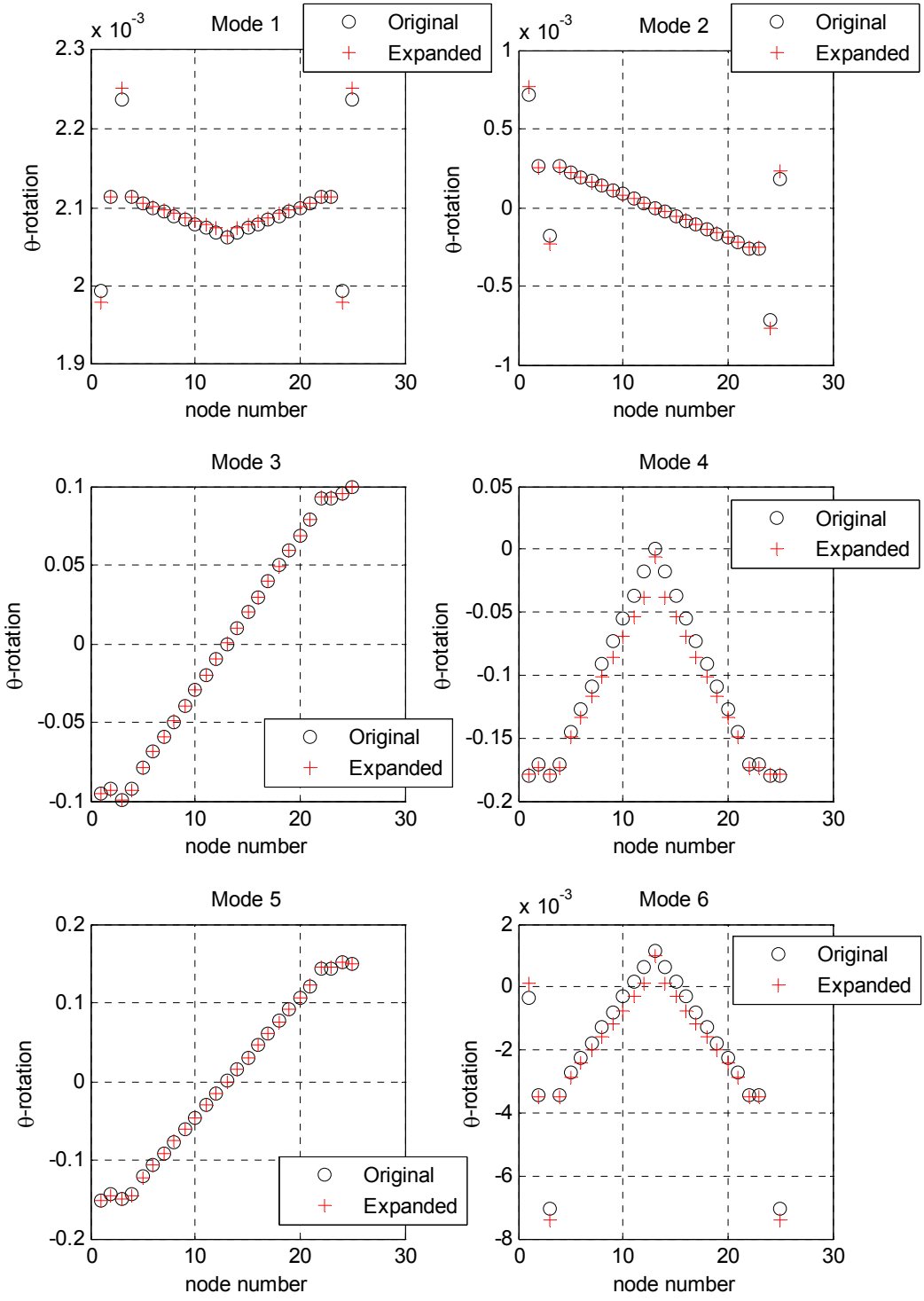

Figure 5.12. Comparison of the rotational dofs of the wing elements calculated from the Guyan's Expansion with the original rotational dofs about the global y-axis of the ideal GARTEUR structure

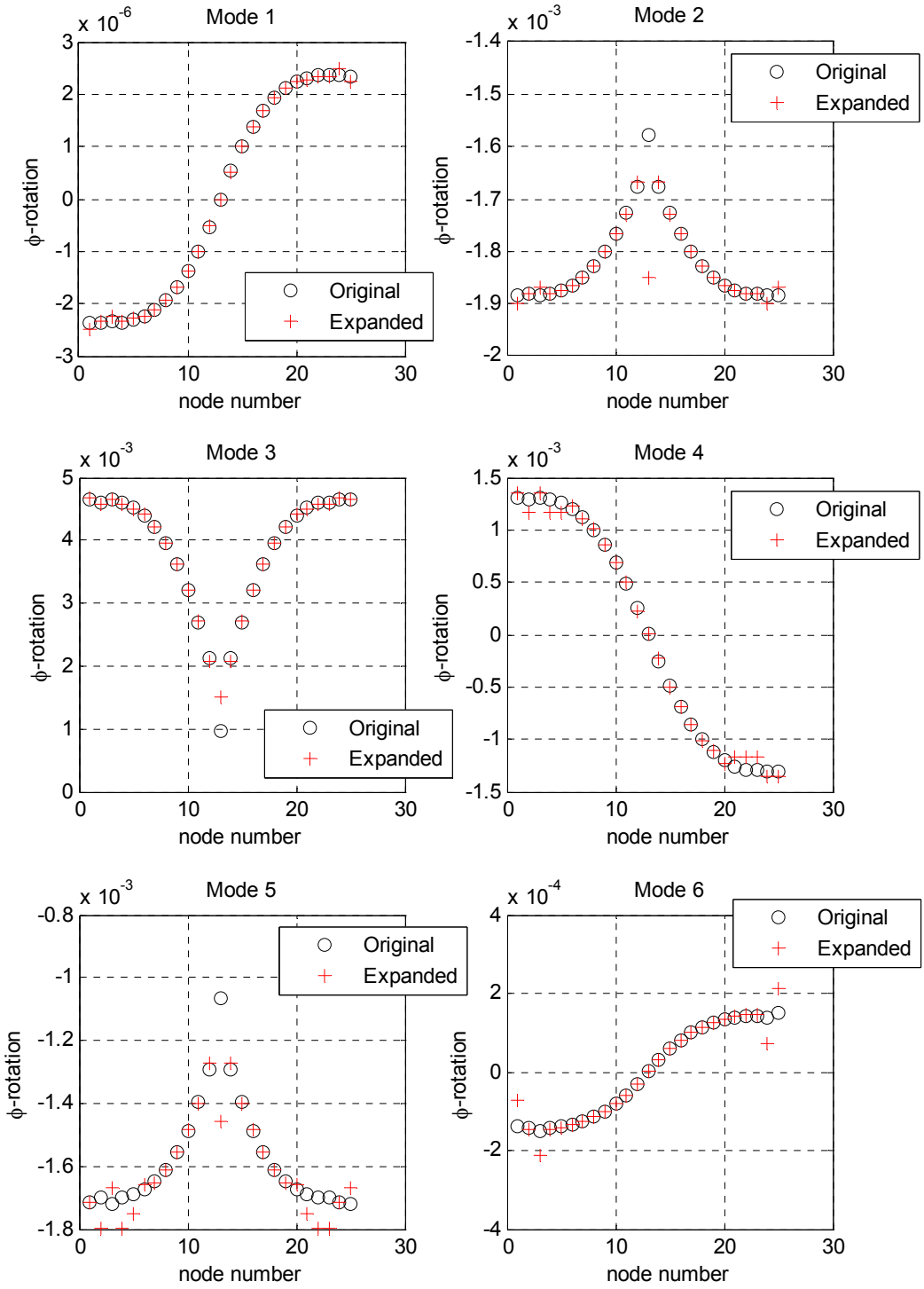

Figure 5.13. Comparison of the rotational dofs of the wing elements calculated from the Guyan's Expansion with the original rotational dofs about the global z-axis of the ideal GARTEUR structure

In case of 4 and higher element groups, solution of the 55 mass orthogonality equations derived from the simulated-experimental modes were always exact up to this point. But, if the mass orthogonality equations are constructed from the 'expanded' simulated-experimental modes, the accuracy of the ρA and ρAI_x parameter estimates drop considerably. In order to improve the accuracy of the parameter estimates, a supplementary equality constraint is imposed to the least square solution of the mass orthogonality equations. That equality constraint is a single equation dictating that the sum of the masses of the entire element groups is equated to the total mass of the ideal GARTEUR structure. Formulation of such an equation is not difficult for a real aircraft structure as well, because during a GVT it is possible to measure the total mass of the aircraft structure.

Least square solution of the mass orthogonality equations supported with the mass equality constraint mentioned above improves the accuracy of ρA parameter estimates up to 6 element groups case. The ρAI_x parameters cannot be estimated accurately but this is not a significant problem, because those parameters do not play a critical role in the determination of the global mass matrix. On the other hand, pseudo-inverse solution of 10 self orthogonality equations does not give sufficiently accurate estimates for ρA parameter of each element group even in the case of 4 element groups.

In the light of the studies mentioned above, regarding the mass orthogonality equations, it is concluded that expansion of the simulated-experimental modes degrade parameter solutions considerably. To improve the accuracy of the parameter estimates, the least square solution of the mass orthogonality equations must be accompanied with the mass equality constraint. Mass orthogonality equations formulated for element groups larger than 6 do not give good results and pseudo-inverse solution of the self orthogonality equations is not an alternative solution technique even in case of 4 element groups.

Study of the stiffness orthogonality equations derived from the 'expanded' simulated-experimental modes also leads up to several important conclusions as stated below:

If the coefficients of passive structural parameters are kept within the coefficient matrix, solutions of certain active parameters given in Table 5.9, especially GJ_e of the wing cannot be determined. But if the coefficient matrix is reduced by removing

the coefficients of the passive parameters as done in the previous section, active parameters are determined more accurately. This observation justifies the following hypothesis mentioned in the previous sections: Coefficients of passive structural parameters are more prone to errors coming from the expansion of truncated experimental modes.

Solutions of stiffness orthogonality equations formulated for element groups larger than 4 cannot predict all of the active parameters. Similarly, the pseudo-inverse solution of the self orthogonality equations does not give accurate estimates for active parameters even in the case of 4 element groups.

As a result, in the case of 4 element groups, it is possible to derive an initial FE model from the solutions of the mass and stiffness orthogonality equations. MAC comparison of that initial model with the simulated-experimental modes is shown in Figure 5.14. Comparison of the natural frequencies of the initial FE model with the simulated-experimental natural frequencies is illustrated in Table 5.14.

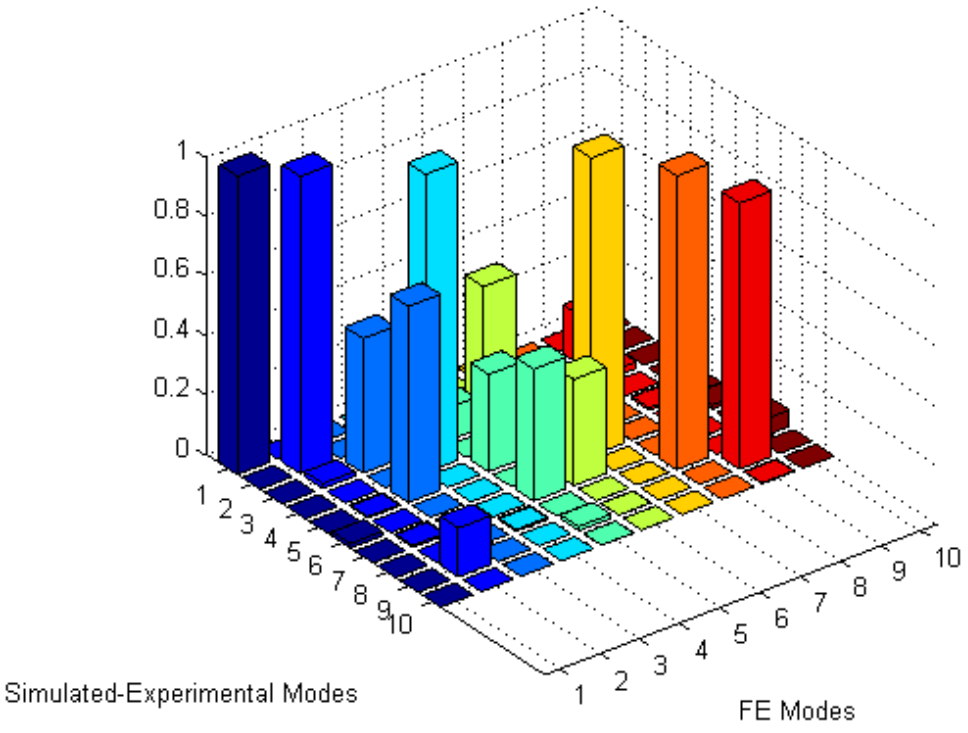

Figure 5.14. MAC comparison of the expanded simulated-experimental modes with the eigenvectors of the initial FE model derived from the reduced stiffness orthogonality equations of the ideal GARTEUR structure in case of the 4 element groups

Table 5.14. Comparison of the simulated-experimental natural frequencies with the natural frequencies of the initial FE model derived from truncated simulated-experimental modes in case of the 4 element groups

Simulated-Experimental Modes	Simulated-Experimental Natural Frequencies (Hz)	Corresponding Modes of the Initial FE Model	Natural Frequencies of the Initial FE Model (Hz)	Difference in the Natural Frequencies (%)
1	5.61	1	5.75	2.48
2	15.82	2	16.65	5.22
3	36.51	6	40.97	12.21
4	36.96	4	31.27	-15.41
5	37.09	3	31.16	-15.98
6	43.22	7	44.25	2.37
7	46.16	5	34.26	-25.78
8	54.81	8	55.82	1.85
9	60.98	9	71.17	16.70
10	67.03	12	128.12	91.13

Starting from that initial FE model and using the iterative algorithm explained in Chapter 3, a very accurate FE model correlating well with the simulated-experimental data is obtained. History plots of the wing and vertical stabilizer parameters throughout the updating procedure are shown in Figures 5.15 and 5.16.

The MAC comparison of the updated FE model with the simulated-experimental data is given in Figure 5.17. Comparison of the natural frequencies of the updated FE model with the simulated-experimental natural frequencies is shown in Table 5.15.

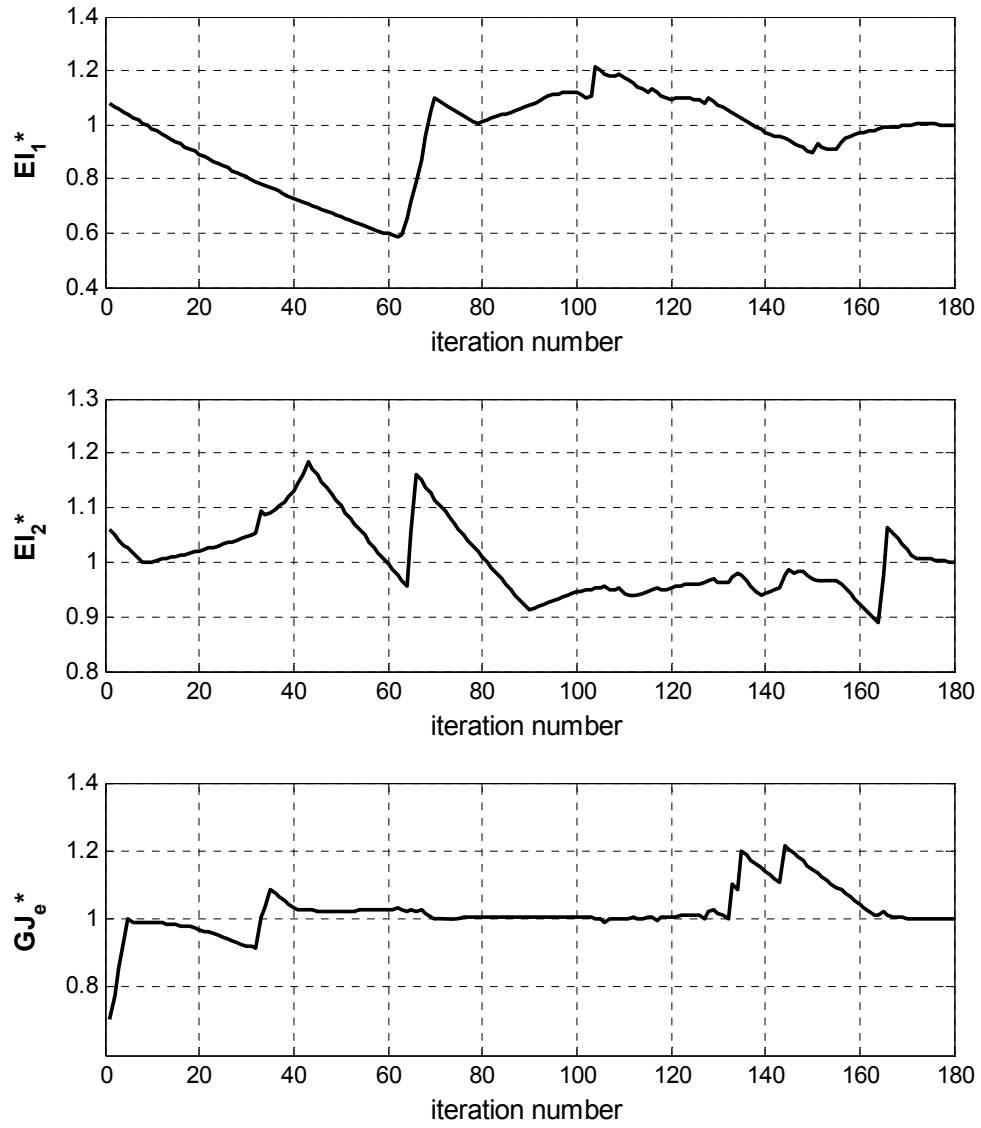

Figure 5.15. History plots of the structural parameters that belong to the wing elements of the FE model derived from the truncated simulated-experimental modes in case of the 4 element groups

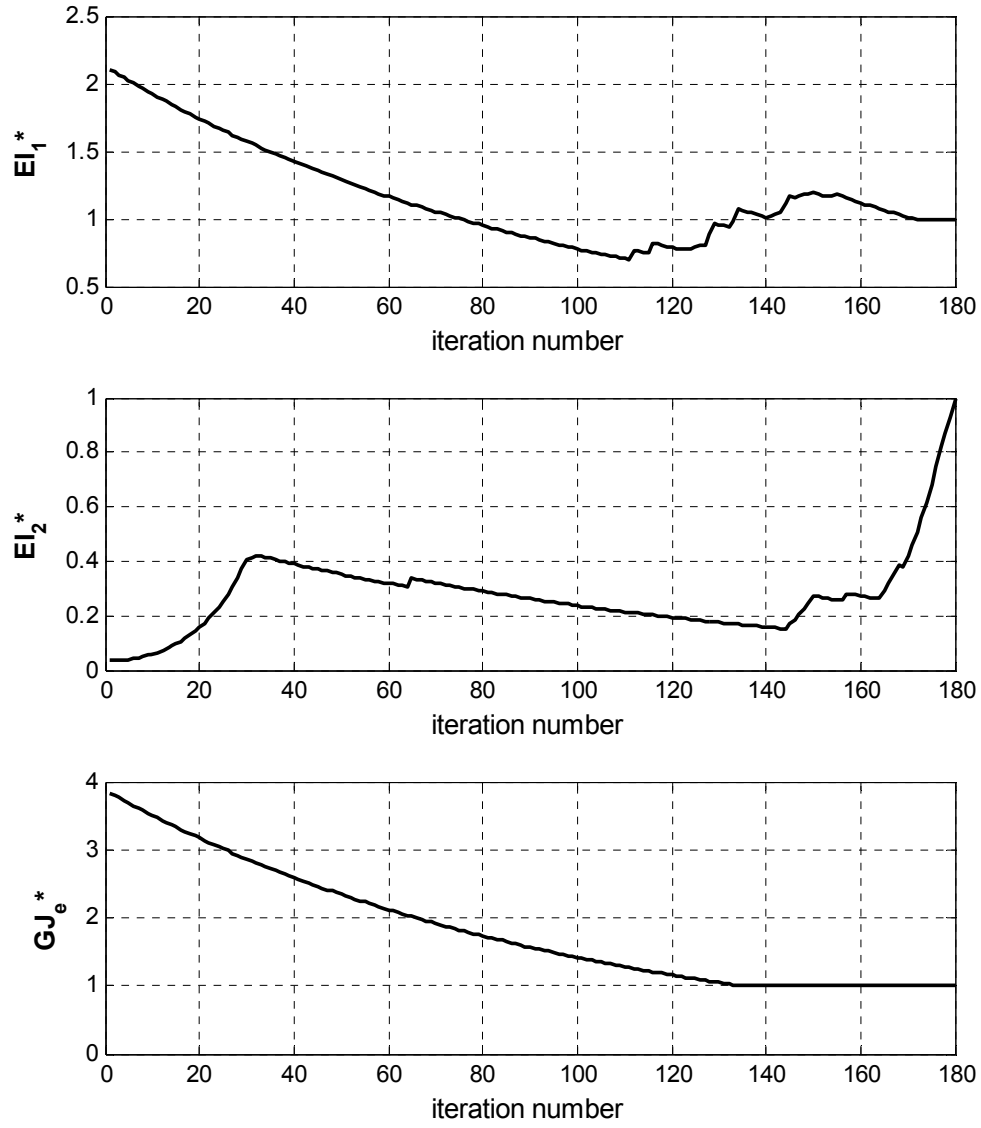

Figure 5.16. History plots of the structural parameters that belong to the vertical stabilizer elements of the FE model derived from the truncated simulated-experimental modes of the ideal GARTEUR structure in case of the 4 element groups

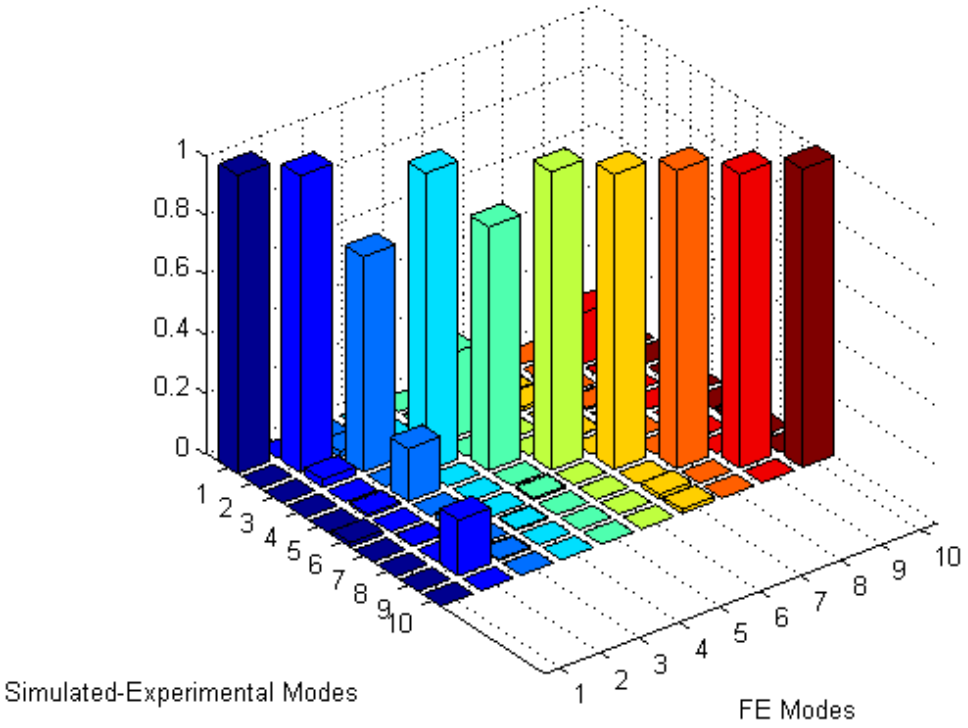

Figure 5.17. MAC comparison of the expanded simulated-experimental modes with the eigenvectors of the updated FE model derived from the reduced stiffness orthogonality equations of the ideal GARTEUR structure in case of the 4 element groups

Table 5.15. Comparison of the simulated-experimental natural frequencies with the natural frequencies of the updated FE model derived from the truncated pseudo-experimental modes in case of the 4 element groups

Simulated-Experimental Modes	Simulated-Experimental Natural Frequencies (Hz)	Corresponding Modes of the Updated FE Model	Natural Frequencies of the Updated FE Model (Hz)	Difference in the Natural Frequencies (%)
1	5.61	1	5.54	-1.35
2	15.82	2	15.66	-1.01
3	36.51	3	34.56	-5.35
4	36.96	4	37.02	0.16
5	37.09	5	37.04	-0.12
6	43.22	6	42.75	-1.10
7	46.16	7	46.19	0.07
8	54.81	8	54.81	0.00
9	60.98	9	61.51	0.86
10	67.03	10	67.03	0.00

5.2.7. Determination of the FE Model of the GARTEUR Structure from the Real Experimental Data

So far, by using the 'ideal GARTEUR structure' concept, quite a lot of knowledge has been gained about the method of the structural identification developed in this thesis work. Now, it is the right time to apply the method to the 'real GARTEUR structure'.

The real experimental data obtained from the modal test of the GARTEUR structure consists of the first 10 elastic mode shapes and corresponding natural frequencies as mentioned in section 5.2.1. Each mode shape includes 66 measurement dofs. Using this experimental data, mass and stiffness orthogonality equations have been formulated for different number of element groups starting from 4 and going up to 9. Important results are stated below:

- Relatively accurate initial estimates of the active FE parameters can only be obtained in case of 4 element groups.
- Least square solution of the mass orthogonality equations has to be solved with an equality constraint that dictates the total mass of the FE model to be equal to the total mass of the real GARTEUR structure.
- Coefficient matrix of the stiffness orthogonality equations has to be reduced by eliminating coefficient of the passive structural parameters. Otherwise, active structural parameters cannot be determined accurately.
- Self and cross orthogonality equations have to be solved altogether because this gives much better results than the pseudo-inverse solution of the self orthogonality equations.

The MAC comparison of the eigenvectors of the initial FE model with the real experimental mode shapes is shown in Figure 5.18. Moreover, eigenvalues of that initial FE model are compared to the experimental natural frequencies in Table 5.16.

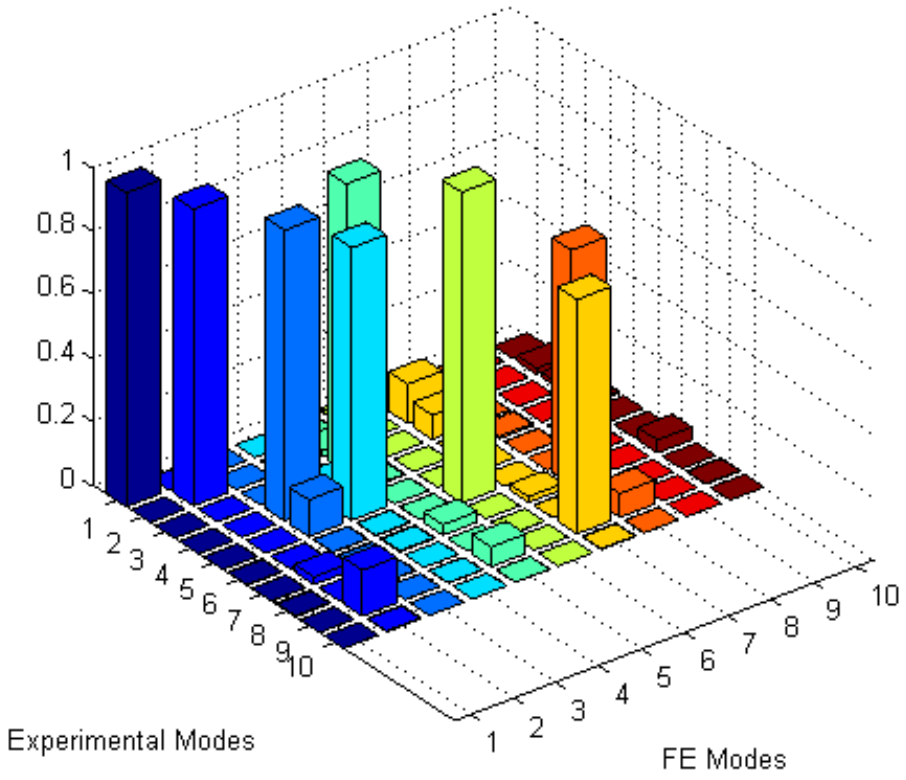

Figure 5.18. MAC comparison of the real experimental modes with the eigenvectors of the initial FE model derived from the reduced stiffness orthogonality equations of the GARTEUR structure in case of the 4 element groups

Table 5.16. Comparison of the experimental natural frequencies of the GARTEUR structure with the natural frequencies of the initial FE model in case of the 4 element groups

Experimental Modes	Experimental Natural Frequencies (Hz)	Corresponding Modes of the Initial FE Model	Natural Frequencies of the Initial FE Model (Hz)	Difference in the Natural Frequencies (%)
1	5.65	1	5.11	-9.49
2	15.73	2	14.09	-10.45
3	36.79	5	37.77	2.66
4	37.51	3	32.43	-13.53
5	37.65	4	32.47	-13.75
6	43.73	6	39.62	-9.39
7	50.32	8	110.95	120.48
8	55.00	12	185.73	237.69
9	60.66	7	68.93	13.64
10	68.23	19	306.35	349.00

After the application of the iterative solution procedure, an ultimate FE model correlating well with the experimental data is achieved. The history plots of the structural parameters of the wing and vertical stabilizer elements throughout the iteration procedure are shown in Figures 5.19 and 5.20.

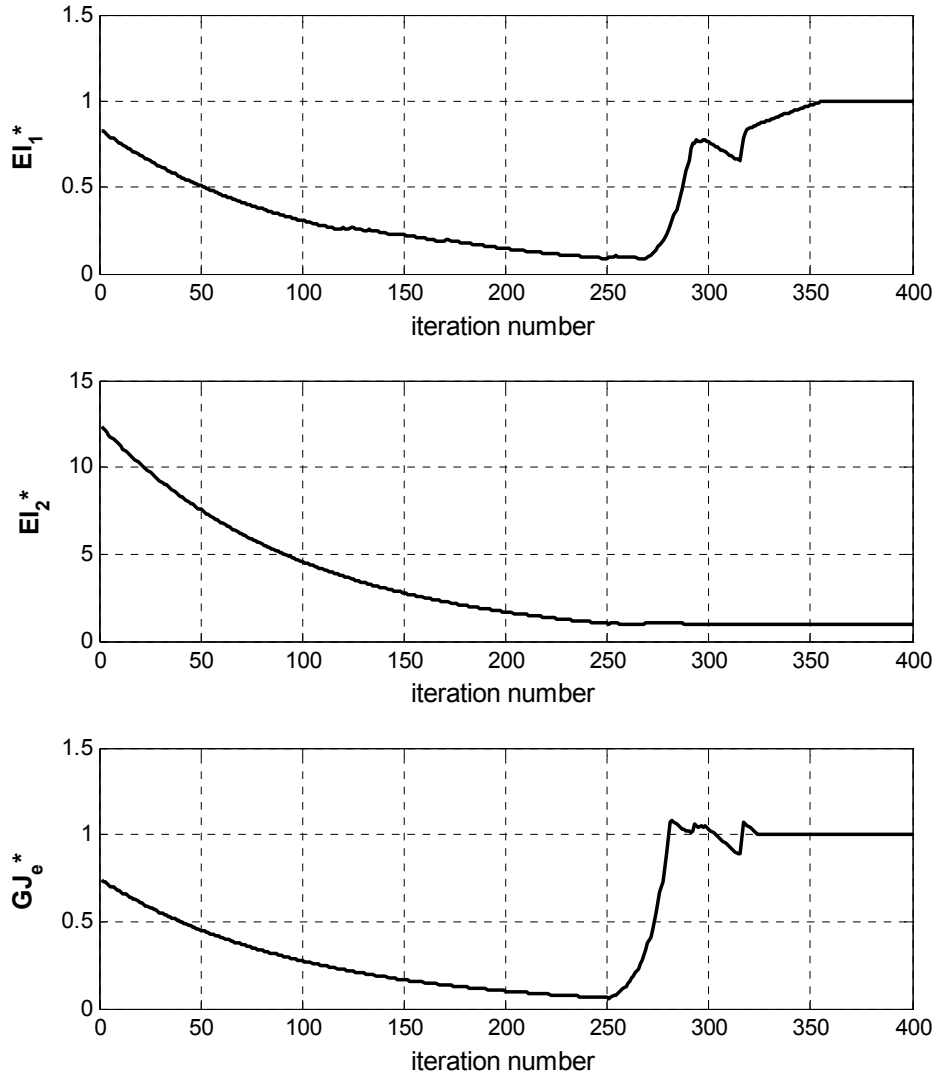

Figure 5.19. History plots of the structural parameters that belong to the wing elements of the FE model derived from the real experimental data of the GARTEUR structure in case of the 4 element groups

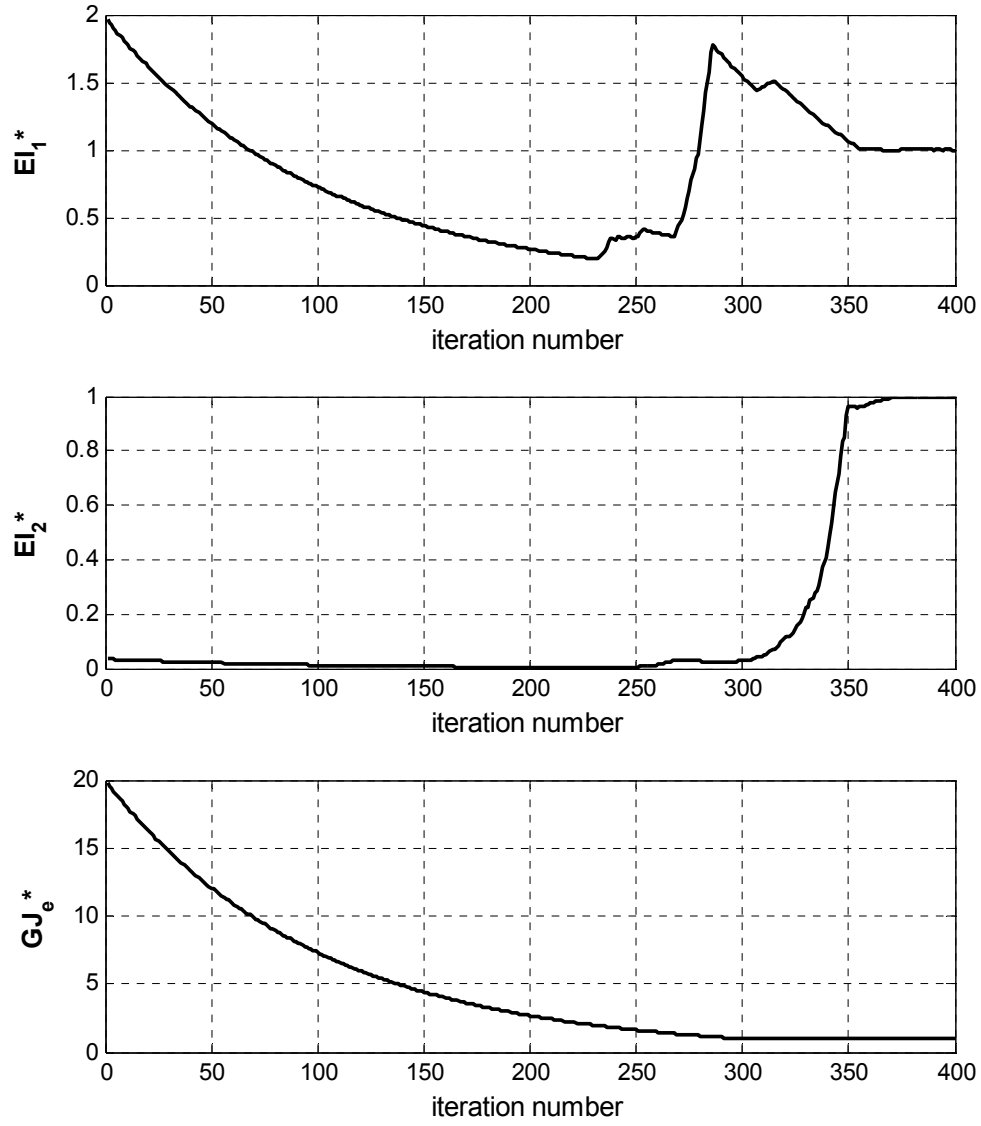

Figure 5.20. History plots of the structural parameters that belong to the vertical stabilizer elements of the FE model derived from the real experimental data of the GARTEUR structure in case of the 4 element groups

The MAC comparison of the eigenvectors of the updated FE model with the experimental mode shapes is given in Figure 5.21. Moreover, natural frequencies of the updated FE model are compared with the experimental natural frequencies in Table 5.17.

Detailed comparisons of the experimental mode shapes with the eigenvectors of the updated FE model are also illustrated in Figures 5.22 to 5.25.

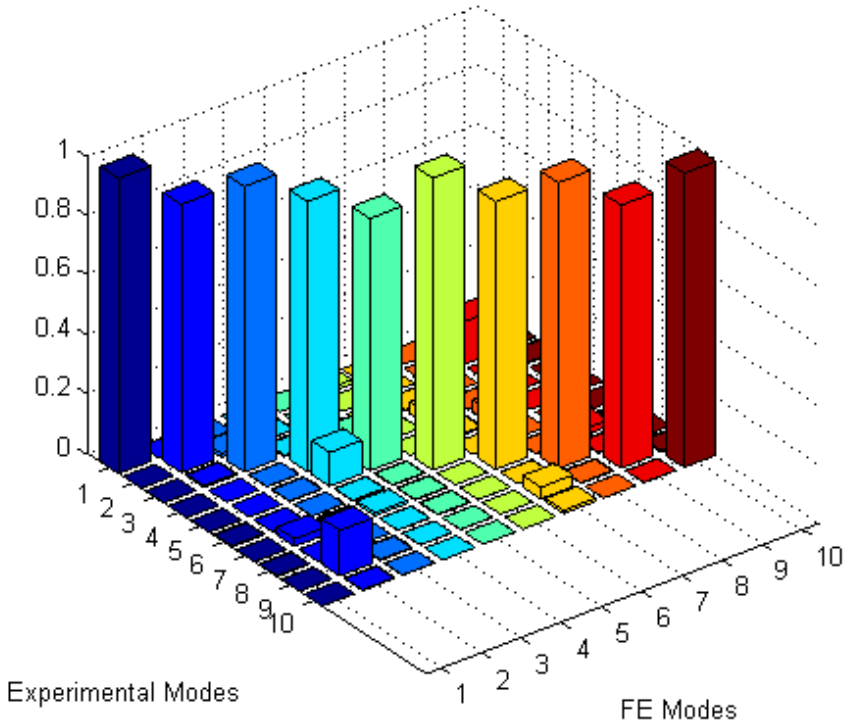

Figure 5.21. MAC comparison of the real experimental modes with the eigenvectors of the updated FE model of the GARTEUR structure in case of the 4 element groups

Table 5.17. Comparison of the experimental natural frequencies of the GARTEUR structure with the natural frequencies of the updated FE model in case of the 4 element groups

Experimental Modes	Experimental Natural Frequencies (Hz)	Corresponding Modes of the Updated FE Model	Natural Frequencies of the Updated FE Model (Hz)	Difference in the Natural Frequencies (%)
1	5.65	1	5.61	-0.71
2	15.73	2	14.51	-7.74
3	36.79	3	35.26	-4.15
4	37.51	4	37.58	0.17
5	37.65	5	37.59	-0.15
6	43.73	6	43.48	-0.57
7	50.32	7	50.33	0.02
8	55.00	8	55.01	0.01
9	60.66	9	61.08	0.69
10	68.23	10	68.23	0.00

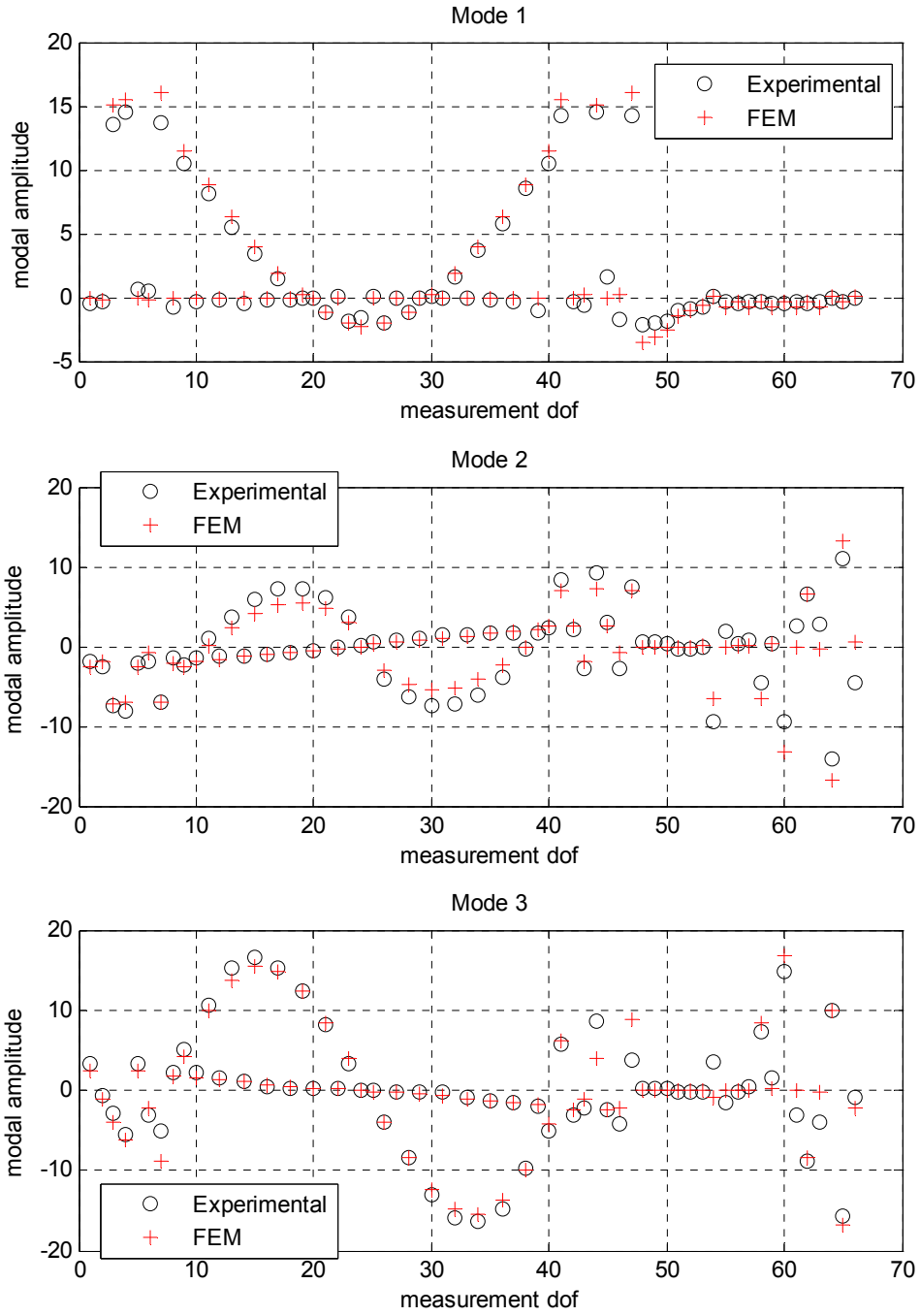

Figure 5.22. Detailed comparison of the experimental mode shapes of the GARTEUR structure with the eigenvectors of the updated FE model in case of the 4 element groups (elastic modes 1 to 3)

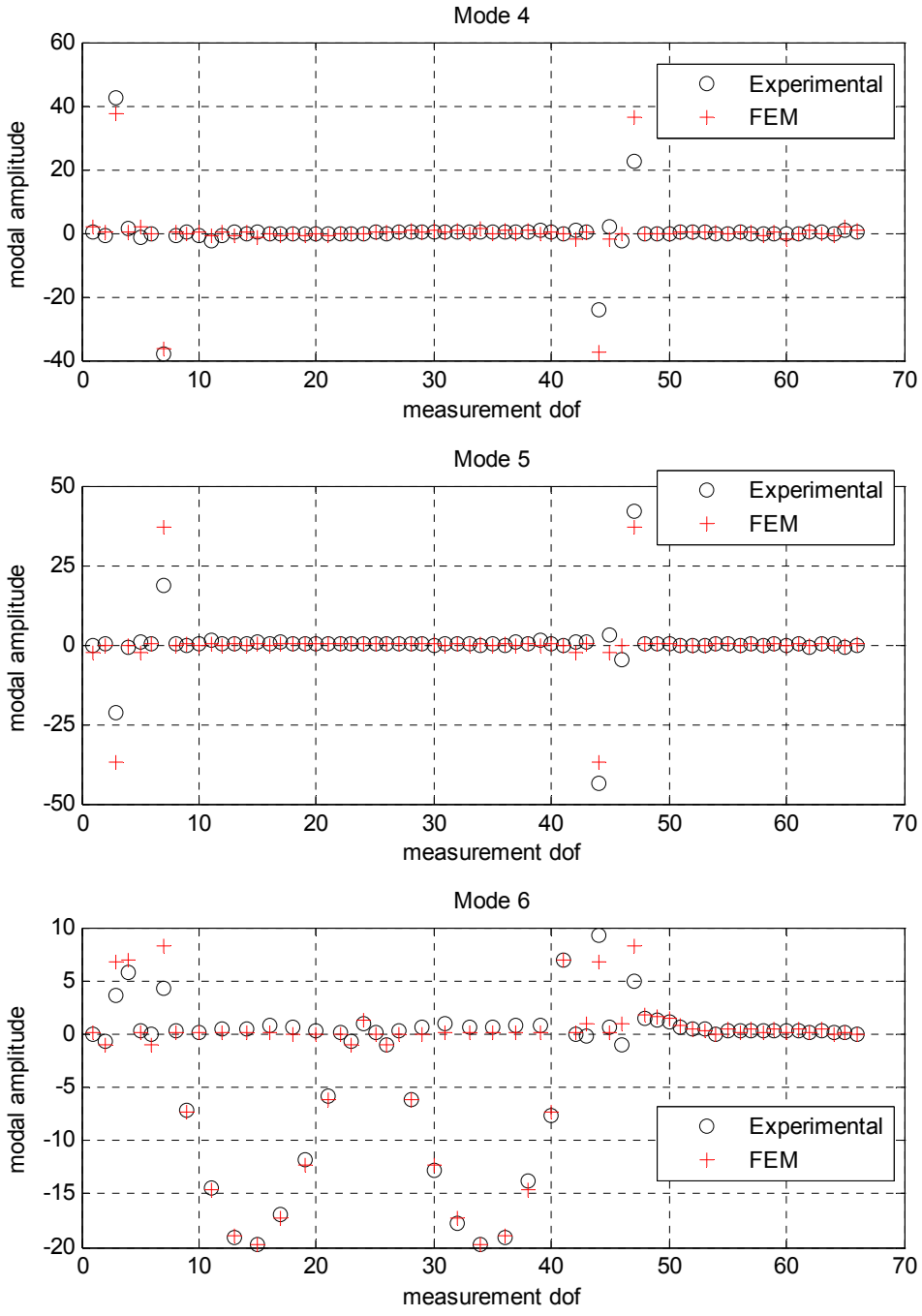

Figure 5.23. Detailed comparison of the experimental mode shapes of the GARTEUR structure with the eigenvectors of the updated FE model in case of the 4 element groups (elastic modes 4 to 6)

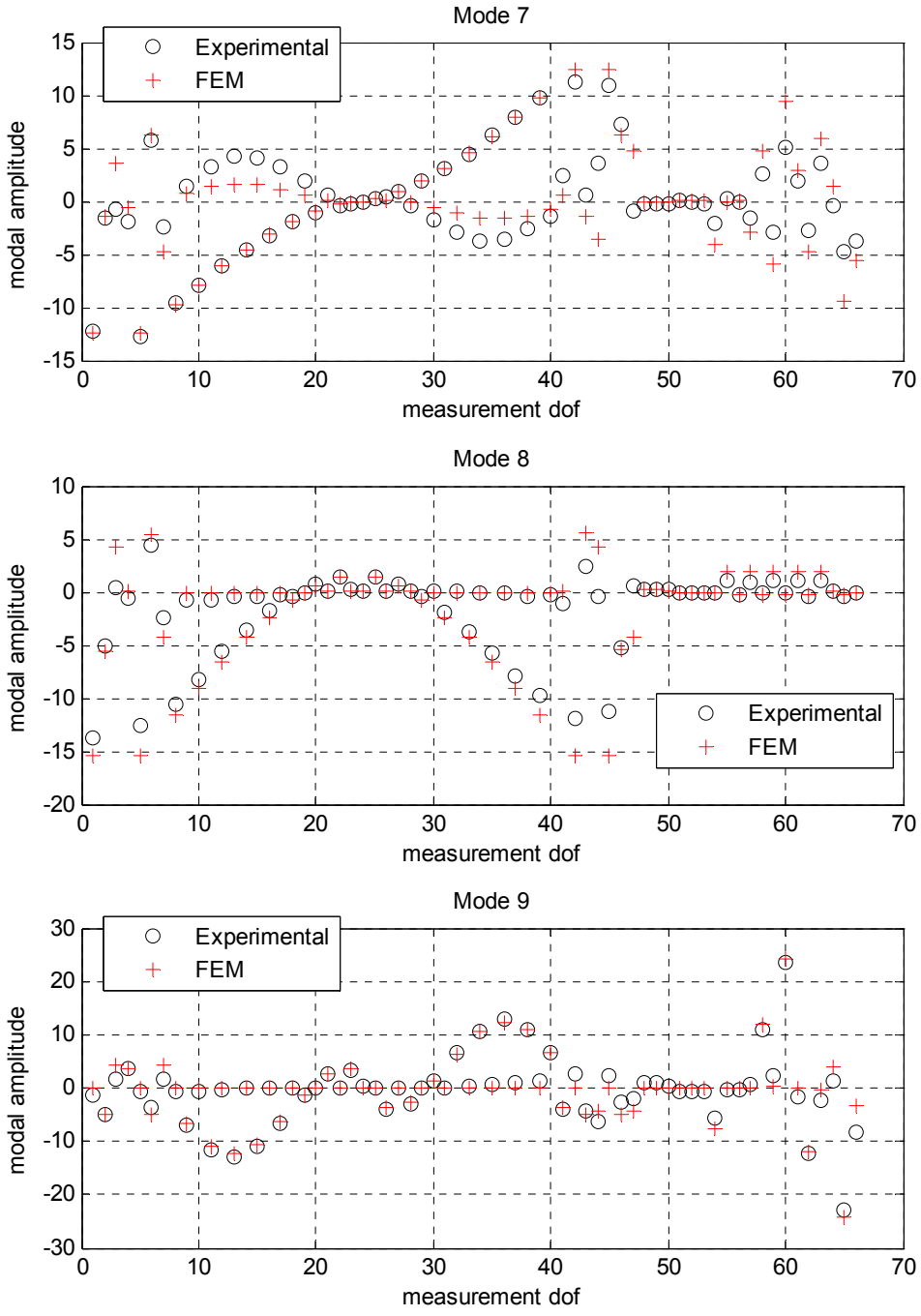

Figure 5.24. Detailed comparison of the experimental mode shapes of the GARTEUR structure with the eigenvectors of the updated FE model in case of the 4 element groups (elastic modes 7 to 9)

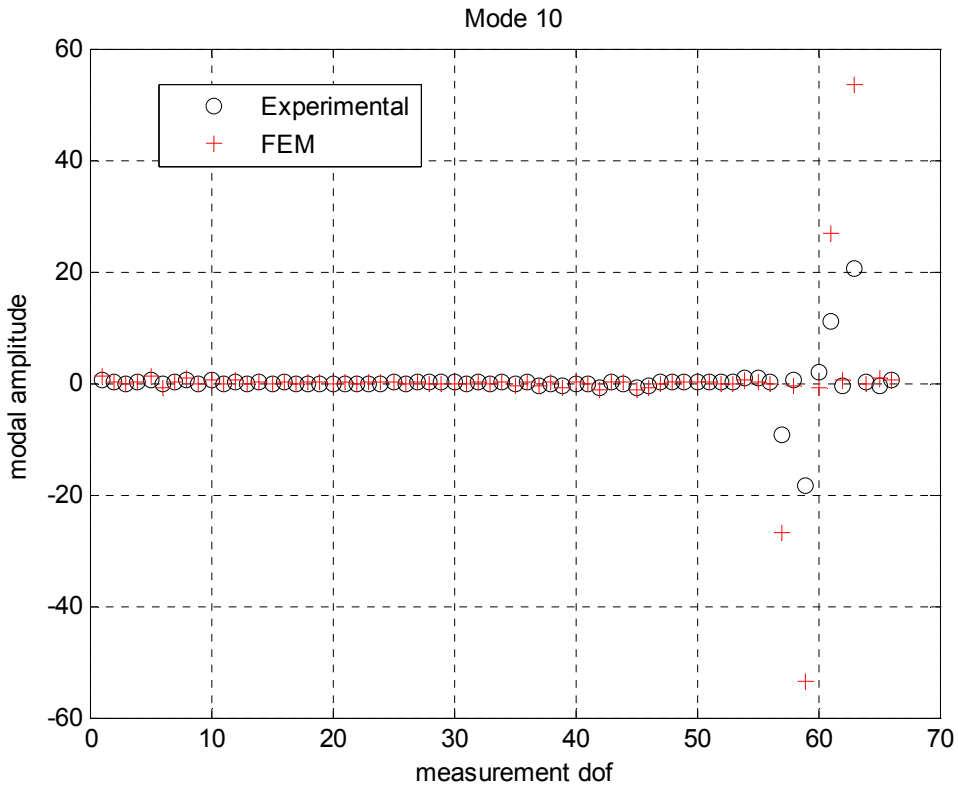

Figure 5.25. Detailed comparison of the experimental mode shapes of the GARTEUR structure with the eigenvectors of the updated FE model in case of the 4 element groups (elastic mode 10)

5.2.8. Increasing the Number of Groups During the Model Updating Procedure

In the previous section, it has been observed that 'initial' estimates of the active FE parameters cannot be obtained accurately if the structural identification equations are constructed by introducing more than 4 finite element groups. This was mainly due to the experimental error and truncated nature of the experimental normal modes. Then, during the iterative procedure as well, structural identification equations have been reconstructed with 4 element groups.

Actually, in the iterative procedure, stiffness orthogonality equations are reconstructed from the FE counterparts of the experimental modes. As a result, experimental error and error due to the Guyan's Expansion are eliminated. For that reason, during the model updating phase, structural identification equations can be constructed by dividing finite elements into more than 4 groups. This is important

because dividing finite elements into 4 groups is not realistic in case of a real aircraft structure. Increasing element groups will bring extra flexibility to the iterative solution procedure and hopefully, a much better correlation between the ultimate FE model and the experimental data will be obtained for a real aircraft structure.

Before going into the case study of the real aircraft structure, the idea of using more element groups in the iterative solution procedure has been tested for the GARTEUR structure as follows:

Since using more than 4 element groups do not improve ‘initial’ estimates of the active FE parameters, the iterative procedure has been initiated with the same initial FE model derived in section 5.2.7. Hence, the MAC comparison of the initial FE model with the experimental data is already given in Figure 5.18. Similarly, the comparison of the natural frequencies of the initial model is given in Table 5.16. However, during the updating procedure of the FE model, structural identification equations have been formulated by dividing wing elements into 4 groups instead of a single group. The group definitions of the fuselage, vertical and horizontal stabilizers were not changed. As a result, the iterative solution procedure has been accomplished with a total of 7 groups instead of 4. The results are quite satisfactory. The MAC comparison of the ultimate FE model with the experimental mode shapes is given in Figure 5.26. Moreover natural frequencies of the updated model are compared to the experimental natural frequencies in Table 5.18. The detailed comparisons of each eigenvector with the corresponding experimental mode shape are shown in Figures 5.27 to 5.30.

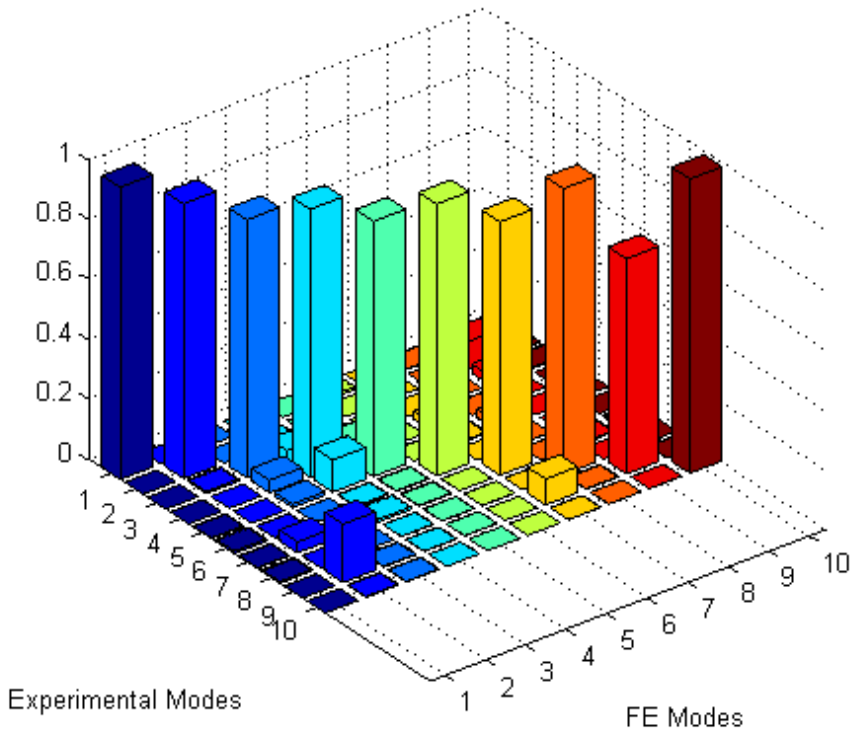

Figure 5.26. MAC comparison of the real experimental modes with the eigenvectors of the updated FE model of the GARTEUR structure in case of using 7 element groups in the iterative solution procedure

Table 5.18. Comparison of the experimental natural frequencies of the GARTEUR structure with the natural frequencies of the updated FE model in case of using 7 element groups in the iterative solution procedure

Experimental Modes	Experimental Natural Frequencies (Hz)	Corresponding Modes of the Updated FE Model	Natural Frequencies of the Updated FE Model (Hz)	Difference in the Natural Frequencies (%)
1	5.65	1	6.27	10.95
2	15.73	2	15.70	-0.21
3	36.79	3	36.79	0.00
4	37.51	4	37.57	0.17
5	37.65	5	37.59	-0.16
6	43.73	6	43.73	0.00
7	50.32	7	50.32	0.00
8	55.00	8	55.01	0.01
9	60.66	9	60.67	0.01
10	68.23	10	68.23	0.00

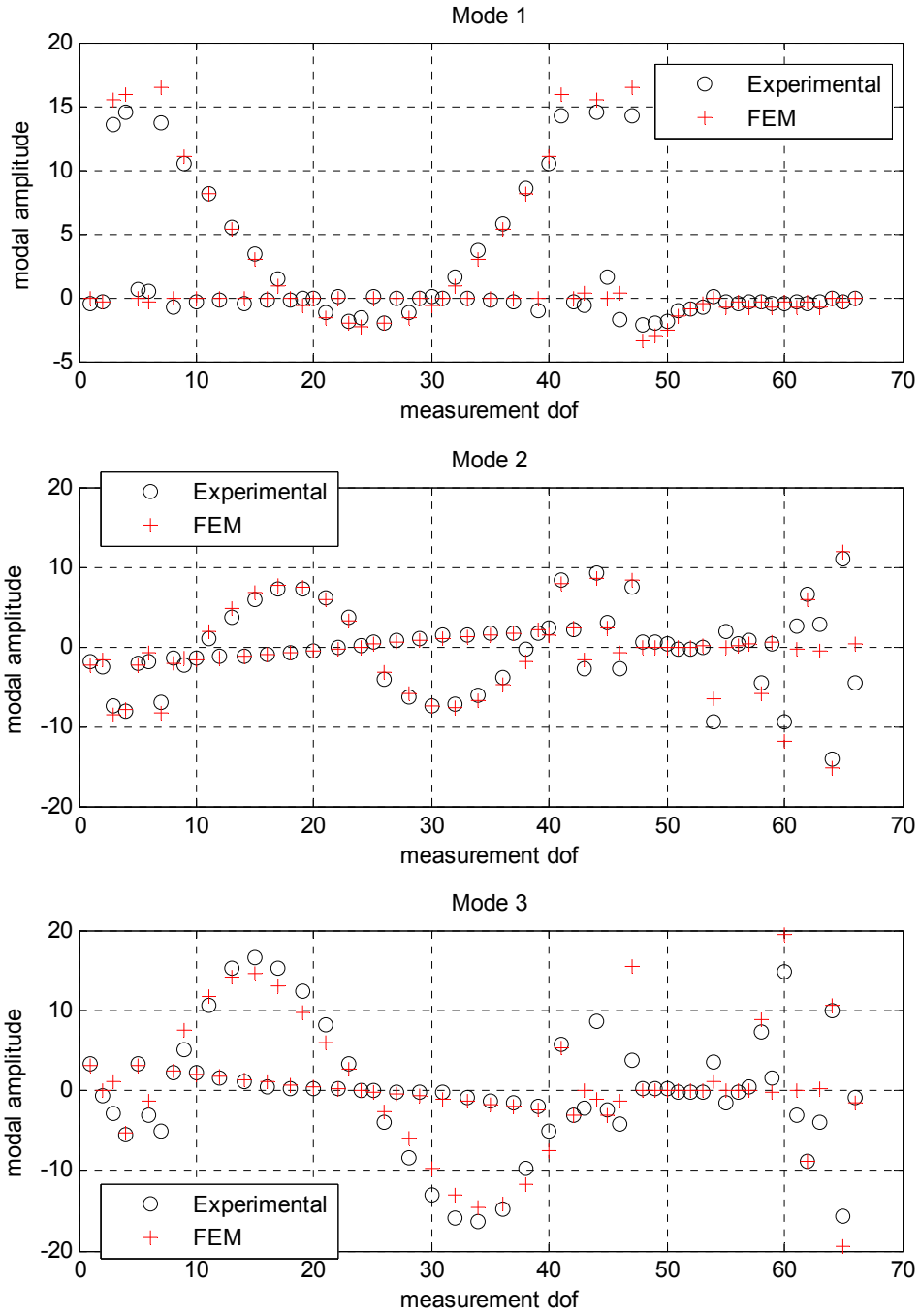

Figure 5.27. Detailed comparison of the experimental mode shapes of the GARTEUR structure with the eigenvectors of the updated FE model in case of using 7 element groups during the iterative solution procedure (elastic modes 1 to 3)

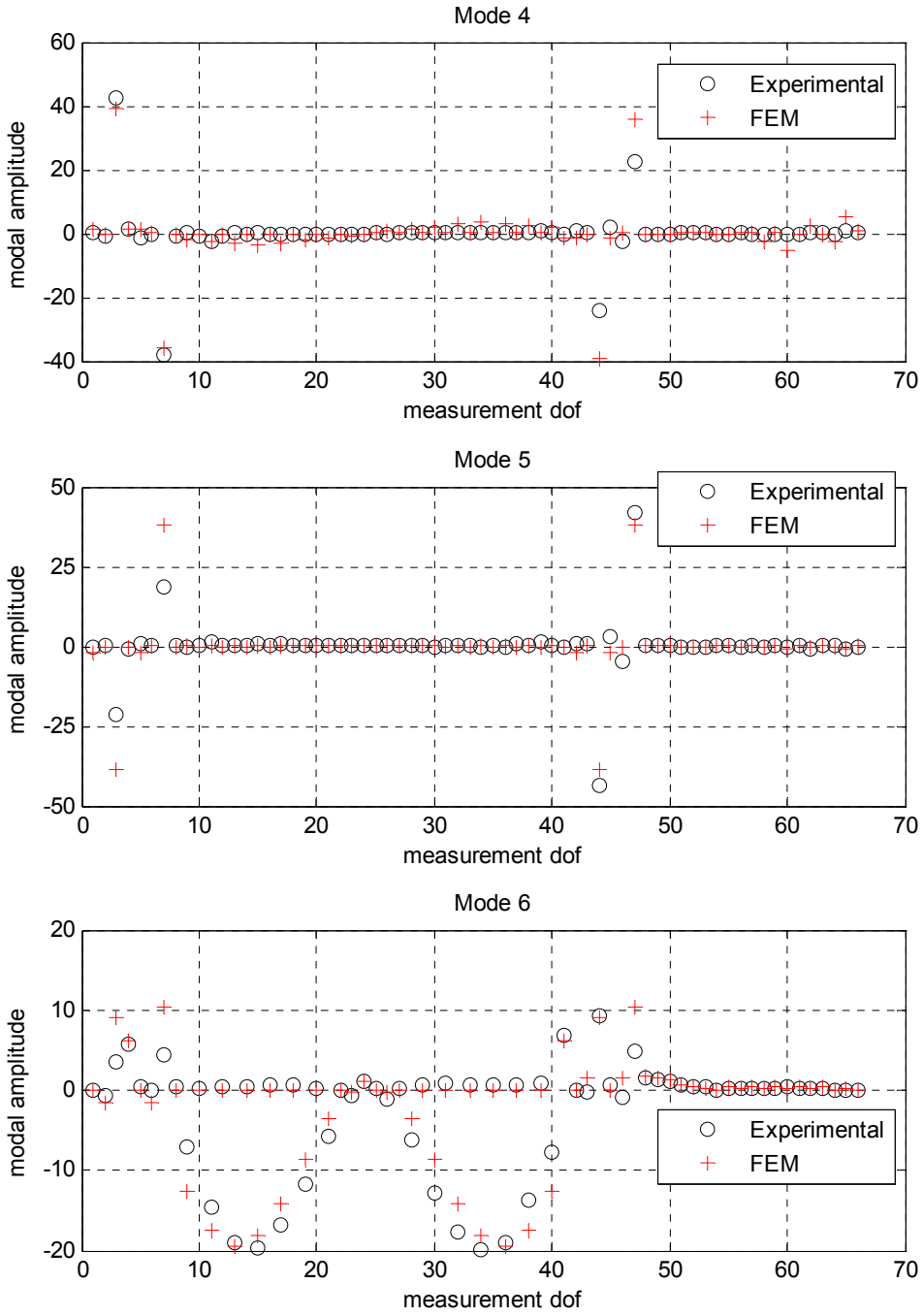

Figure 5.28. Detailed comparison of the experimental mode shapes of the GARTEUR structure with the eigenvectors of the updated FE model in case of using 7 element groups during the iterative solution procedure (elastic modes 4 to 6)

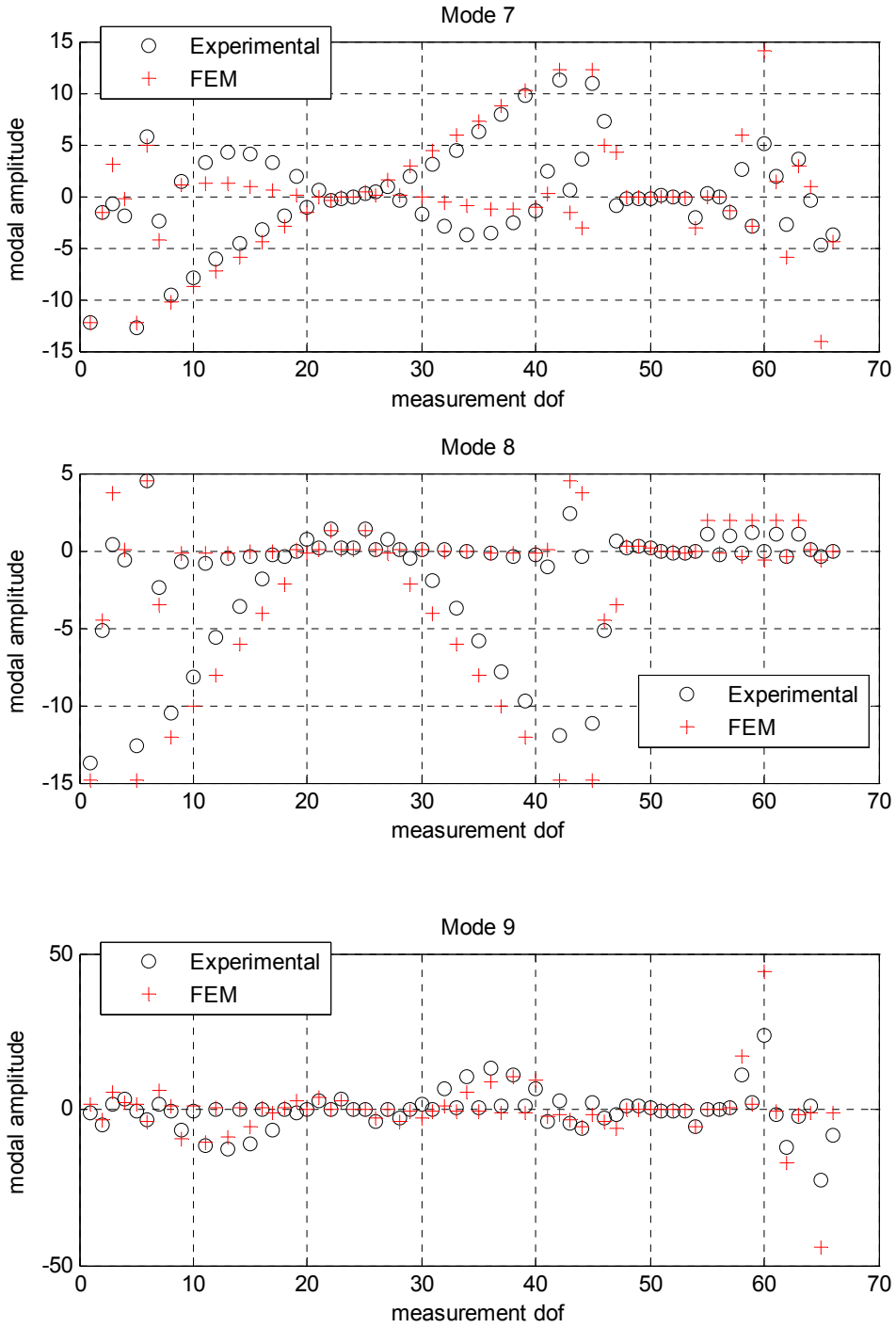

Figure 5.29. Detailed comparison of the experimental mode shapes of the GARTEUR structure with the eigenvectors of the updated FE model in case of using 7 element groups during the iterative solution procedure (elastic modes 7 to 9)

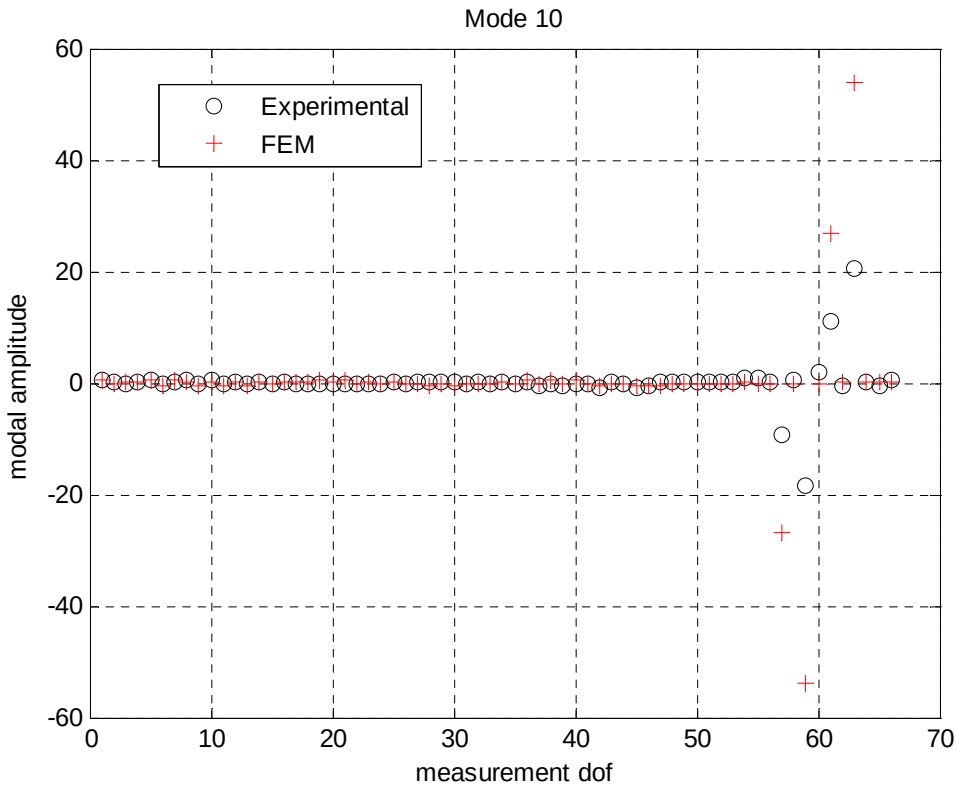

Figure 5.30. Detailed comparison of the experimental mode shapes of the GARTEUR structure with the eigenvectors of the updated FE model in case of using 7 element groups during the iterative solution procedure (elastic mode 10)

5.3. REAL AIRCRAFT STRUCTURE

In this second case study, the method developed in Chapter 3 is applied to determine FE model of a real aircraft structure by using measured modes obtained from its Ground Vibration Test (GVT).

The application of the method starts with an FE mesh constructed by connecting measurement points of the aircraft structure with 3 D Euler-Bernoulli beam elements as shown in Figures 5.31 and 5.32. The FE mesh consists of 232 beam elements, 144 nodes and 864 dofs.

GVT of an aircraft structure is accomplished for different configurations such as empty aircraft, aircraft filled with fuel, aircraft loaded with a munition etc. The experimental data used in this case study consists of the first 10 measured mode shapes using 101 measurement dofs and corresponding natural frequencies of the empty aircraft configuration.

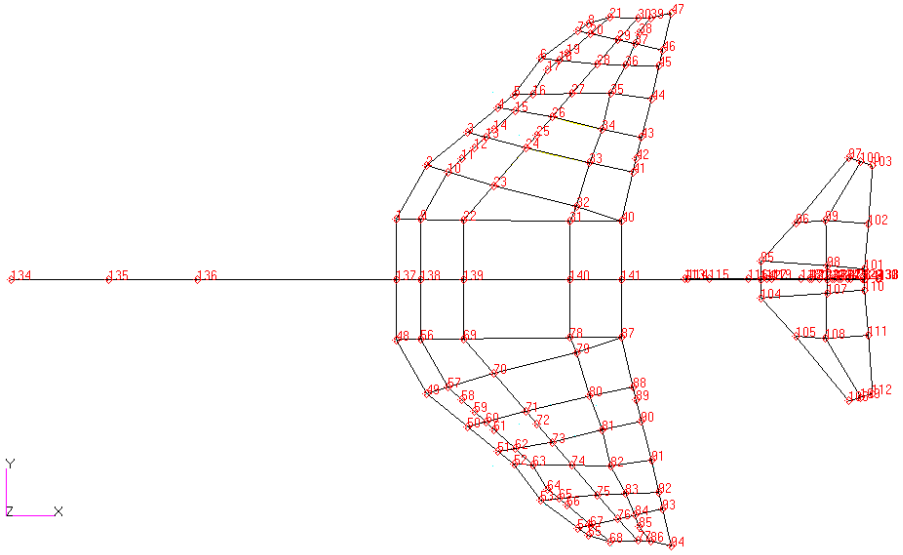

Figure 5.31. Top view of the FE mesh of a real aircraft structure obtained by connecting its GVT measurement points

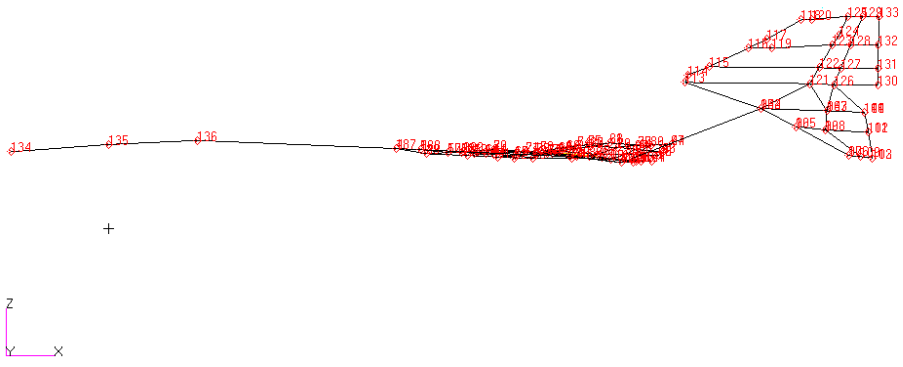

Figure 5.32. Side view of the FE mesh of a real aircraft structure obtained by connecting its GVT measurement points

After constructing an FE mesh of the aircraft structure, the next step is to determine initial estimates of geometric and material properties of the FE model. To do so, first of all, 10 measured modes are expanded to the size of the FE model by using Guyan's Expansion with an arbitrary stiffness matrix. The arbitrary stiffness matrix is obtained with the same approach used in the case study of the GARTEUR's scaled aircraft model: All beam elements are assigned geometric properties of a square cross section of unit area and material properties of aluminum.

By using 10 measured modes, it is possible to construct at most 55 structural identification equations from the mass orthogonality and another 55 equations from the stiffness orthogonality. As a result, as previously done in case study of the GARTEUR's scaled aircraft model, elements of the FE model are classified into 4 groups with the assumption that elements within the same group have the same geometric and material properties. This reduces the number of unknowns below the number of equations. Element group definitions are given in Table 5.19.

Table 5.19. Element groups of the FE model of the real aircraft structure

GROUP NO	STRUCTURAL COMPONENT
1	WING
2	HORIZONTAL STABILIZER
3	VERTICAL STABILIZER
4	FUSELAGE

After deriving structural identification equations, mass orthogonality equations are accompanied with an equality constraint that equates total mass of the FE model to the total mass of the aircraft structure measured during its GVT. Moreover, coefficients of the $(\rho AI_x)_g$ terms (subscript g stands for group number) are eliminated from equations and only $(\rho A)_g$ parameters remain as unknowns to be determined.

On the other hand, stiffness orthogonality equations are reduced by eliminating columns of the coefficient matrix that belong to $(EA)_g$, $(EI_{12})_g$ and $(GJ_e)_g$ parameters. If coefficients of those parameters are included in the stiffness orthogonality equations, physically meaningless, negative parameter estimates appear in the solution. Moreover, it degrades solutions of the active parameters, namely $(EI_1)_g$, and $(EI_2)_g$.

Solutions of the mass orthogonality equations give only estimates of $(\rho A)_g$ parameters, but in order to construct the mass matrix, estimates of $(\rho AI_x)_g$ are also required. In the case study of the GARTEUR's scaled aircraft model, it was observed that $(\rho AI_x)_g$ are not required to be as accurate as $(\rho A)_g$ parameters. As a result, rough estimates of $(\rho AI_x)_g$ were determined by calculating $(I_x)_g$ terms from estimates of cross sectional areas $(A)_g$. Estimates of $(A)_g$ terms were calculated by assigning density of aluminum to the estimates of $(\rho A)_g$ parameters. In case of a real aircraft structure, the same approach is used to obtain estimates of $(\rho AI_x)_g$ parameters and the global mass matrix of the initial FE model is completely determined.

Finally, the global stiffness matrix of the initial FE model is constructed by using estimates of the active structural parameters $(EI_1)_g$ and $(EI_2)_g$ determined from the stiffness orthogonality equations and by assigning arbitrary values to passive structural parameters several orders of magnitude larger than active terms.

MAC comparison of the eigenvectors obtained from the initial FE model with those measured experimentally is given in Figure 5.33. Moreover, percentage differences between natural frequencies found from the initial FE model and experimental ones are given in Table 5.20.

Unfortunately, starting with this initial FE model, the iterative solution procedure does not converge to an FE model correlating well with experimental data. However, by changing initial estimates of active structural parameters with a trial and error procedure, it is possible to obtain a much better initial FE model. MAC comparison of the eigenvectors obtained from that 'new' initial FE model with those measured experimentally is given in Figure 5.34. Moreover, percentage differences between

natural frequencies found from the ‘new’ initial FE model and experimental ones are given in Table 5.21.

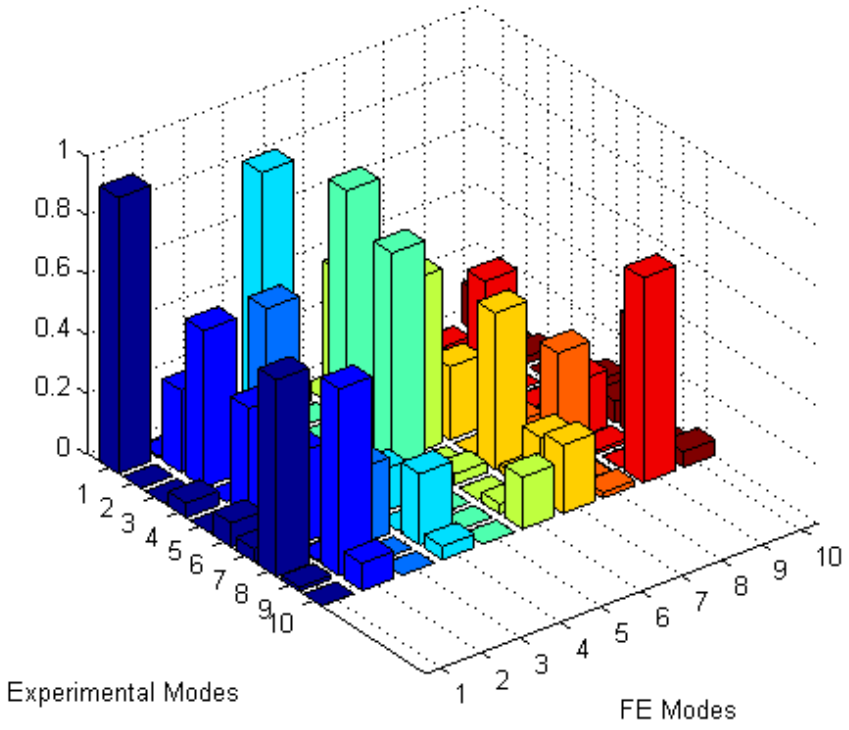

Figure 5.33. MAC comparison of experimental modes of a real aircraft structure with eigenvectors of its initial FE model in case of 4 element groups

Table 5.20. Comparison of natural frequencies of a real aircraft structure with natural frequencies of its initial FE model in case of 4 element groups

Experimental Modes	Corresponding Modes of the Initial FE Model	MAC number	Difference in the Natural Frequencies (%)
1	1	0.92	-8.39
2	4	0.90	47.28
3	2	0.53	-12.40
4	5	0.89	45.68
5	6	0.59	38.67
6	5	0.78	20.05
7	7	0.52	63.99
8	1	0.66	-57.84
9	2	0.63	-50.20
10	9	0.69	48.08

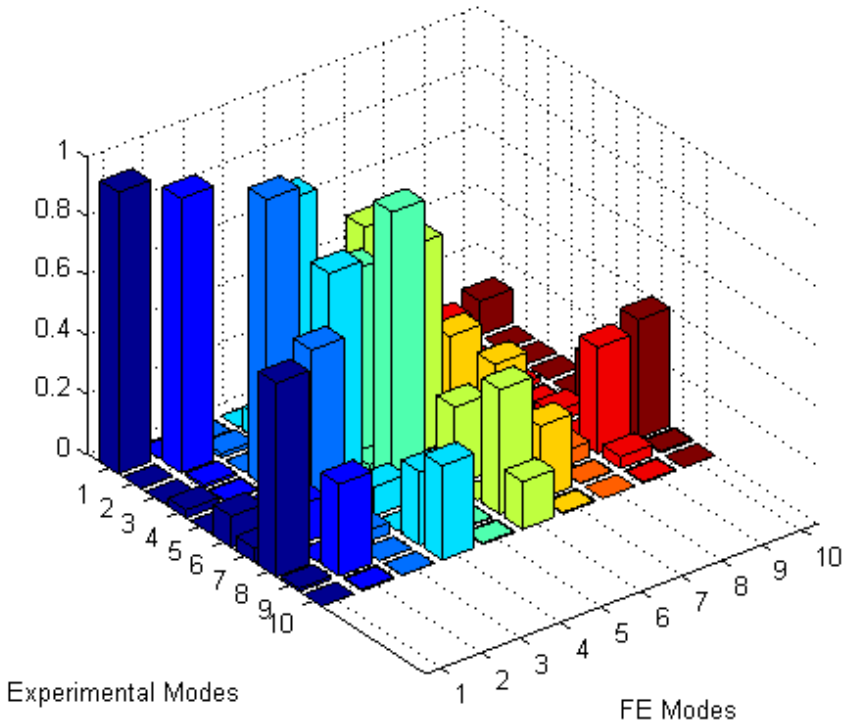

Figure 5.34. MAC comparison of experimental modes of a real aircraft structure with eigenvectors of its 'new' initial FE model in case of 4 element groups

Table 5.21. Comparison of natural frequencies of a real aircraft structure with natural frequencies of its 'new' initial FE model in case of 4 element groups

Experimental Modes	Corresponding Modes of the Initial FE Model	MAC number	Difference in the Natural Frequencies (%)
1	1	0.94	0.05
2	2	0.92	0.76
3	4	0.86	0.04
4	3	0.97	-10.29
5	4	0.71	-9.55
6	5	0.92	-17.54
7	16	0.52	181.64
8	1	0.65	-53.95
9	6	0.42	-16.62
10	4	0.32	-44.38

Starting with the 'new' initial FE model mentioned above, the iterative solution procedure achieves an FE model whose first 4 modes correlate well with

experimental data. MAC comparison of that updated FE model with measured modes is given in Figure 5.35. Moreover, percentage differences between natural frequencies of the updated FE model and experimental natural frequencies are given in Table 5.22.

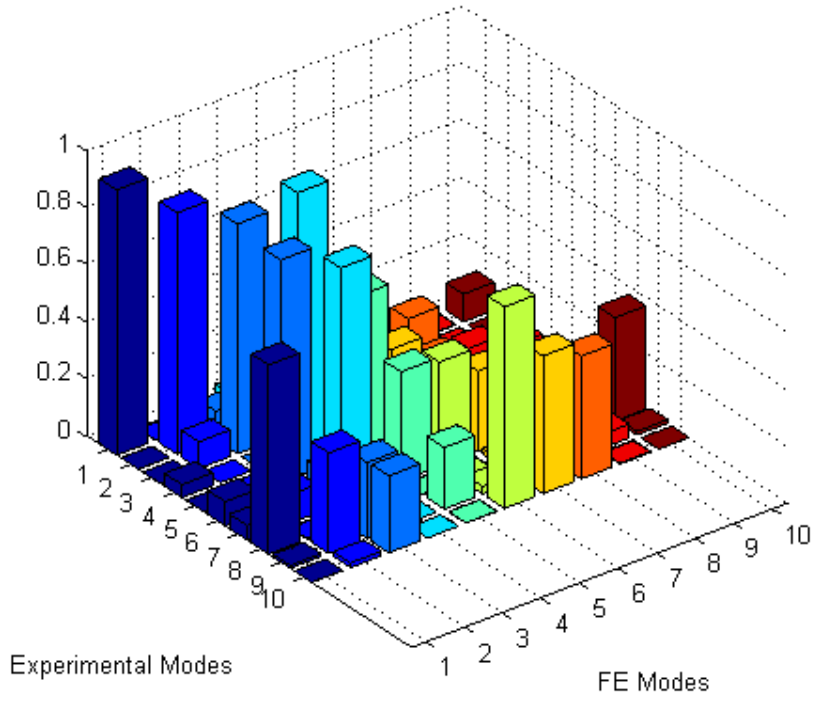

Figure 5.35. MAC comparison of experimental modes of a real aircraft structure with eigenvectors of its updated FE model in case of 4 element groups

Table 5.22. Comparison of natural frequencies of a real aircraft structure with natural frequencies of its updated FE model in case of 4 element groups

Experimental Modes	Corresponding Modes of the Updated FE Model	MAC number	Difference in the Natural Frequencies (%)
1	1	0.93	-9.44
2	2	0.84	-5.43
3	3	0.80	2.89
4	4	0.91	1.58

History plots of the structural parameters during the iterative solution procedures are given in Figures 5.36 to 5.38. Finally, detailed comparison of the first 4 modes of the updated FE model with the corresponding experimental modes are given in Figures 5.39 to 5.42.

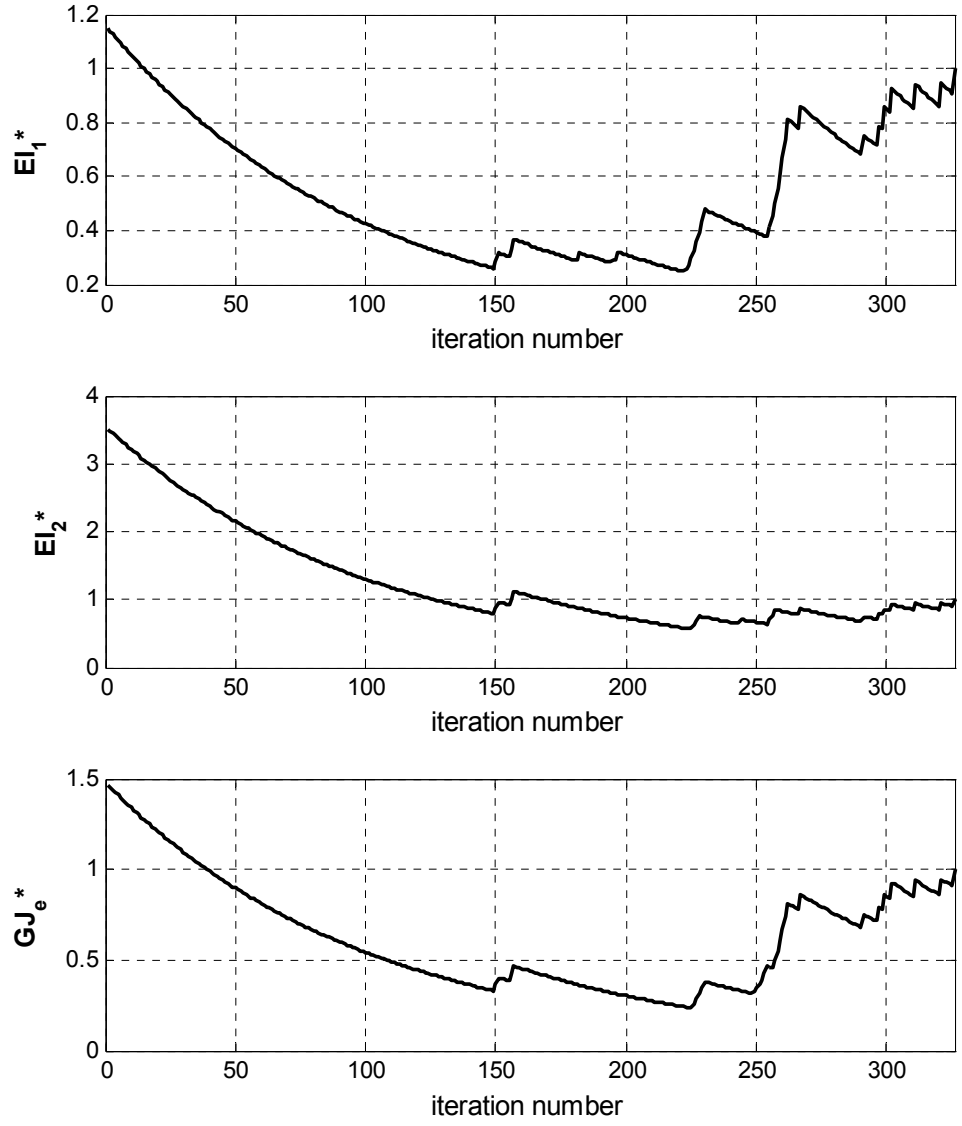

Figure 5.36. History plots of the structural parameters that belong to the wing elements of the FE model derived from experimental data of a real aircraft structure in case of 4 element groups

It is concluded that the method developed herein is a promising technique to determine FE models of real aircraft structures but it requires further improvements because correlation of the first 4 elastic modes is not sufficient for a reliable flutter analysis. Detailed discussion of the results, important conclusions and various recommendations for future work to improve the method are given in Chapter 6.

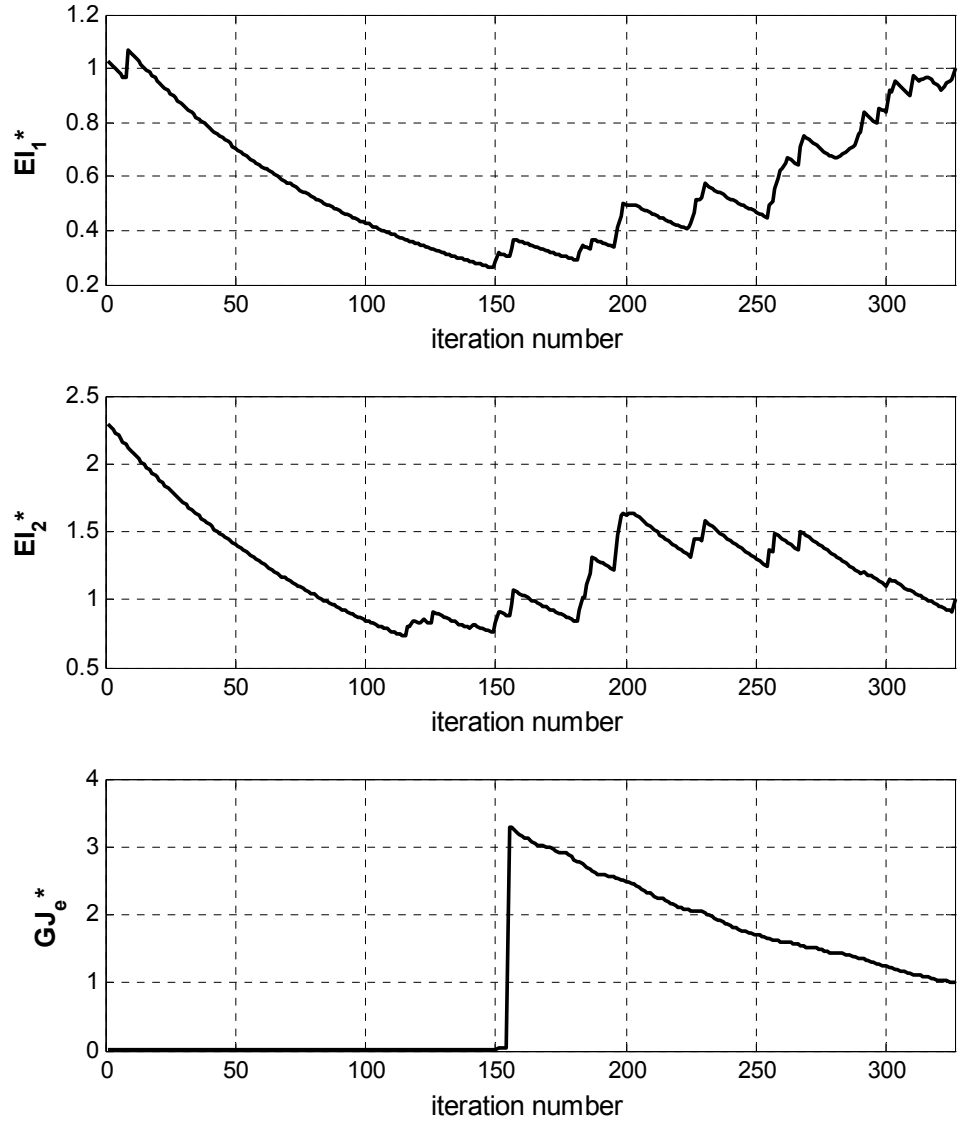

Figure 5.37. History plots of the structural parameters that belong to the horizontal stabilizer of the FE model derived from experimental data of a real aircraft structure in case of 4 element groups

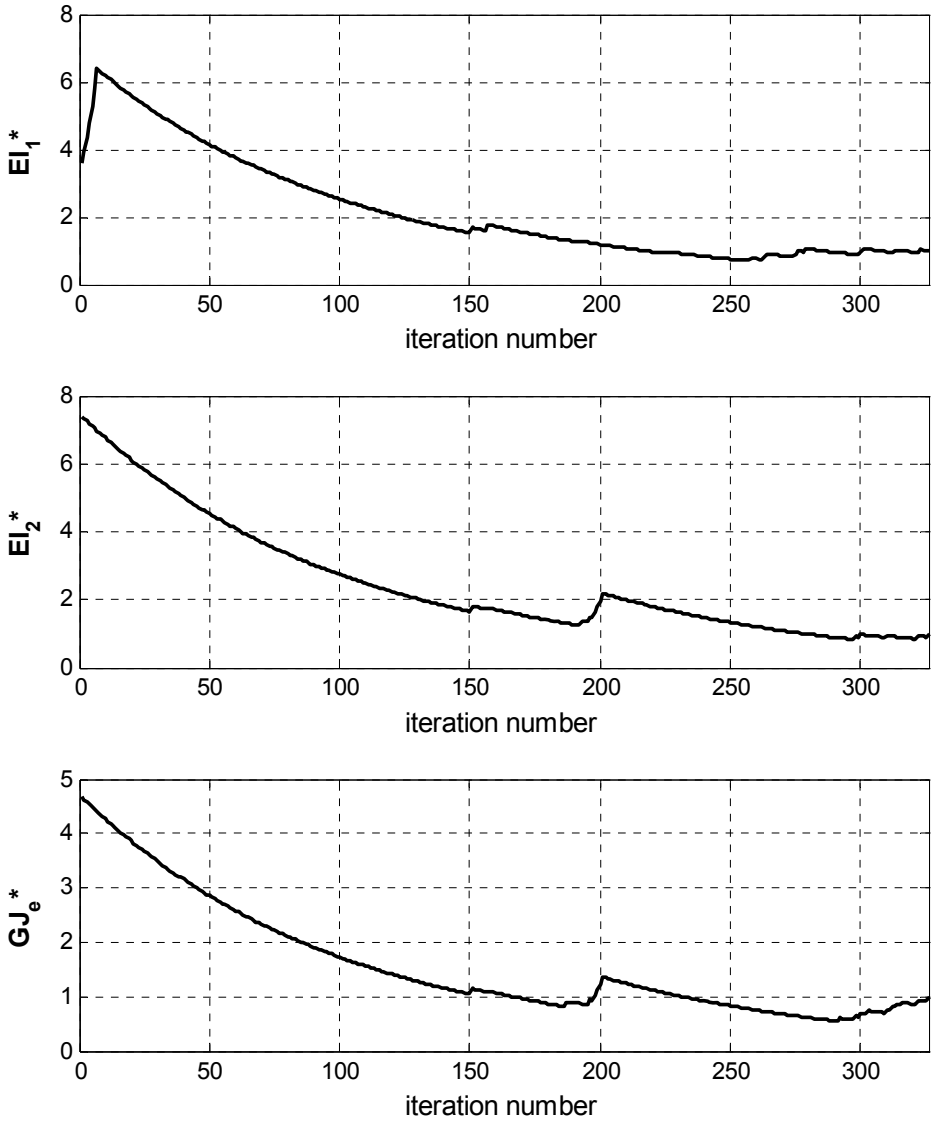

Figure 5.38. History plots of the structural parameters that belong to the vertical stabilizer of the FE model derived from experimental data of a real aircraft structure in case of 4 element groups

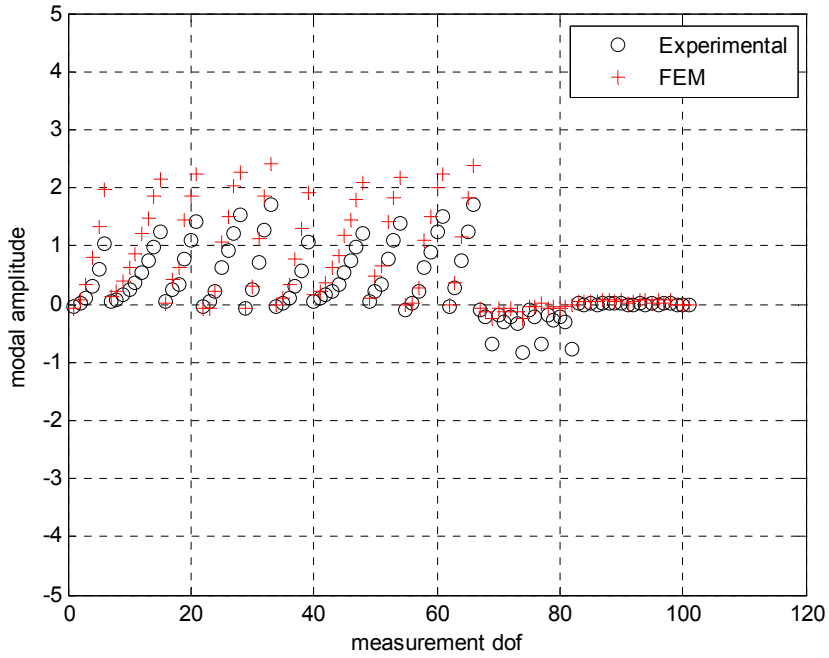

Figure 5.39. Detailed comparison of the 1st elastic experimental mode shape of a real aircraft structure with the 1st elastic mode shape of the updated FE model in case of 4 element groups

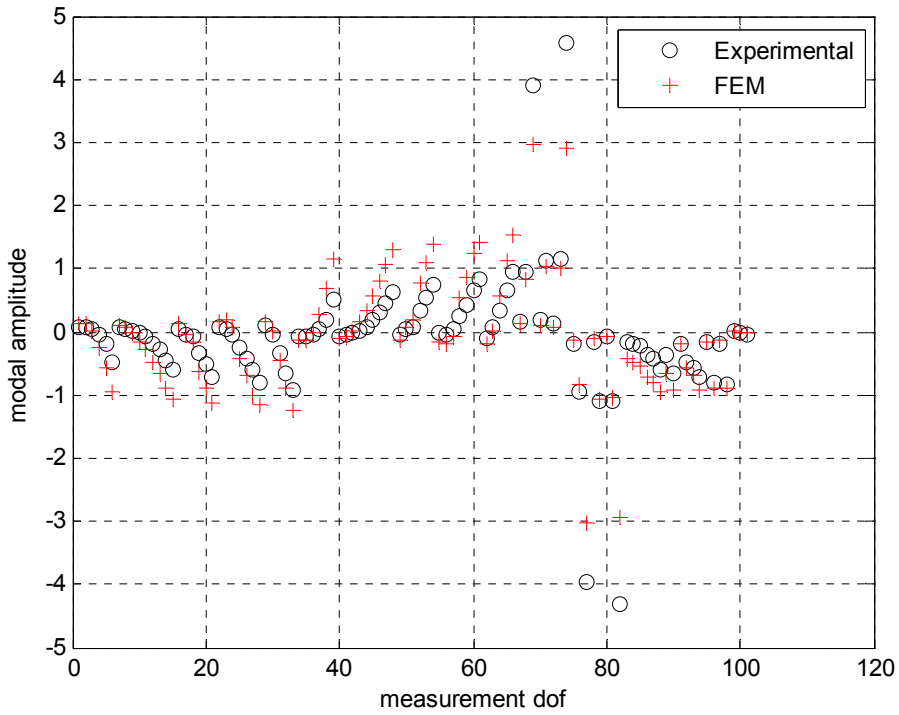

Figure 5.40. Detailed comparison of the 2nd elastic experimental mode shape of a real aircraft structure with the 2nd elastic mode shape of the updated FE model in case of 4 element groups

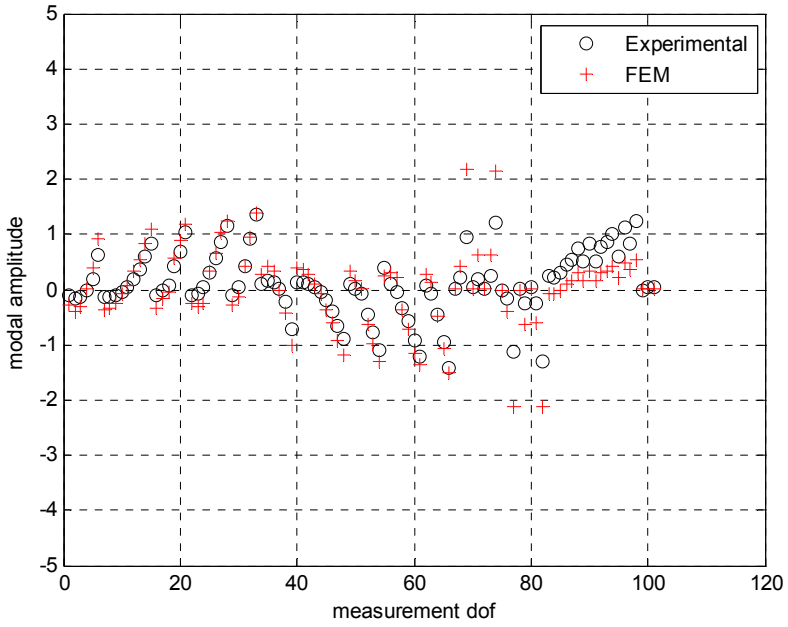

Figure 5.41. Detailed comparison of the 3rd elastic experimental mode shape of a real aircraft structure with the 3rd elastic mode shape of the updated FE model in case of 4 element groups

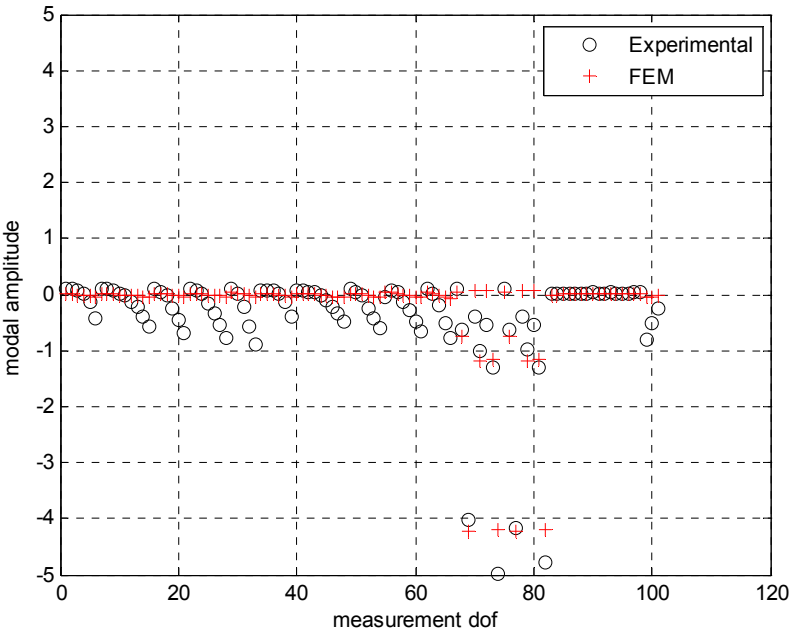

Figure 5.42. Detailed comparison of the 4th elastic experimental mode shape of a real aircraft structure with the 4th elastic mode shape of the updated FE model in case of 4 element groups

CHAPTER 6

DISCUSSION, CONCLUSIONS AND RECOMMENDATIONS FOR FUTURE WORK

6.1. DISCUSSION

The theory developed in this thesis work aimed to overcome important disadvantages of the state-of-the art model updating techniques used to determine FE models of real aircraft structures correlating well with experimental modal data. One such disadvantage stems from the requirement of a relatively accurate initial FE model of the aircraft structure to guarantee convergence to an ultimate FE model in good correlation with measured modes. The general trend to satisfy such a requirement is to construct a very detailed, complex initial FE model that duplicates morphology of a real aircraft as much as possible. Of course, this approach requires enormous time and engineering work which makes it a real disadvantage. To overcome this problem, may be for the first time, the following critical question that attacks the aforementioned prejudice about the complexity level of an initial FE model was asked: Is it really a must to conduct the model updating with the conventional FE mesh that duplicates the morphology of a real aircraft structure? To find an answer, the method developed in this thesis work used a very simple FE mesh constructed by connecting measurement points used in the Ground Vibration Test (GVT) of an aircraft structure with 3 D Euler Bernoulli beam elements. This approach became successful to some extend as discussed in the subsequent sections.

Another disadvantage of currently available model updating techniques is related to their iterative updating procedure. Most common indirect model updating methods such as the Inverse Eigen Sensitivity Method makes use of sensitivities of experimental mode shapes and natural frequencies with respect to FE parameters to correct analytical models of aircraft structures. Sensitivity analysis is

accomplished by giving small perturbations to structural parameters which result some changes in natural frequencies and components of normal modes. The ratio of those changes to perturbations of FE parameters gives a measure of sensitivity of modal parameters to structural parameters. With that perturbation approach, the sensitivity analysis becomes a black box that avoids the analyst to develop a deeper understanding about the physical mechanism that makes modal properties more sensitive to certain FE parameters than others. At this point, the method developed herein opens that black box by converting mass and stiffness orthogonality relations of experimental normal modes into appropriate structural identification equations that relate FE parameters of an aircraft structure to the experimental natural frequencies. In the first case study of Chapter 5 related with the GARTEUR's scaled aircraft model, it is shown that each self orthogonality equation derived from the stiffness orthogonality of a mode shape is proportional to a physical quantity, namely the strain energy of that mode shape. Coefficient of each structural parameter in a self orthogonality equation is a measure of contribution of that parameter to the strain energy of the relevant mode. Parameters with large coefficients are called 'active' parameters. On the other hand, parameters with small coefficients are called 'passive' structural parameters. Modal properties are more sensitive to active parameters than passive structural parameters. Obviously, structural identification equations developed in this thesis work are more useful than perturbation method to see the big picture and to choose the most appropriate design parameters in order to correct FE model of a real aircraft structure.

The method of this thesis work also shows that structural identification equations mentioned above are very useful both in the initial estimates of FE parameters and in the subsequent updating procedure of those parameters to obtain an ultimate FE model correlating well with experimental data.

Although the method developed herein has several advantages over currently available model updating methods, it is not perfect. It brings its own challenges and drawbacks. All these problems are discussed in the next section.

6.2. CONCLUSIONS

Considering the theory introduced in Chapter 3 and results of the case studies given in Chapter 5, the following conclusions are obtained:

- Application of the theory introduced in Chapter 3 to the scaled aircraft model developed by GARTEUR gave the opportunity to determine and solve practical problems that stem from experimental error and error due to expansion of the truncated measured modes. As a result, the method has been improved further and by using only the first 10 measured elastic modes of the GARTEUR's scaled aircraft model, dynamically equivalent FE model of that structure correlating well with experimental modal data has been obtained successfully.

- The method of this thesis work showed that it is possible to obtain FE model of a real aircraft structure correlating well with experimental data by using a much simpler FE mesh than conventional method based on duplicating morphology of a real aircraft structure. In the second case study of Chapter 5, an FE model whose first 4 elastic modes correlating well with the first 4 measured modes of a real aircraft structure has been successfully obtained.

- Of course, correlation of the first 4 elastic modes is not sufficient for reliable aeroelastic analysis of an aircraft structure. For the time being, there are several problems that avoid correlation of more than 4 modes: First of all, structural identification equations used to determine initial estimates of structural parameters are derived from truncated experimental mode shapes. Experimental error and error introduced during the expansion of measured modes to the size of the FE model considerably degrade solutions of structural identification equations. As a result, relatively rough estimates of structural parameters are obtained. With these rough parameter estimates, at least in the case study of Chapter 5, it was not possible to obtain an initial FE model including FE counterparts of all first 10 measured modes of a real aircraft structure. Secondly, in order to reduce number of unknown parameters below limited number of structural identification equations, FE parameters have been classified into few groups with the assumption that elements within the same group have the same geometric and material properties. This assumption is not very realistic for a real aircraft structure and it imposes too much constraint on the correction of the FE parameters. As a result, achieving a much better correlation becomes a challenge.

  In any way, it has to be remembered that the method developed herein successfully obtained FE model of a real aircraft structure whose first 4 elastic modes correlating well with experimental modal data. In doing this, much less

effort has been spent than common model updating procedures. For that reason, the theory developed herein merits to be studied and improved further because if appropriate improvements can be achieved, it is a promising method that may replace common model updating techniques in near future. Accordingly, some important recommendations for future work to improve the method are given in the next section.

6.3. RECOMMENDATIONS FOR FUTURE WORK

In the method developed herein, structural identification equations used to determine initial estimates of FE parameters are derived from experimental normal modes expanded the size of the FE model. Currently, the expansion procedure is accomplished by using Guyan's expansion with an arbitrary stiffness matrix. Of course, this is not an exact method and it introduces some error to the structural identification equations degrading accuracy of initial estimates of FE parameters. As an alternative approach, unmeasured degrees of freedom (dofs) of an aircraft structure such as rotational dofs can be estimated by fitting surface splines to the measured dofs. Smooth surface splines may result more accurate estimates of slave coordinates compared to the Guyan's Expansion that does guarantee smoothness of the expanded experimental mode shapes. This approach worth to be studied because it may improve accuracy of the structural identification equations and hopefully a much better initial FE model may be obtained for an aircraft structure. This is important because an accurate initial FE model has a very important role on the determination of an ultimate FE model correlating well with experimental data.

Another important recommendation aims to bring some relaxation to the approach that divides FE elements into few element groups and that forces elements within the same group to have the same geometric and material properties. In the current approach, element group are fixed at the beginning of the iterative procedure and they are not changed throughout the iterations. As an alternative approach, a dynamic group definition that changes throughout the iterative procedure several times may be used. This may bring extra flexibility to the updated FE parameters and eventually a much better correlation between FE model and experimental data may be obtained.

A final recommendation will be made to improve the iterative procedure. In the current iterative algorithm, structural identification equations obtained from the stiffness orthogonality are constructed by using FE counterparts of experimental mode shapes. Unfortunately, in case of a real aircraft structure initial FE model may not include FE counterparts of all experimental modes at a good correlation level. In such a case, substituting expanded experimental modes with eigenvectors representing the same mode shape at a poor correlation level may improve iterative procedure.

REFERENCES

[1] A. Berman, William G. Flannelly, *Theory of Incomplete Models of Dynamic Structures.* AIAA Journal, 9(8), 1481-1486, 1971

[2] Thoren, A. R., *Derivation of Mass and Stiffness Matrices from Dynamic Test Data*. AIAA Paper, AIAA/ASME/SAE 13th Structures, Structural Dynamics and Materials Conference, San Antonio, Texas, April 1972

[3] Collins, J.D., Hart, G. C., Hasselman, T.K., and Kennedy, B., *Statistical Identification of Structures*. AIAA Journal, 12, 185-190, February 1974

[4] Berman, A., *System Identification of a Complex Structure*. AIAA Paper, 75-809, AIAA/ASME/SAE 16th Structures, Structural Dynamics and Materials Conference, Denver, Colo., May 1975

[5] Menahem Baruch, Itzhack Y. Bar Itzhack, *Optimal Weighted Orthogonalization of Measured Modes.* AIAA Journal, 16(4), 346-351, 1978

[6] A. Berman, E.J. Nagy, *Improvement of a Large Analytical Model Using Test Data.* AIAA Journal, 21(8), 1168-1173, 1983

[7] J. Sidhu, D.J. Ewins, *Correlation of Finite Element and Modal Test Studies of a Practical Structure*. Proc of 2nd IMAC, 756-762, Orlando, Florida 1984

[8] Menahem Baruch, *Methods of Reference Basis for Identification of Linear Dynamic Structures.* Vol. 22(4), 561-663, 1984

[9] B. Ceasar, *Update and Identification of Dynamic Mathematical Models. Proc of 4th IMAC*, 394-401, Los Angeles, California 1986.

[10] H.P. Gypsin, *Critical Application of the Error Matrix Method for Localization of FE Modeling Inaccuracies*. Proceedings of 4th IMAC, 1339-1351, K.U.Leuven, 1986

[11] Choudhury, R.A., Llieonart, G., He, J., *A New Approach for Identification of Spatial Matrices by Using Measured Frequency Response Function Data.* Proc. of IMAC 1995, 1484-1489, Nashville, Tenessee, 13-16 Feb., 1995

[12] Mastroddi, F., Benedetti, L., *A Generalization of Spatial Model Identification by Using FRF Data*. ESA Conference on Spacecraft Structures, Materials and Mechanical Testing, 1319-1326, Noordwijk, The Netherlands, 27-29 March 1996

[13] J. Carvalho, B. N. Datta, A. Gupta and M. Lagadapati, A Direct Method for Model Updating with Incomplete Measured Data and with Spurious Modes, Mechanical Systems and Signal Processing, 21, 2715-2731, 2007

[14] R. L. Fox, M. P. Kapoor, *Rate of Change of Eigenvectors and Eigenvalues*, *AIAA Journal 12*(6), 2426-2429, 1968

[15] J.M.W. Lee, G.R. Parker, *Application of Design Sensitivity Analysis to Improve Correlation between Analytical and Test Mode*. MSC 1989 World Users' Conference Proceedings, Los Angeles, California, USA, 1989

[16] D. Göge, 2003, *Automatic Updating of Large Aircraft Models Using Experimental Data from Ground Vibration Testing*. Aerospace Science and Technology 7 33-45, 2003

[17] M. Tuğrul Kozak, *Investigation of Model Updating Techniques and Their Applications to Aircraft Structure.* MS Thesis, Department of Mechanical Engineering, METU, 2006

[18] M.T. Kozak, M. Öztürk, H.N. Özgüven, *A Method in Model Updating Using Miscorrelation Index Sensitivity*. Mechanical Systems and Signal Processing, 23(6), 1747-1758, 2008

[19] J.N. Reddy, *An Introduction to the Finite Element Method*, Third Edition, McGraw-Hill

[20] Young W. Known, Hyochoong Bang, *The Finite Element Method Using MATLAB*. CRC Press

[21] A. Berman, *Mass Matrix Correction Using An Incomplete Set of Measured Modes*, AIAA Journal, 17(10), 1147-1148, October 1979

[22] A. Berman, *Comment on Optimal Weighted Orthogonalization of Measured Modes*. AIAA Journal, 17(8), 927-928, August 1979

[23] Guyan R. J., *Reduction of Mass and Stiffness Matrices.* AIAA Journal, Vol. 3, 380, 1965

[24] Heylen W., *Optimization of Model Matrices by Means of Experimentally Obtained Dynamic Data.* Proceedings of 1th IMAC, 33-38, Orlando Florida, 1982

[25] http://en.wikipedia.org

APPENDIX A

VARIATIONAL PRINCIPLES IN STRUCTURAL MECHANICS

A.1. INTRODUCTION

The static and/or dynamic equilibrium equations of large and complex structures such as an aircraft structure cannot be solved exactly. Therefore, in order to solve complex engineering problems, an approximate solution procedure called '*the finite element* (FE) *method*' has been developed in the last century. In a structural mechanical sense, the FE method divides an intricate structural domain into simpler subdomains i.e. finite elements and seeks an approximate solution of the governing equilibrium equations over each subdomain. Assembly of the subdomain solutions finally gives rise to the global solution for the entire structure.

Since the focal point of this thesis study is the development and investigation of a novel method to derive the FE model of a real aircraft structure, it is very meaningful to introduce the general procedure followed in the derivation of FE formulation of engineering structures.

The development of the FE method starts with the derivation of the equilibrium equations of an engineering structure by an appropriate variational principle. For that reason, Appendix A is dedicated to the introduction of two fundamental variational principles: '*Minimization of Total Potential Energy*' and '*Hamilton's Principle*'.

A.2. MINIMIZATION OF TOTAL POTENTIAL ENERGY

'*Minimization of Total Potential Energy*' is a variational principle that applies only to elastic (linear or nonlinear) continua. Its mathematical formulation starts with the following implicit definition of the strain energy function at a point in a structure:

$$\sigma_{ij} = \frac{\partial U_0}{\partial \varepsilon_{ij}} \tag{A.1}$$

where U_0 is the strain energy, σ_{ij} are the stress components and ε_{ij} are the strain components.

Reformulating equation (A.1), the definition of the strain energy can be put in an explicit form as follows:

$$U_0 = \int_0^{\varepsilon_{ij}} \sigma_{ij}\, d\varepsilon_{ij} \tag{A.2}$$

For linear elastic bodies, the integral expression of equation (A.2) is evaluated as follows:

$$\int_0^{\varepsilon_{ij}} \sigma_{ij}\, d\varepsilon_{ij} = \frac{1}{2}\sigma_{ij}\ \varepsilon_{ij} \tag{A.3}$$

The total strain energy of a linear elastic structure over its entire volume is then expressed as below:

$$U = \int_V U_0\, dV = \int_V \frac{1}{2}\sigma_{ij}\ \varepsilon_{ij}\ dV \tag{A.4}$$

The total strain energy is nothing but the internal reaction of a structure to the externally applied body and surface forces. And the potential energy of the external body and surface traction forces is given as follows:

$$V = -\int_V f_i\ u_i\ dV\ - \int_S t_i\ u_i\ dS \tag{A.5}$$

where f_i are the components of the total body force per unit volume, t_i are the components of the total surface traction force per unit surface and u_i are the components of the displacement field.

The total potential energy of a linear elastic body in 3 D is defined as:

$$\Pi = U + V \tag{A.6}$$

Hence,

$$\Pi = \int_V \frac{1}{2}\sigma_{ij}\ \varepsilon_{ij}\ dV - \int_V f_i\ u_i\ dV - \int_S t_i\ u_i\ dS \tag{A.7}$$

'*Minimization of Total Potential Energy*' or '*The Principle of Stationary Potential Energy*' states that a linear elastic structure subjected to body and surface traction forces deforms in a manner to minimize its total potential energy.

Mathematically, minimum total potential energy of a linear elastic structure is achieved by equating the first variation of its total potential energy to zero as follows:

$$\delta\ \Pi = 0 \tag{A.8}$$

More explicitly,

$$\delta\ \Pi = \delta\ U + \delta\ V = 0 \tag{A.9}$$

Hence,

$$\int_V \sigma_{ij}\ \delta\varepsilon_{ij}\ dV - \int_V f_i\ \delta u_i\ dV - \int_S t_i\ \delta u_i\ dS = 0 \tag{A.10}$$

Equation (A.10) is a general expression applicable to the linear structures with any degree of complexity (in the elastic region) and is used to derive the static equilibrium equations, the solution of which gives the deformation field of the relevant structure.

Engineering structures are not always subjected to the static loading. In case of the dynamic problems, dynamic equilibrium equations have to be derived. This is accomplished by the application of another variational principle called '*Hamilton's Principle*' which is the subject of the next section.

A.3. HAMILTON'S PRINCIPLE

The main assumption of the '*Hamilton's Principle*' is that an ideal conservative linear elastic structure can be characterized by two energy functions: the kinetic energy K and the potential energy Π.

The definition of the potential energy Π of a linear elastic body has been already given within the expression (A.7). The definition of its kinetic energy K is given as follows:

$$K = \int_V \frac{1}{2}\rho \frac{\partial u_i}{\partial t} \frac{\partial u_i}{\partial t} \, dV \tag{A.11}$$

where ρ is the density and u_i are the components of the displacement field.

Before introducing '*Hamilton's Principle*', a final definition, namely '*Lagrangian*' of an elastic body has to be given:

$$L = K - \Pi \tag{A.12}$$

Hamilton's Principle states that the deformation history of a linear elastic structure between times t_1 and t_2 develops in a manner to minimize the time integral of its Lagrangian.

Mathematically, the time integral of the Lagrangian L of a linear elastic body subjected to dynamic loads is minimized by equating its first variation to zero as follows:

$$\delta \int_{t_1}^{t_2} L \, dt = 0 \tag{A.13}$$

More explicitly,

$$\int_{t_1}^{t_2} \left\{ \int_V \rho \frac{\partial^2 u_i}{\partial t^2} \delta u_i \, dV - \int_V \sigma_{ij} \delta \varepsilon_{ij} \, dV + \int_V f_i \, \delta u_i \, dV + \int_S t_i \, \delta u_i \, dS \right\} dt = 0 \tag{A.14}$$

Equation (A.14) is a general expression applicable to conservative linear structures with any degree of complexity (in the elastic region) and is used to derive the dynamic equilibrium equations, the solution of which gives the deformation history of the relevant structure.

APPENDIX B

FREE VIBRATION EQUATIONS OF A 3 D EULER-BERNOULLI BEAM ELEMENT

B.1. INTRODUCTION

The sort of the structural analysis required for any type of engineering structure defines also the approach used in the finite element (FE) modeling of that structure. For example, if the flutter analysis of an aircraft structure is required, a FE model consisting of beam and shell elements proves to be sufficient. But if the concern was the stress analysis of aircraft components subjected to aerodynamic loads, the FE model prepared for the flutter analysis would not be useful. In such a case, FE models of the individual components isolated from the whole aircraft structure by relevant free body diagrams would be necessary. And this time, each FE model would possess a few thousands of degree of freedom and it would consist of solid elements instead of beam and shell elements.

The objective of this thesis study is to investigate whether it is possible to derive a stick (beam) FE model of an aircraft structure directly from experimental data for flutter analysis. For that reason the general procedure of FE formulation of engineering structures will be explained over a specific element type, namely the 3 D Euler-Bernoulli beam element.

Before giving the solution i.e. the FE formulation of a 3 D Euler- Bernoulli beam element, a clear problem statement is to be given first. For that reason, Appendix B is dedicated to derive the dynamic equilibrium equations of a 3 D Euler-Bernoulli beam element by applying Hamilton's Principle introduced in Appendix A.

B.2. POTENTIAL AND KINETIC ENERGIES OF A 3 D EULER-BERNOLLI BEAM ELEMENT

The total potential energy expression for a linear elastic structure is given as follows:

$$\Pi = \int_V \frac{1}{2}\sigma_{ij}\ \varepsilon_{ij}\ dV - \int_V f_i\ u_i\ dV\ - \int_S t_i\ u_i\ dS \tag{B.1}$$

In this thesis study, the eigenvalue problem for free vibration of aircraft structures is under consideration. In the free vibration study, the body forces and the surface traction forces are discarded from the total potential energy expression and total potential energy is expressed as follows:

$$\Pi = \int_V \frac{1}{2}\sigma_{ij}\ \varepsilon_{ij}\ dV \tag{B.2}$$

In the Euler-Bernoulli beam theory, the deformation of beam elements under bending loads is studied and the main assumption of the theory is that plane cross sections remain *plane* and *normal* to the longitudinal axis after bending. In the most general case, a beam element can carry axial and torsional loads as well as bending loads. So the total potential energy of a beam element can be expressed as follows:

$$\Pi = U_a + U_b + U_t \tag{B.3}$$

where U_a, U_b and U_t are the components of the stain energy due to the axial, bending and torsional loads respectively.

The axial strain energy of a linear elastic beam element is given as:

$$U_a = \int_V \frac{1}{2}\sigma_{xx}^a\ \varepsilon_{xx}^a\ dV \tag{B.4}$$

where σ_{xx}^a and ε_{xx}^a are the stress and strain components along the x-axis (longitudinal axis) due to axial loads, respectively.

The stain ε_{xx}^a is related to the axial deformation u of a beam element as follows:

$$\varepsilon_{xx}^a = \frac{\partial u}{\partial x} \tag{B.5}$$

Within the scope of this thesis study only the structures made of isotropic materials will be considered, so the constitutive law for an isotropic material is:

$$\sigma_{xx}^{a} = E\ \varepsilon_{xx}^{a} \tag{B.6}$$

where E is the elastic modulus.

Replacing equations (B.5) and (B.6) into (B.4), the strain energy due to the axial loading takes the form:

$$\Pi = \int_0^L \int_A \frac{1}{2} E \left(\frac{\partial u}{\partial x}\right)^2 \, dA \, dx = \int_0^L \frac{1}{2} EA \left(\frac{\partial u}{\partial x}\right)^2 \, dx \tag{B.7}$$

where L is the length and A is the cross sectional area of the beam element.

The bending stain energy of a linear elastic beam element is given as follows:

$$U_b = \int_V \frac{1}{2} \sigma_{xx}^{b} \ \varepsilon_{xx}^{b} \ dV \tag{B.8}$$

where σ_{xx}^{b} and ε_{xx}^{b} are the stress and strain components along the longitudinal axis due to the bending loads.

The stain ε_{xx}^{b} is related to the radii of curvature of a beam element in its xy and xz planes as follows:

$$\varepsilon_{xx}^{b} = \frac{y}{\rho_{xy}} + \frac{z}{\rho_{xz}} \tag{B.9}$$

where ρ_{xy} and ρ_{xz} are the radii of curvature in the xy and xz planes respectively.

On the other hand, the transverse deflections of a beam element are related to the radii of curvature as shown below:

$$\frac{1}{\rho_{xy}} = \frac{\partial^2 v / \partial x^2}{\left[1 + \left(\partial v / \partial x\right)^2\right]^{3/2}} \tag{B.10}$$

$$\frac{1}{\rho_{xz}} = \frac{\partial^2 \omega / \partial x^2}{\left[1 + \left(\partial \omega / \partial x\right)^2\right]^{3/2}} \tag{B.11}$$

where v and ω are the transverse deflections in the xy and xz planes of the local coordinate frame of the beam element.

In case of small deformations, the denominators of the right hand side expressions of (B.10) and (B.11) are close to one. As a result, the relations (B.10) and (B.11) are reduced to:

$$\frac{1}{\rho_{xy}} = \frac{\partial^2 v}{\partial x^2} \tag{B.12}$$

$$\frac{1}{\rho_{xz}} = \frac{\partial^2 \omega}{\partial x^2} \tag{B.13}$$

Replacing (B.12) and (B.13) into (B.9), the bending stain expression turns out to be:

$$\varepsilon_{xx}^{b} = y\frac{\partial^2 v}{\partial x^2} + z\frac{\partial^2 \omega}{\partial x^2} \tag{B.14}$$

Using the constitutive law given in (B.6) and evaluating the bending stain energy expression given in (B.8) with relation (B.14):

$$U_b = \int_0^L \int_A \frac{1}{2} E \left(y\frac{\partial^2 v}{\partial x^2} + z\frac{\partial^2 \omega}{\partial x^2} \right)^2 \, dA \, dx \tag{B.15}$$

Expanding the expression in the parenthesis of (B.15):

$$U_b = \int_0^L \frac{1}{2} E \left[\left(\frac{\partial^2 v}{\partial x^2}\right)^2 \int_A y^2 \, dA + \left(\frac{\partial^2 v}{\partial x^2}\right)\left(\frac{\partial^2 \omega}{\partial x^2}\right) \int_A yz \, dA + \left(\frac{\partial^2 \omega}{\partial x^2}\right)^2 \int_A z^2 \, dA \right] dx \tag{B.16}$$

Evaluating the area integrals within (B.16), the bending strain energy turns out to be:

$$U_b = \int_0^L \frac{1}{2} E I_1 \left(\frac{\partial^2 v}{\partial x^2}\right)^2 dx + \int_0^L \frac{1}{2} E I_{12} \left(\frac{\partial^2 v}{\partial x^2}\right)\left(\frac{\partial^2 \omega}{\partial x^2}\right) dx + \int_0^L \frac{1}{2} E I_2 \left(\frac{\partial^2 \omega}{\partial x^2}\right)^2 dx \tag{B.17}$$

where I_1 and I_2 are the second moment of areas about the z and y axes respectively and I_{12} is the product moment of area in the yz plane.

Finally the torsional stain energy of a linear elastic beam element is given as follows:

$$U_t = \int_V \frac{1}{2}\left(\tau_{xy}\gamma_{xy} + \tau_{xz}\gamma_{xz}\right) dV \tag{B.18}$$

where, $\tau_{xy}, \tau_{xz}, \gamma_{xy}$ and γ_{xz} are the torsional shear stresses and strains, respectively.

Analogous to the axial loading, the torsional stain energy can be expressed in terms of rotational displacement about longitudinal axis of the beam element as follows:

$$U_t = \int_0^L \frac{1}{2} G J_e \left(\frac{\partial \alpha}{\partial x}\right)^2 dx \tag{B.19}$$

where G is shear modulus, J_e is *equivalent* polar moment of area and α is rotational displacement about x axis of the beam element.

Combining the terms within (B.7), (B.17) and (B.19), the total potential energy of a 3 D Euler-Bernoulli beam element can be written as:

$$\Pi = \int_0^L \frac{1}{2} EA \left(\frac{\partial u}{\partial x}\right)^2 dx + \int_0^L \frac{1}{2} G J_e \left(\frac{\partial \alpha}{\partial x}\right)^2 dx + \int_0^L \frac{1}{2} EI_1 \left(\frac{\partial^2 v}{\partial x^2}\right)^2 dx +$$

$$+ \int_0^L \frac{1}{2} EI_{12} \left(\frac{\partial^2 v}{\partial x^2}\right)\left(\frac{\partial^2 \omega}{\partial x^2}\right) dx + \int_0^L \frac{1}{2} EI_2 \left(\frac{\partial^2 \omega}{\partial x^2}\right)^2 dx \tag{B.20}$$

The kinetic energy expression of a 3 D Euler-Bernoulli beam element is very obvious and does not require lengthy derivations as in case of the total potential energy:

$$K = \int_0^L \frac{1}{2} \rho A \left[\left(\frac{\partial u}{\partial t}\right)^2 + \left(\frac{\partial v}{\partial t}\right)^2 + \left(\frac{\partial \omega}{\partial t}\right)^2\right] dx + \int_0^L \frac{1}{2} \rho A I_x \left(\frac{\partial \alpha}{\partial t}\right)^2 dx \tag{B.21}$$

where I_x is the moment of inertia per *unit mass* about the x axis.

As the potential and kinetic energy terms of a 3 D Euler-Bernoulli beam element have been derived, the free vibration equations shall be derived by using 'Hamilton's Principle' in the following section.

B.3. FREE VIBRATION EQUATIONS OF A 3 D EULER-BERNOULLI BEAM ELEMENT

The general Lagrangian expression for engineering structures is given as below:

$$L = K - \Pi \tag{B.22}$$

In free vibration problem of a 3 D undamped linear elastic beam element made of isotropic material, the Lagrangian expression is stated by substituting (B.20) and (B.21) into (B.22) as follows:

$$\begin{aligned} L = \int_0^L \frac{1}{2}\rho A \left[\left(\frac{\partial u}{\partial t}\right)^2 + \left(\frac{\partial v}{\partial t}\right)^2 + \left(\frac{\partial \omega}{\partial t}\right)^2\right] dx + \int_0^L \frac{1}{2}\rho I_x \left(\frac{\partial \alpha}{\partial t}\right)^2 dx - \int_0^L \frac{1}{2} EA \left(\frac{\partial u}{\partial x}\right)^2 dx + \\ - \int_0^L \frac{1}{2} G J_e \left(\frac{\partial \alpha}{\partial x}\right)^2 dx - \int_0^L \frac{1}{2} E I_1 \left(\frac{\partial^2 v}{\partial x^2}\right)^2 dx - \int_0^L \frac{1}{2} E I_{12} \left(\frac{\partial^2 v}{\partial x^2}\right)\left(\frac{\partial^2 \omega}{\partial x^2}\right) dx + \\ - \int_0^L \frac{1}{2} E I_2 \left(\frac{\partial^2 \omega}{\partial x^2}\right)^2 dx \end{aligned} \tag{B.23}$$

Hamilton's Principle states that:

$$\delta \int_{t_1}^{t_2} L \, dt = 0 \tag{B.24}$$

Since the Lagrangian in (B.23) is a lengthy expression, evaluation of (B.24) has to be accomplished by dividing it into its components:

$$\delta \int_{t_1}^{t_2} L \, dt = \int_{t_1}^{t_2} (\delta K - \delta \Pi) \, dt = 0 \tag{B.25}$$

Total potential energy Π can be further divided into its components as follows:

$$\delta \int_{t_1}^{t_2} L \, dt = \int_{t_1}^{t_2} (\delta K - \delta U_a - \delta U_b - \delta U_t) \, dt = 0 \tag{B.27}$$

The first term in equation (B.27) can be evaluated as follows:

$$\int_{t_1}^{t_2} \delta K \, dt = \int_0^L \int_{t_1}^{t_2} \left\{\rho A\left[\left(\frac{\partial \delta u}{\partial t}\right)\frac{\partial u}{\partial t} + \left(\frac{\partial \delta v}{\partial t}\right)\frac{\partial v}{\partial t} + \left(\frac{\partial \delta \omega}{\partial t}\right)\frac{\partial \omega}{\partial t}\right] + \rho I_x \left(\frac{\partial \delta \alpha}{\partial t}\right)\frac{\partial \alpha}{\partial t}\right\} dt \, dx \tag{B.28}$$

Expression (B.28) is further evaluated by using integration by parts to obtain the variational operators outside of the partial derivatives and the following expression is obtained:

$$\int_{t_1}^{t_2} \delta K \, dt = -\int_0^L \int_{t_1}^{t_2} \left\{ \rho A \left[\left(\frac{\partial^2 u}{\partial t^2} \right) \delta u + \left(\frac{\partial^2 v}{\partial t^2} \right) \delta v + \left(\frac{\partial^2 \omega}{\partial t^2} \right) \delta \omega \right] + \rho A I_x \left(\frac{\partial^2 \alpha}{\partial t^2} \right) \delta \alpha \right\} dt \, dx +$$

$$+ \int_0^L \left\{ \left[\rho A \frac{\partial u}{\partial t} \delta u \right]_{t_1}^{t_2} + \left[\rho A \frac{\partial v}{\partial t} \delta v \right]_{t_1}^{t_2} + \left[\rho A \frac{\partial \omega}{\partial t} \delta \omega \right]_{t_1}^{t_2} + \left[\rho A I_x \frac{\partial \alpha}{\partial t} \delta \alpha \right]_{t_1}^{t_2} \right\} dx \qquad \text{(B.29)}$$

The second term in equation (B.27) related with the axial strain energy can be expressed as follows:

$$\int_{t_1}^{t_2} \delta U_a \, dt = \int_{t_1}^{t_2} \int_0^L EA \frac{\partial u}{\partial x} \frac{\partial \delta u}{\partial x} dx \, dt \qquad \text{(B.30)}$$

Applying integration by parts and arranging terms, (B.30) is translated into the following expression:

$$\int_{t_1}^{t_2} \delta U_a \, dt = \int_{t_1}^{t_2} \left[- \int_0^L \frac{\partial}{\partial x} \left(EA \frac{\partial u}{\partial x} \right) \delta u \, dx + \left(EA \frac{\partial u}{\partial x} \delta u \right)_0^L \right] dt \qquad \text{(B.31)}$$

The third term of equation (B.27) is expanded as follows:

$$\int_{t_1}^{t_2} \delta U_b \, dt = \int_{t_1}^{t_2} \left[\int_0^L EI_1 \frac{\partial^2 v}{\partial x^2} \frac{\partial^2 \delta v}{\partial x^2} dx + \int_0^L EI_{12} \frac{\partial^2 \omega}{\partial x^2} \frac{\partial^2 \delta v}{\partial x^2} dx + \int_0^L EI_{12} \frac{\partial^2 v}{\partial x^2} \frac{\partial^2 \delta \omega}{\partial x^2} dx + \right.$$

$$\left. + \int_0^L EI_2 \frac{\partial^2 \omega}{\partial x^2} \frac{\partial^2 \delta \omega}{\partial x^2} dx \right] dt \qquad \text{(B.32)}$$

Applying integration by parts twice to (B.32) in order to get variational operators outside of the partial derivatives and arranging the terms, the following expression is obtained:

$$\int_{t_1}^{t_2} \delta U_b \, dt = \int_{t_1}^{t_2} \left\{ \int_0^L \frac{\partial^2}{\partial x^2} \left(EI_1 \frac{\partial^2 v}{\partial x^2} \right) \delta v \, dx + \int_0^L \frac{\partial^2}{\partial x^2} \left(EI_{12} \frac{\partial^2 v}{\partial x^2} \right) \delta \omega \, dx + \int_0^L \frac{\partial^2}{\partial x^2} \left(EI_{12} \frac{\partial^2 \omega}{\partial x^2} \right) \delta v \, dx + \right.$$

$$\left. + \int_0^L \frac{\partial^2}{\partial x^2} \left(EI_2 \frac{\partial^2 \omega}{\partial x^2} \right) \delta \omega \, dx - \left[\frac{\partial}{\partial x} \left(EI_1 \frac{\partial^2 v}{\partial x^2} \right) \delta v \right]_0^L + \left[EI_1 \frac{\partial^2 v}{\partial x^2} \frac{\partial \delta v}{\partial x} \right]_0^L + \right.$$

$$-\left[\frac{\partial}{\partial x}\left(EI_{12}\frac{\partial^2\omega}{\partial x^2}\right)\delta v\right]_0^L+\left[EI_{12}\frac{\partial^2\omega}{\partial x^2}\frac{\partial\delta v}{\partial x}\right]_0^L-\left[\frac{\partial}{\partial x}\left(EI_{12}\frac{\partial^2 v}{\partial x^2}\right)\delta\omega\right]_0^L+$$

$$+\left[EI_{12}\frac{\partial^2 v}{\partial x^2}\frac{\partial\delta\omega}{\partial x}\right]_0^L-\left[\frac{\partial}{\partial x}\left(EI_2\frac{\partial^2\omega}{\partial x^2}\right)\delta\omega\right]_0^L+\left[EI_2\frac{\partial^2\omega}{\partial x^2}\frac{\partial\delta\omega}{\partial x}\right]_0^L\Bigg\}dt \qquad (B.33)$$

Finally, the last term in equation (B.27) related with the torsional strain energy is evaluated as follows:

$$\int_{t_1}^{t_2}\delta\ U_t\ dt=\int_{t_1}^{t_2}\int_0^L GJ_e\frac{\partial\alpha}{\partial x}\frac{\partial\delta\alpha}{\partial x}\,dx\ dt \qquad (B.34)$$

Applying integration by parts and arranging the terms, (B.34) takes the form:

$$\int_{t_1}^{t_2}\delta\ U_t\ dt=\int_{t_1}^{t_2}\left[-\int_0^L\frac{\partial}{\partial x}\left(GJ_e\frac{\partial\alpha}{\partial x}\right)\delta\alpha\ dx+\left(GJ_e\frac{\partial\alpha}{\partial x}\delta\alpha\right)_0^L\right]dt \qquad (B.35)$$

If expressions (B.29), (B.31), (B.33) and (B.35) are combined within the same expression it will be noticed that multipliers of variations of common parameters like $\delta u, \delta v$ etc. can be combined within common parentheses. Besides, according to the variational calculus, the first variations of dependent parameters indicate arbitrary changes of those parameters, yet left hand side of the equation (B.27) always has to be equal to zero. The only way to satisfy equation (B.27) under any circumstance is to equate terms within the common parentheses mentioned above to zero as follows:

$$\rho A\ \frac{\partial^2 u}{\partial t^2}-\frac{\partial}{\partial x}\left(EA\frac{\partial u}{\partial x}\right)=0 \qquad (B.36)$$

$$\rho A\ \frac{\partial^2 v}{\partial t^2}+\frac{\partial^2}{\partial x^2}\left(EI_1\frac{\partial^2 v}{\partial x^2}\right)+\frac{\partial^2}{\partial x^2}\left(EI_{12}\frac{\partial^2\omega}{\partial x^2}\right)=0 \qquad (B.37)$$

$$\rho A\ \frac{\partial^2\omega}{\partial t^2}+\frac{\partial^2}{\partial x^2}\left(EI_2\frac{\partial^2\omega}{\partial x^2}\right)+\frac{\partial^2}{\partial x^2}\left(EI_{12}\frac{\partial^2 v}{\partial x^2}\right)=0 \qquad (B.38)$$

$$\rho A\, I_x\ \frac{\partial^2\alpha}{\partial t^2}-\frac{\partial}{\partial x}\left(GJ_e\frac{\partial\alpha}{\partial x}\right)=0 \qquad (B.39)$$

Equations from (B.36) to (B.39) are the governing equilibrium equations of the free vibration problem of the 3 D Euler-Bernoulli beam element. Solutions of those equations give nothing but the translational and rotational displacements of the beam element as a function of time and position in its local coordinate frame.

Equation (B.27) does not only introduce dynamic equilibrium equations but also initial and boundary conditions as follows:

$$\left[EA \frac{\partial u}{\partial x} \delta u \right]_0^L = 0 \tag{B.40}$$

$$\left[\frac{\partial}{\partial x}\left(EI_1 \frac{\partial^2 v}{\partial x^2} \right)\delta v + \frac{\partial}{\partial x}\left(EI_{12} \frac{\partial^2 \omega}{\partial x^2} \right)\delta v \right]_0^L = 0 \tag{B.41}$$

$$\left[\frac{\partial}{\partial x}\left(EI_2 \frac{\partial^2 \omega}{\partial x^2} \right)\delta \omega + \frac{\partial}{\partial x}\left(EI_{12} \frac{\partial^2 v}{\partial x^2} \right)\delta \omega \right]_0^L = 0 \tag{B.42}$$

$$\left[GJ_e \frac{\partial \alpha}{\partial x} \delta \alpha \right]_0^L = 0 \tag{B.43}$$

$$\left[\rho A \frac{\partial u}{\partial t} \delta u \right]_{t_1}^{t_2} = 0 \tag{B.44}$$

$$\left[\rho A \frac{\partial v}{\partial x} \delta v \right]_{t_1}^{t_2} = 0 \tag{B.45}$$

$$\left[\rho A \frac{\partial \omega}{\partial x} \delta \omega \right]_{t_1}^{t_2} = 0 \tag{B.46}$$

$$\left[\rho A I_x \frac{\partial \alpha}{\partial x} \delta \alpha \right]_{t_1}^{t_2} = 0 \tag{B.47}$$

APPENDIX C

WEIGHTED-INTEGRAL AND WEAK FORMULATIONS OF FREE VIBRATION EQUATIONS OF A 3 D EULER-BERNOULLI BEAM ELEMENT

C.1. INTRODUCTION

The free vibration equations derived in Appendix B for a 3 D Euler-Bernoulli beam element cannot be solved exactly for complex engineering structures such as an aircraft structure. For that reason, approximate solutions of the displacement fields are to be sought over the entire problem domain. In case of linear differential equations such as free vibration equations of a beam element, an approximate solution can be expressed as follows:

$$u(x) \approx U_N(x) = \sum_{j=1}^{N} c_j \phi_j(x) + \phi_0(x) \tag{C.1}$$

where U_N is the *N*-parameter approximate solution, ϕ_j and ϕ_0 are approximation functions (ex: simple polynomials) and c_j are unknown coefficients to be determined.

N unknown coefficients within an approximate solution requires the derivation of *N* linearly independent equations. One of the techniques used to derive those equations is called the '*method of weighted residuals*' in which differential equations are translated into weighted integral statements. Weighted integral statements of governing differential equations are further manipulated to obtain '*weak forms*' of the differential equations. Appendix C is dedicated to the explanation and derivation of weighted integral statements and weak forms of the free vibration equations of a 3 D

Euler-Bernoulli beam element. Thus, the last step before the introduction of finite element formulations for beam elements will be accomplished.

C.2. THE METHOD OF WEIGHTED RESIDUALS

Consider the following general differential equation:

$$A(u) = f \qquad \text{in } \Omega \tag{C.2}$$

where A is a differential operator (linear or nonlinear), u is the dependent variable and f is the known function of the independent variables.

The function u has to satisfy boundary conditions associated with the differential equation (C.2) as well as the equation itself.

In the method of weighted residuals, the solution u is approximated as given in the expression (C.1). Substituting U_N into equation (C.2) and replacing f to the left hand side of the equation, the following expression is obtained:

$$R \equiv A(U_N) - f = A\left(\sum_{j=1}^{N} c_j \ \phi_j + \phi_0 \right) - f \neq 0 \tag{C.3}$$

where R, the residual of the approximation, is non-zero.

In the method of weighted residuals, sufficient number of algebraic equations of unknown parameters c_j are derived by requiring the residual R to vanish in a weighted integral sense as follows:

$$\int_{\Omega} \psi_i \ R(c_j) \ d\Omega = 0 \qquad (i = 1, 2, ..., N) \tag{C.4}$$

where ψ_i are the *weight functions* and Ω is the problem domain.

It is important to notice that the set of the weight functions $\{\psi_i\}$ must be linearly independent in order that algebraic equations within (C.4) are linearly independent as well.

The method of weighted residuals takes different names according to the kind of the weight functions that it uses, such as '*Galerkin Method*', *'Least-Squares Method'* etc. Several weighted residual methods are introduced in the following subsections.

C.2.1. The Petrov-Galerkin Method

The weighted-residual method is called the '*Petrov-Galerkin Method*' when the weight functions ψ_i are not equated to approximating functions ϕ_i i.e. $\psi_i \neq \phi_i$. In this method, weighted integral statements of (C.4) can be arranged as follows:

$$\sum_{j=1}^{N}\left[\int_{\Omega}\psi_i\ A(\phi_j)\ d\Omega\right] c_j = \int_{\Omega}\psi_i\ \left[f - A(\phi_0)\right] d\Omega \tag{C.5}$$

Equations (C.5) can be expressed in a more compact form as follows:

$$\sum_{j=1}^{N} A_{ij}\ c_j = F_i \tag{C.6}$$

In the Petrov-Galerkin Method the coefficient matrix is not symmetric:

$$A_{ij} = \int_{\Omega}\psi_i\ A(\phi_j)\ d\Omega \neq A_{ji} \tag{C.7}$$

C.2.2. The Galerkin Method

The weighted-residual method is called the '*Galerkin Method*' when the weight function ψ_i is taken to be equal to the approximation function ϕ_i. In this method, weighted integral statements of (C.4) are arranged as follows:

$$\sum_{j=1}^{N}\left[\int_{\Omega}\phi_i\ A(\phi_j)\ d\Omega\right] c_j = \int_{\Omega}\phi_i\ \left[f - A(\phi_0)\right] d\Omega \tag{C.8}$$

As in the case of Petrov-Galerkin Method, in the Galerkin Method as well the coefficient matrix is not symmetric:

$$A_{ij} = \int_{\Omega}\phi_i\ A(\phi_j)\ d\Omega \neq A_{ji} \tag{C.9}$$

C.2.3. The Least-Squares Method

In the '*Least-Squares Method*', algebraic equations in (C.4) are derived by minimizing the integral of the square of the residual as follows:

$$\frac{\partial}{\partial c_i}\int_{\Omega} R^2(c_j)\ d\Omega = 0 \tag{C.10}$$

Evaluating partial derivatives of $R^2(c_j)$, the set of equations (C.10) takes the form:

$$\int_{\Omega}\frac{\partial R}{\partial c_i}\ R\ d\Omega = 0 \tag{C.11}$$

Comparison of (C.11) with (C.4) shows that:

$$\psi_i = \frac{\partial R}{\partial c_i} \tag{C.12}$$

If A is a linear operator, $\psi_i = A(\phi_i)$ and weighted integral statements of (C.4) are written as follows:

$$\sum_{j=1}^{N}\left[\int_{\Omega} A(\phi_i)\ A(\phi_j)\ d\Omega\right] c_j = \int_{\Omega} A(\phi_i)\ \left[f - A(\phi_0)\right] d\Omega \tag{C.13}$$

In case of the Least-Squares Method, the coefficient matrix turns out to be symmetric but it involves the same order of differentiation as in the governing differential equation (C.2):

$$A_{ij} = \int_{\Omega} A(\phi_i)\ A(\phi_j)\ d\Omega = A_{ji} \tag{C.14}$$

C.2.4. The Collocation Method

In *the 'Collocation Method'*, algebraic equations in (C.4) are determined by forcing the residual to vanish identically at N selected points $X^i \equiv (x^i, y^i, z^i)$ in the domain Ω as follows:

$$R\left(X^i, c_j\right) = 0 \qquad (i = 1,2,\ldots,N) \tag{C.15}$$

Actually, the Collocation Method is nothing but a special case of the method of weighted residuals with $\psi_i = \delta(X - X^i)$, where $\delta(X)$ is the Dirac delta function defined as follows:

$$\int_{\Omega} f(X)\ \delta(X - \xi)\ dX = f(\xi) \tag{C.16}$$

According to the definition given in (C.16), weighted integral statement of the governing differential equation (C.2) turns out to be:

$$\int_{\Omega} \delta(X - X^i)\ R(X, c_j)\ dX = 0 \tag{C.16}$$

Obviously, weighted residual methods are sufficient to derive necessary number of algebraic equations among coefficients c_j. Consequently, the approximate solution U_N of the governing differential equation (C.4) can be determined. But, those methods require that approximation functions ϕ_i must have non-zero derivatives up to the order appearing in the original differential equation (C.4). Moreover, since weighted integral statements do not include any of the specified boundary conditions (essential or natural) approximate solution U_N is required to satisfy all specified boundary conditions of the problem. However, if the weight functions ψ_i are chosen to be equal to approximation functions ϕ_i, then half of the derivatives can be *shifted* from ϕ_i to ψ_i by using integration by parts. The resulting form of the integral statements is called the '*weak form'*. Several advantages of the weak form over the weighted integral statements can be stated as follows [19]: First, it requires *weaker* continuity of the approximation functions ϕ_i, second it always results a symmetric coefficient matrix, and third the natural boundary conditions of the problem are included in the weak form, and therefore the approximate solution U_N is required to satisfy only the essential boundary conditions of the problem. Those relaxations brought to the weighted integral statements play crucial role in the development of finite element models of a problem. For that reason, next section is dedicated to the derivation of weak forms of free vibration equations of a 3 D Euler-Bernoulli beam element.

C.3. WEAK FORMS OF THE FREE VIBRATION EQUATIONS OF A 3 D EULER-BERNOULLI BEAM ELEMENT

Free vibration equations of a 3 D Euler-Bernoulli beam element derived in Appendix B are given as follows:

$$\rho A \frac{\partial^2 u}{\partial t^2} - \frac{\partial}{\partial x}\left(EA \frac{\partial u}{\partial x} \right) = 0 \tag{C.17}$$

$$\rho A \frac{\partial^2 v}{\partial t^2} + \frac{\partial^2}{\partial x^2}\left(EI_1 \frac{\partial^2 v}{\partial x^2} \right) + \frac{\partial^2}{\partial x^2}\left(EI_{12} \frac{\partial^2 \omega}{\partial x^2} \right) = 0 \tag{C.18}$$

$$\rho A \frac{\partial^2 \omega}{\partial t^2} + \frac{\partial^2}{\partial x^2}\left(EI_2 \frac{\partial^2 \omega}{\partial x^2} \right) + \frac{\partial^2}{\partial x^2}\left(EI_{12} \frac{\partial^2 v}{\partial x^2} \right) = 0 \tag{C.19}$$

$$\rho A I_x \frac{\partial^2 \alpha}{\partial t^2} - \frac{\partial}{\partial x}\left(GJ_e \frac{\partial \alpha}{\partial x} \right) = 0 \tag{C.20}$$

The weighted integral statement of equation (C.17) is given as follows:

$$\int_0^L \psi \left(\rho A \frac{\partial^2 u}{\partial t^2} - \frac{\partial}{\partial x}\left(EA \frac{\partial u}{\partial x} \right) \right) dx = 0 \tag{C.21}$$

The weak form of the integral statement in (C.21) is obtained as:

$$\int_0^L \psi \left(\rho A \frac{\partial^2 u}{\partial t^2} \right) dx + \int_0^L \frac{\partial \psi}{\partial x}\left(EA \frac{\partial u}{\partial x} \right) dx - \left[\psi \; EA \; \frac{\partial u}{\partial x} \right]_0^L = 0 \tag{C.22}$$

The weighted integral statement of equation (C.18) is written as follows:

$$\int_0^L \psi \left(\rho A \frac{\partial^2 v}{\partial t^2} + \frac{\partial^2}{\partial x^2}\left(EI_1 \frac{\partial^2 v}{\partial x^2} \right) + \frac{\partial^2}{\partial x^2}\left(EI_{12} \frac{\partial^2 \omega}{\partial x^2} \right) \right) dx = 0 \tag{C.23}$$

The weak form of the integral statement (C.23) is obtained by using integration by parts as follows:

$$\int_0^L \psi \left(\rho A \frac{\partial^2 v}{\partial t^2} \right) dx + \int_0^L \frac{\partial^2 \psi}{\partial x^2}\left(EI_1 \frac{\partial^2 v}{\partial x^2} \right) dx + \int_0^L \frac{\partial^2 \psi}{\partial x^2}\left(EI_{12} \frac{\partial^2 \omega}{\partial x^2} \right) dx +$$

$$+\left[\psi\frac{\partial}{\partial x}\left(EI_1\frac{\partial^2 v}{\partial x^2}\right)\right]_0^L-\left[EI_1\frac{\partial^2 v}{\partial x^2}\frac{\partial\psi}{\partial x}\right]_0^L+\left[\psi\frac{\partial}{\partial x}\left(EI_{12}\frac{\partial^2\omega}{\partial x^2}\right)\right]_0^L-\left[EI_{12}\frac{\partial^2\omega}{\partial x^2}\frac{\partial\psi}{\partial x}\right]_0^L=0 \qquad \text{(C.24)}$$

Similarly, the weak forms of the differential equations (C.19) and (C.20) are found to be:

$$\int_0^L \psi\left(\rho A\,\frac{\partial^2\omega}{\partial t^2}\right)\,dx\;+\int_0^L\;\frac{\partial^2\psi}{\partial x^2}\left(EI_2\,\frac{\partial^2\omega}{\partial x^2}\right)\,dx\;+\int_0^L\;\frac{\partial^2\psi}{\partial x^2}\left(EI_{12}\,\frac{\partial^2 v}{\partial x^2}\right)\,dx\;+$$

$$+\left[\psi\frac{\partial}{\partial x}\left(EI_2\frac{\partial^2\omega}{\partial x^2}\right)\right]_0^L-\left[EI_2\frac{\partial^2\omega}{\partial x^2}\frac{\partial\psi}{\partial x}\right]_0^L+\left[\psi\frac{\partial}{\partial x}\left(EI_{12}\frac{\partial^2 v}{\partial x^2}\right)\right]_0^L-\left[EI_{12}\frac{\partial^2 v}{\partial x^2}\frac{\partial\psi}{\partial x}\right]_0^L=0 \qquad \text{(C.25)}$$

$$\int_0^L\psi\left(\rho AI_x\,\frac{\partial^2\alpha}{\partial t^2}\right)dx+\int_0^L\,\frac{\partial\psi}{\partial x}\left(GJ_e\,\frac{\partial\alpha}{\partial x}\right)\,dx\;\;-\left[\psi\;GJ_e\;\frac{\partial\alpha}{\partial x}\right]_0^L=0 \qquad \text{(C.26)}$$

The finite element formulation of a 3 D Euler-Bernoulli beam element is based on the weak formulations given in equations (C.22), (C.24), (C.25) and (C.26) and it is the subject of Appendix D.

APPENDIX D

FINITE ELEMENT FORMULATION OF A 3 D EULER-BERNOULLI BEAM ELEMENT

D.1. INTRODUCTION

Appendix D is dedicated to derive the finite element model of a 3 D Euler-Bernoulli beam element starting from the weak forms of the free vibration equations introduced in Appendix C.

As shown in Appendix B, there are four free vibration equations in terms of the displacement degrees of freedom u, v and ω as well as the rotational degree of freedom α about x axis of the beam. Approximate solution of each equation will be obtained separately and finally all solutions are going to be superposed to determine the finite element model of an Euler-Bernoulli beam element in 3 D.

D.2. FINITE ELEMENT MODEL RELATED TO AXIAL DISPLACEMENT OF AN EULER-BERNOULLI BEAM

The free vibration equation related with the displacement field u of an Euler-Bernoulli beam element is stated as follows:

$$\rho A \frac{\partial^2 u}{\partial t^2} - \frac{\partial}{\partial x}\left(EA \frac{\partial u}{\partial x} \right) = 0 \qquad \text{(D.1)}$$

The weighted integral statement of equation (D.1) in weak form is given as:

$$\int_0^L \psi\left(\rho A \frac{\partial^2 u}{\partial t^2}\right) dx + \int_0^L \frac{\partial \psi}{\partial x}\left(EA \frac{\partial u}{\partial x}\right) dx - \left[\psi \; EA \; \frac{\partial u}{\partial x}\right]_0^L = 0 \qquad (D.2)$$

where ψ are the weight functions.

Examination of the boundary terms within (D.2) indicates that the essential boundary conditions involve the specification of u and the natural boundary conditions involve the specification of axial forces at the end points of the Euler-Bernoulli beam element.

Secondary variables within the boundary terms of (D.2) can be put in more compact form as follows:

$$Q_{u1}^e \equiv -\left(EA \frac{\partial u}{\partial x}\right)_{x=0} \qquad (D.3)$$

$$Q_{u2}^e \equiv \left(EA \frac{\partial u}{\partial x}\right)_{x=L} \qquad (D.4)$$

where Q_{u1}^e and Q_{u2}^e are called '*generalized forces*'.

Substituting left hand side terms of (D.3) and (D.4) and replacing boundary terms to the right hand side of the equation (D.2), the weak form turns out to be:

$$\int_0^L \psi\left(\rho A \frac{\partial^2 u}{\partial t^2}\right) dx + \int_0^L \frac{\partial \psi}{\partial x}\left(EA \frac{\partial u}{\partial x}\right) dx = \psi(L,t)Q_{u2}^e + \psi(0,t)Q_{u1}^e \qquad (D.5)$$

The weak form (D.5) requires that the interpolation (i.e. approximation) function of the beam element be continuous with non zero derivatives wrt variable x up to order one. So the approximation function u_h^e must be differentiable wrt x at least once and satisfy the following essential boundary conditions:

$$u_h^e(0,t) = u_1^e(t), \qquad u_h^e(L,t) = u_2^e(t) \qquad (D.6)$$

Since there are two conditions stated in (D.6), a two parameter polynomial must be selected for the approximate solution u_h^e:

$$u(x,t) \approx u_h^e(x,t) = c_1^e(t) + c_2^e(t) \; x \qquad (D.7)$$

Primary nodal variables (i.e. generalized displacements) $u_1^e(t)$ and $u_2^e(t)$ are related to the unknown coefficients $c_1^e(t)$ and $c_2^e(t)$ as follows:

$$u_1^e(t) = c_1^e(t) \tag{D.8}$$

$$u_2^e(t) = c_1^e(t) + c_2^e(t)L \tag{D.9}$$

Equalities (D.8) and (D.9) can be put in a matrix form as:

$$\begin{Bmatrix} u_1^e(t) \\ u_2^e(t) \end{Bmatrix} = \begin{bmatrix} 1 & 0 \\ 1 & L \end{bmatrix} \begin{Bmatrix} c_1^e(t) \\ c_2^e(t) \end{Bmatrix} \tag{D.10}$$

Inverting matrix equation to express $c_i^e(t)$ in terms of $u_1^e(t)$ and $u_2^e(t)$, and substituting the result into (D.7), the approximate solution can be stated as follows:

$$u_h^e(x,t) = u_1^e \left(1 - \frac{x}{L}\right) + u_2^e \frac{x}{L} \tag{D.11}$$

Expression (D.11) can be put in a more compact form with the following definitions:

$$H_1^e(x) \equiv \left(1 - \frac{x}{L}\right) \tag{D.12}$$

$$H_2^e(x) \equiv \frac{x}{L} \tag{D.13}$$

Substituting (D.12) and (D.13) into (D.11), approximation function takes the form:

$$u_h^e(x,t) = u_1^e \, H_1^e(x) + u_2^e \, H_2^e(x) \tag{D.14}$$

where $H_1^e(x)$ and $H_2^e(x)$ are in general called '*shape functions'* or '*interpolation functions'*.

The finite element model related only with the axial displacement u of the Euler-Bernoulli beam is obtained by substituting u_h^e for u and $H_j^e(x)$ for the weight function ψ into the weak form (D.5).

Two algebraic equations obtained for the finite element model are as follows:

$$\int_0^L H_1^e\left[\rho A\frac{\partial^2}{\partial t^2}\left(u_1^e H_1^e + u_2^e H_2^e\right)\right]dx + \int_0^L \frac{\partial H_1^e}{\partial x}\left[EA\frac{\partial}{\partial x}\left(u_1^e H_1^e + u_2^e H_2^e\right)\right]dx =$$

$$H_1^e(L)Q_{u2}^e + H_1^e(0)Q_{u1}^e \qquad \text{(D.15)}$$

$$\int_0^L H_2^e\left[\rho A\frac{\partial^2}{\partial t^2}\left(u_1^e H_1^e + u_2^e H_2^e\right)\right]dx + \int_0^L \frac{\partial H_2^e}{\partial x}\left[EA\frac{\partial}{\partial x}\left(u_1^e H_1^e + u_2^e H_2^e\right)\right]dx =$$

$$H_1^e(L)Q_{u2}^e + H_1^e(0)Q_{u1}^e \qquad \text{(D.16)}$$

Equations (D.15) and (D.16) can be put into the following matrix form:

$$\int_0^L \rho A\begin{bmatrix}\left(H_1^e\right)^2 & H_1^e H_2^e\\ H_1^e H_2^e & \left(H_2^e\right)^2\end{bmatrix}dx\begin{Bmatrix}\ddot{u}_1^e\\ \ddot{u}_2^e\end{Bmatrix} + \int_0^L \rho A\begin{bmatrix}\left(\frac{\partial H_1^e}{\partial x}\right)^2 & \frac{\partial H_1^e}{\partial x}\frac{\partial H_2^e}{\partial x}\\ \frac{\partial H_1^e}{\partial x}\frac{\partial H_2^e}{\partial x} & \left(\frac{\partial H_2^e}{\partial x}\right)^2\end{bmatrix}dx\begin{Bmatrix}u_1^e\\ u_2^e\end{Bmatrix} = \begin{Bmatrix}Q_{u1}^e\\ Q_{u2}^e\end{Bmatrix} \qquad \text{(D.17)}$$

where $\ddot{u}_1^e$ and $\ddot{u}_2^e$ are the acceleration terms.

Evaluating integral terms within the matrix expressions, equation (D 17) yields:

$$\rho AL\begin{bmatrix}1/3 & 1/6\\ 1/6 & 1/3\end{bmatrix}\begin{Bmatrix}\ddot{u}_1^e\\ \ddot{u}_2^e\end{Bmatrix} + \frac{EA}{L}\begin{bmatrix}1 & -1\\ -1 & 1\end{bmatrix}\begin{Bmatrix}u_1^e\\ u_2^e\end{Bmatrix} = \begin{Bmatrix}Q_{u1}^e\\ Q_{u2}^e\end{Bmatrix} \qquad \text{(D.18)}$$

In case of free vibration, there are no nodal forces acting on the boundaries of the beam element, so the right hand side of equation (D.18) turns out to be zero as follows:

$$\rho AL\begin{bmatrix}1/3 & 1/6\\ 1/6 & 1/3\end{bmatrix}\begin{Bmatrix}\ddot{u}_1^e\\ \ddot{u}_2^e\end{Bmatrix} + \frac{EA}{L}\begin{bmatrix}1 & -1\\ -1 & 1\end{bmatrix}\begin{Bmatrix}u_1^e\\ u_2^e\end{Bmatrix} = \begin{Bmatrix}0\\ 0\end{Bmatrix} \qquad \text{(D.19)}$$

The first and second matrix expressions at the left hand side of equation (D.19) have very important physical meanings: they are the mass and stiffness matrices of the Euler-Bernoulli beam related with the displacement field u (i.e. axial displacement) within its local coordinate frame. Obviously, mass and stiffness matrices represent inertial and elastic properties of the beam element in its axial direction.

Linear ordinary differential equations expressed (D.19) can be solved with relevant initial conditions for boundary terms $u_1^e(t)$ and $u_2^e(t)$ as a function of time. Replacing those boundary displacements in (D.14) gives an approximate solution for the free vibration response of the beam element in its axial direction.

The power of the finite element model becomes more obvious when a large problem, domain for example an aircraft structure, is divided into sub domains i.e. finite elements. This way, governing differential equation (D.1) is solved approximately for each finite element as explained above and the global solution is obtained by simply assembling finite element solutions.

It is important to note that boundary solutions $u_1^e(t)$ and $u_2^e(t)$ of a finite element model obtained from (D.19) are exact solutions, i.e. they satisfy governing differential equation (D.1) exactly. Consequently, if a problem domain is divided into more and more finite elements, number of boundary points will accordingly increase and exact solutions will be obtained at more and more discrete positions within the problem domain. In the finite element modeling terminology, the boundary points of a finite element are called '*nodes'*. Within the same terminology, dividing the global problem domain into finite elements is called '*meshing'*.

Classical approximate solution techniques such as the '*Rayleigh-Ritz method*' seek an approximate solution covering the entire problem domain which cannot be achieved in case of complex engineering structures such as an aircraft structure. Consequently, the problem domain is to be divided into simpler subdomains as in the case of the finite element method. This way, approximate solutions can be obtained over each sub domain no matter how complex the entire structure. Then, finite element solutions can be easily assembled to obtain the global solution over the entire problem domain. This is the major advantage of the finite element method over classical solution techniques.

D.3. FINITE ELEMENT MODEL RELATED TO AXIAL ROTATION OF AN EULER-BERNOULLI BEAM

The free vibration equation related to the rotational displacement field α of an Euler-Bernoulli beam element is stated as follows:

$$\rho A I_x \frac{\partial^2 \alpha}{\partial t^2} - \frac{\partial}{\partial x}\left(G J_e \frac{\partial \alpha}{\partial x} \right) = 0 \tag{D.20}$$

Equation (D.20) is very analogous to the governing free vibration equation for the displacement field u given in the previous section. For that reason, the lengthy derivation procedure will not be repeated here. As a result, the finite element formulation of the free vibration problem of an Euler-Bernoulli beam for the rotational displacement field α in its local coordinate frame is stated as follows:

$$\rho A I_x L \begin{bmatrix} 1/3 & 1/6 \\ 1/6 & 1/3 \end{bmatrix} \begin{Bmatrix} \ddot{\alpha}_1^e \\ \ddot{\alpha}_2^e \end{Bmatrix} + \frac{G J_e}{L} \begin{bmatrix} 1 & -1 \\ -1 & 1 \end{bmatrix} \begin{Bmatrix} \alpha_1^e \\ \alpha_2^e \end{Bmatrix} = \begin{Bmatrix} 0 \\ 0 \end{Bmatrix} \tag{D.21}$$

D.4. FINITE ELEMENT MODEL RELATED TO THE TRANSVERSE DISPLACEMENTS FIELDS OF AN EULER-BERNOULLI BEAM

The free vibration equations related with displacement fields v and ω of an Euler-Bernoulli beam are given as follows:

$$\rho A \frac{\partial^2 v}{\partial t^2} + \frac{\partial^2}{\partial x^2}\left(EI_1 \frac{\partial^2 v}{\partial x^2} \right) + \frac{\partial^2}{\partial x^2}\left(EI_{12} \frac{\partial^2 \omega}{\partial x^2} \right) = 0 \tag{D.22}$$

$$\rho A \frac{\partial^2 \omega}{\partial t^2} + \frac{\partial^2}{\partial x^2}\left(EI_2 \frac{\partial^2 \omega}{\partial x^2} \right) + \frac{\partial^2}{\partial x^2}\left(EI_{12} \frac{\partial^2 v}{\partial x^2} \right) = 0 \tag{D.23}$$

The weighted integral statements of equations (D.22) and (D.23) in weak form are obtained as follows:

$$\int_0^L \psi \left(\rho A \frac{\partial^2 v}{\partial t^2} \right) dx + \int_0^L \frac{\partial^2 \psi}{\partial x^2} \left(EI_1 \frac{\partial^2 v}{\partial x^2} \right) dx + \int_0^L \frac{\partial^2 \psi}{\partial x^2} \left(EI_{12} \frac{\partial^2 \omega}{\partial x^2} \right) dx +$$

$$+ \left[\psi \frac{\partial}{\partial x}\left(EI_1 \frac{\partial^2 v}{\partial x^2} \right) \right]_0^L - \left[EI_1 \frac{\partial^2 v}{\partial x^2} \frac{\partial \psi}{\partial x} \right]_0^L + \left[\psi \frac{\partial}{\partial x}\left(EI_{12} \frac{\partial^2 \omega}{\partial x^2} \right) \right]_0^L - \left[EI_{12} \frac{\partial^2 \omega}{\partial x^2} \frac{\partial \psi}{\partial x} \right]_0^L = 0 \tag{D.24}$$

$$\int_0^L \psi\left(\rho A \frac{\partial^2 \omega}{\partial t^2}\right) dx + \int_0^L \frac{\partial^2 \psi}{\partial x^2}\left(EI_2 \frac{\partial^2 \omega}{\partial x^2}\right) dx + \int_0^L \frac{\partial^2 \psi}{\partial x^2}\left(EI_{12} \frac{\partial^2 v}{\partial x^2}\right) dx +$$

$$+\left[\psi \frac{\partial}{\partial x}\left(EI_2 \frac{\partial^2 \omega}{\partial x^2}\right)\right]_0^L - \left[EI_2 \frac{\partial^2 \omega}{\partial x^2}\frac{\partial \psi}{\partial x}\right]_0^L + \left[\psi \frac{\partial}{\partial x}\left(EI_{12} \frac{\partial^2 v}{\partial x^2}\right)\right]_0^L - \left[EI_{12} \frac{\partial^2 v}{\partial x^2}\frac{\partial \psi}{\partial x}\right]_0^L = 0 \quad \text{(D.25)}$$

Secondary variables or generalized forces within the boundary terms of equations (D.24) and (D.25) can be put in a more compact form as follows:

$$Q_{v1}^e \equiv -\frac{\partial}{\partial x}\left(EI_1 \frac{\partial^2 v}{\partial x^2}\right)\bigg|_{x=L} - \frac{\partial}{\partial x}\left(EI_{12} \frac{\partial^2 \omega}{\partial x^2}\right)\bigg|_{x=L} \quad \text{(D.26)}$$

$$Q_{v2}^e \equiv EI_1 \frac{\partial^2 v}{\partial x^2}\bigg|_{x=L} + EI_{12} \frac{\partial^2 \omega}{\partial x^2}\bigg|_{x=L} \quad \text{(D.27)}$$

$$Q_{v3}^e \equiv \frac{\partial}{\partial x}\left(EI_1 \frac{\partial^2 v}{\partial x^2}\right)\bigg|_{x=0} + \frac{\partial}{\partial x}\left(EI_{12} \frac{\partial^2 \omega}{\partial x^2}\right)\bigg|_{x=0} \quad \text{(D.28)}$$

$$Q_{v4}^e \equiv -EI_1 \frac{\partial^2 v}{\partial x^2}\bigg|_{x=0} - EI_{12} \frac{\partial^2 \omega}{\partial x^2}\bigg|_{x=0} \quad \text{(D.29)}$$

$$Q_{\omega 1}^e \equiv -\frac{\partial}{\partial x}\left(EI_2 \frac{\partial^2 \omega}{\partial x^2}\right)\bigg|_{x=L} - \frac{\partial}{\partial x}\left(EI_{12} \frac{\partial^2 v}{\partial x^2}\right)\bigg|_{x=L} \quad \text{(D.30)}$$

$$Q_{\omega 2}^e \equiv -EI_2 \frac{\partial^2 \omega}{\partial x^2}\bigg|_{x=L} - EI_{12} \frac{\partial^2 v}{\partial x^2}\bigg|_{x=L} \quad \text{(D.31)}$$

$$Q_{\omega 3}^e \equiv \frac{\partial}{\partial x}\left(EI_2 \frac{\partial^2 \omega}{\partial x^2}\right)\bigg|_{x=0} + \frac{\partial}{\partial x}\left(EI_{12} \frac{\partial^2 v}{\partial x^2}\right)\bigg|_{x=0} \quad \text{(D.32)}$$

$$Q_{\omega 4}^e \equiv EI_2 \frac{\partial^2 \omega}{\partial x^2}\bigg|_{x=0} + EI_{12} \frac{\partial^2 v}{\partial x^2}\bigg|_{x=0} \quad \text{(D.33)}$$

Arranging the terms of (D.24) and (D.25) according to the definitions given in (D.26) to (D.33), weighted integral terms can be expressed as follows:

$$\int_0^L \psi\left(\rho A \frac{\partial^2 v}{\partial t^2}\right) dx + \int_0^L \frac{\partial^2 \psi}{\partial x^2}\left(EI_1 \frac{\partial^2 v}{\partial x^2}\right) dx + \int_0^L \frac{\partial^2 \psi}{\partial x^2}\left(EI_{12} \frac{\partial^2 \omega}{\partial x^2}\right) dx =$$

$$\psi(L,t)Q_{v1}^e + \left(\frac{\partial \psi}{\partial x}\right)_{x=L} Q_{v2}^e + \psi(0,t)Q_{v3}^e + \left(\frac{\partial \psi}{\partial x}\right)_{x=0} Q_{v4}^e \qquad \text{(D.34)}$$

$$\int_0^L \psi\left(\rho A \frac{\partial^2 \omega}{\partial t^2}\right) dx + \int_0^L \frac{\partial^2 \psi}{\partial x^2}\left(EI_2 \frac{\partial^2 \omega}{\partial x^2}\right) dx + \int_0^L \frac{\partial^2 \psi}{\partial x^2}\left(EI_{12} \frac{\partial^2 v}{\partial x^2}\right) dx =$$

$$\psi(L,t)Q_{\omega 1}^e + \left(-\frac{\partial \psi}{\partial x}\right)_{x=L} Q_{\omega 2}^e + \psi(0,t)Q_{\omega 3}^e + \left(-\frac{\partial \psi}{\partial x}\right)_{x=0} Q_{\omega 4}^e \qquad \text{(D.35)}$$

The weak forms (D.34) and (D.35) require that the interpolation (i.e. approximation) function of the beam element be continuous with non zero derivatives up to order two. So the approximation functions v_h^e and ω_h^e must be differentiable at least twice and satisfy the following essential boundary conditions of a beam element:

$$v_h^e(0,t) = v_1^e(t), \quad v_h^e(L,t) = v_2^e(t), \quad \phi_h^e(0,t) = \phi_1^e(t), \quad \phi_h^e(L,t) = \phi_2^e(t) \qquad \text{(D.36)}$$

$$\omega_h^e(0,t) = \omega_1^e(t), \quad \omega_h^e(L,t) = \omega_2^e(t), \quad \theta_h^e(0,t) = \theta_1^e(t), \quad \theta_h^e(L,t) = \theta_2^e(t) \qquad \text{(D.37)}$$

where θ_h^e and ϕ_h^e are approximation functions of rotational degrees of freedom θ and ϕ about the y and z axes respectively.

Since there is a total of four conditions for each of the displacement fields *v* and ω of a beam element, four parameter polynomials must be selected for the approximation functions v_h^e and ω_h^e as follows:

$$v(x,t) \approx v_h^e(x,t) = c_1^e(t) + c_2^e(t)\ x + c_3^e(t)\ x^2 + c_4^e(t)\ x^3 \qquad \text{(D.38)}$$

$$\omega(x,t) \approx \omega_h^e(x,t) = c_5^e(t) + c_6^e(t)\ x + c_7^e(t)\ x^2 + c_8^e(t)\ x^3 \qquad \text{(D.39)}$$

Primary nodal variables (i.e. generalized displacements) are related to the unknown coefficients $c_j^e(t)$ as follows:

$$v_h^e(0,t) = v_1^e(t) = c_1^e(t) \tag{D.40}$$

$$\phi_h^e(0,t) = \left(\frac{\partial v_h^e}{\partial x} \right)\Bigg|_{x=0} = \phi_1^e(t) = c_2^e(t) \tag{D.41}$$

$$v_h^e(L,t) = v_2^e(t) = c_1^e(t) + c_2^e(t)\ L + c_3^e(t)\ L^2 + c_4^e(t)\ L^3 \tag{D.42}$$

$$\phi_h^e(L,t) = \left(\frac{\partial v_h^e}{\partial x} \right)\Bigg|_{x=L} = \phi_2^e(t) = c_2^e(t) + 2c_3^e(t)\ L + 3c_4^e(t)\ L^2 \tag{D.43}$$

$$\omega_h^e(0,t) = \omega_1^e(t) = c_5^e(t) \tag{D.44}$$

$$\theta_h^e(0,t) = \left(-\frac{\partial \omega_h^e}{\partial x} \right)\Bigg|_{x=0} = \theta_1^e(t) = -c_6^e(t) \tag{D.45}$$

$$\omega_h^e(L,t) = \omega_2^e(t) = c_5^e(t) + c_6^e(t)\ L + c_7^e(t)\ L^2 + c_8^e(t)\ L^3 \tag{D.46}$$

$$\theta_h^e(L,t) = \left(-\frac{\partial \omega_h^e}{\partial x} \right)\Bigg|_{x=L} = \theta_2^e(t) = -c_6^e(t) - 2c_7^e(t)\ L - 3c_8^e(t)\ L^2 \tag{D.47}$$

Equalities (D.40) to (D.47) can be put into matrix form as follows:

$$\begin{Bmatrix} v_1^e \\ \phi_1^e \\ v_2^e \\ \phi_2^e \end{Bmatrix} = \begin{bmatrix} 1 & 0 & 0 & 0 \\ 0 & 1 & 0 & 0 \\ 1 & L & L^2 & L^3 \\ 0 & 1 & 2L & 3L^2 \end{bmatrix} \begin{Bmatrix} c_1^e \\ c_2^e \\ c_3^e \\ c_4^e \end{Bmatrix} \tag{D.48}$$

$$\begin{Bmatrix} \omega_1^e \\ \theta_1^e \\ \omega_2^e \\ \theta_2^e \end{Bmatrix} = \begin{bmatrix} 1 & 0 & 0 & 0 \\ 0 & -1 & 0 & 0 \\ 1 & L & L^2 & L^3 \\ 0 & -1 & -2L & -3L^2 \end{bmatrix} \begin{Bmatrix} c_5^e \\ c_6^e \\ c_7^e \\ c_8^e \end{Bmatrix} \tag{D.49}$$

Inverting matrix equations (D.48) and (D.49) and substituting the results into (D.38) and (D.39), approximate solutions are expressed as below:

$$v_h^e(x,t) = v_1^e(t)\ H_1^e(x) + \phi_1^e(t)\ H_2^e(x) + v_2^e(t)\ H_3^e(x) + \phi_2^e(t)\ H_4^e(x) \tag{D.50}$$

$$\omega_h^e(x,t) = \omega_1^e(t)\, H_5^e(x) + \theta_1^e(t)\, H_6^e(x) + \omega_2^e(t)\, H_7^e(x) + \theta_2^e(t)\, H_8^e(x) \tag{D.51}$$

where

$$H_1^e(x) = H_5^e(x) \equiv 1 - \frac{3x^2}{L^2} + \frac{2x^3}{L^3} \tag{D.52}$$

$$H_2^e(x) = -H_6^e(x) \equiv x - \frac{2x^2}{L} + \frac{x^3}{L^2} \tag{D.53}$$

$$H_3^e(x) = H_7^e(x) \equiv \frac{3x^2}{L^2} - \frac{2x^3}{L^3} \tag{D.54}$$

$$H_4^e(x) = -H_8^e(x) \equiv -\frac{x^2}{L} + \frac{x^3}{L^2} \tag{D.55}$$

$H_j^e(x)$ are nothing but the shape functions of the approximate solutions $v_h^e(t)$ and $\omega_h^e(t)$.

The finite element model related with axial displacement v and ω of the Euler-Bernoulli beam is obtained by substituting v_h^e and ω_h^e for v and ω, respectively, and also $H_j^e(x)$ for the weight function ψ, in the weak forms (D.34) and (D.35):

$$\int_0^L [H_v]^T \rho A [H_v]\, dx \begin{Bmatrix} \ddot{v}_1^e \\ \ddot{\phi}_1^e \\ \ddot{v}_2^e \\ \ddot{\phi}_2^e \end{Bmatrix} + \int_0^L [B_v]^T E I_1 [B_v]\, dx \begin{Bmatrix} v_1^e \\ \phi_1^e \\ v_2^e \\ \phi_2^e \end{Bmatrix} + \int_0^L [B_v]^T E I_{12} [B_\omega]\, dx \begin{Bmatrix} \omega_1^e \\ \theta_1^e \\ \omega_2^e \\ \theta_2^e \end{Bmatrix} = \begin{Bmatrix} Q_{v1}^e \\ Q_{v2}^e \\ Q_{v3}^e \\ Q_{v4}^e \end{Bmatrix} \tag{D.56}$$

$$\int_0^L [H_\omega]^T \rho A [H_\omega]\, dx \begin{Bmatrix} \ddot{\omega}_1^e \\ \ddot{\theta}_1^e \\ \ddot{\omega}_2^e \\ \ddot{\theta}_2^e \end{Bmatrix} + \int_0^L [B_\omega]^T E I_2 [B_\omega]\, dx \begin{Bmatrix} \omega_1^e \\ \theta_1^e \\ \omega_2^e \\ \theta_2^e \end{Bmatrix} + \int_0^L [B_\omega]^T E I_{12} [B_v]\, dx \begin{Bmatrix} v_1^e \\ \phi_1^e \\ v_2^e \\ \phi_2^e \end{Bmatrix} = \begin{Bmatrix} Q_{\omega 1}^e \\ Q_{\omega 2}^e \\ Q_{\omega 3}^e \\ Q_{\omega 4}^e \end{Bmatrix} \tag{D.57}$$

where

$$[H_v] = \left\{ H_1^e \;\; H_2^e \;\; H_3^e \;\; H_4^e \right\} \tag{D.58}$$

$$[B_v] = \left\{ \frac{\partial^2 H_1^e}{\partial x^2} \;\; \frac{\partial^2 H_2^e}{\partial x^2} \;\; \frac{\partial^2 H_3^e}{\partial x^2} \;\; \frac{\partial^2 H_4^e}{\partial x^2} \right\} \tag{D.59}$$

$$[H_\omega] = \left\{ H_5^e \;\; H_6^e \;\; H_7^e \;\; H_8^e \right\} \tag{D.60}$$

$$[B_\omega] = \left\{ \frac{\partial^2 H_5^e}{\partial x^2} \;\; \frac{\partial^2 H_6^e}{\partial x^2} \;\; \frac{\partial^2 H_7^e}{\partial x^2} \;\; \frac{\partial^2 H_8^e}{\partial x^2} \right\} \tag{D.61}$$

Evaluating integral terms in the equations (D.56) and (D.57), the following linear ordinary differential equations are obtained for free vibrations of a beam element:

$$\frac{\rho A}{420}\begin{bmatrix} 156 & 22L & 54 & -13L \\ 22L & 4L^2 & 13L & -3L^2 \\ 54 & 13L & 156 & -22L \\ -13L & -3L^2 & -22L & 4L^2 \end{bmatrix}\begin{Bmatrix} \ddot{v}_1^e \\ \ddot{\phi}_1^e \\ \ddot{v}_2^e \\ \ddot{\phi}_2^e \end{Bmatrix} + \frac{EI_1}{L^3}\begin{bmatrix} 12 & 6L & -12 & 6L \\ 6L & 4L^2 & -6L & 2L^2 \\ -12 & -6L & 12 & -6L \\ 6L & 2L^2 & -6L & 4L^2 \end{bmatrix}\begin{Bmatrix} v_1^e \\ \phi_1^e \\ v_2^e \\ \phi_2^e \end{Bmatrix} +$$

$$+ \frac{EI_{12}}{L^3}\begin{bmatrix} 12 & -6L & -12 & -6L \\ 6L & -4L^2 & -6L & -2L^2 \\ -12 & 6L & 12 & 6L \\ 6L & -2L^2 & -6L & -4L^2 \end{bmatrix}\begin{Bmatrix} \omega_1^e \\ \theta_1^e \\ \omega_2^e \\ \theta_2^e \end{Bmatrix} = \begin{Bmatrix} 0 \\ 0 \\ 0 \\ 0 \end{Bmatrix} \tag{D.62}$$

$$\frac{\rho A}{420}\begin{bmatrix} 156 & -22L & 54 & 13L \\ -22L & 4L^2 & -13L & -3L^2 \\ 54 & -13L & 156 & 22L \\ 13L & -3L^2 & 22L & 4L^2 \end{bmatrix}\begin{Bmatrix} \ddot{\omega}_1^e \\ \ddot{\theta}_1^e \\ \ddot{\omega}_2^e \\ \ddot{\theta}_2^e \end{Bmatrix} + \frac{EI_2}{L^3}\begin{bmatrix} 12 & -6L & -12 & -6L \\ -6L & 4L^2 & 6L & 2L^2 \\ -12 & 6L & 12 & 6L \\ -6L & 2L^2 & 6L & 4L^2 \end{bmatrix}\begin{Bmatrix} \omega_1^e \\ \theta_1^e \\ \omega_2^e \\ \theta_2^e \end{Bmatrix} +$$

$$\frac{EI_{12}}{L^3}\begin{bmatrix} 12 & 6L & -12 & 6L \\ -6L & -4L^2 & 6L & -2L^2 \\ -12 & -6L & 12 & -6L \\ -6L & -2L^2 & 6L & -4L^2 \end{bmatrix}\begin{Bmatrix} v_1^e \\ \phi_1^e \\ v_2^e \\ \phi_2^e \end{Bmatrix} = \begin{Bmatrix} 0 \\ 0 \\ 0 \\ 0 \end{Bmatrix} \tag{D.63}$$

D.5. ELEMENT MASS AND STIFFNESS MATRICES OF A 3 D EULER-BERNOULLI BEAM

Finite element formulations of a 3 D Euler-Bernoulli beam element given in equations (D.19), (D.21), (D.62) and (D.63) are assembled together within the following matrix equation:

$$\left[\overline{m_e^l}\right]\{\ddot{q}_e\} + \left[\overline{k_e^l}\right]\{q_e\} = \{0\} \tag{D.64}$$

where $\left[\overline{m_e^l}\right]$ and $\left[\overline{k_e^l}\right]$ are element mass and stiffness matrices of a 3 D Euler-Bernoulli beam in its local coordinate frame and $\{q_e\}$ is the vector of nodal displacements.

The explicit forms of element mass and stiffness matrices are given in Tables D.1 and D.2 respectively. And the displacement vector $\{q_e\}$ for element e is defined as follows:

$$\{q_e\} = \left\{u_1^e \;\; v_1^e \;\; \omega_1^e \;\; \alpha_1^e \;\; \theta_1^e \;\; \phi_1^e \;\; u_2^e \;\; v_2^e \;\; \omega_2^e \;\; \alpha_2^e \;\; \theta_2^e \;\; \phi_2^e\right\}^T \tag{D.65}$$

D.6. ASSEMBLY OF ELEMENT MATRICES INTO GLOBAL MASS AND STIFFNESS MATRICES

The finite element model of a complex engineering structure is constructed by assembling element matrices into global mass and stiffness matrices as follows:

1. The structure of interest is divided into k appropriate elements with a total of n dofs. This process is called meshing.

2. Mass and stiffness matrices of each element in local coordinates are transformed into the global coordinate frame by an appropriate transformation matrix as shown below:

$$\left[\overline{m_e}\right]_{mxm} = \left[T_e\right]^T_{mxm} \left[\overline{m_e^l}\right]_{mxm} \left[T_e\right]_{mxm} \tag{D.66}$$

$$\left[\overline{k_e}\right]_{mxm} = \left[T_e\right]^T_{mxm} \left[\overline{k_e^l}\right]_{mxm} \left[T_e\right]_{mxm} \tag{D.67}$$

where $\left[\overline{m_e}\right]$ and $\left[\overline{k_e}\right]$ are the element mass and stiffness matrices, respectively, expressed in the global coordinate frame, and $\left[T_e\right]$ is the element transformation matrix. Subscript m indicates the degree of freedom of an individual element. If it is a beam element with 2 nodes, m is equal to 12 as shown in (D.65).

3. Before the assembly operation, element matrices must be expanded into the size of the finite element model, i.e. mxm mass and stiffness matrices must be expanded into sparse matrices of size nxn where n is the total degree of freedom of the entire structure. All of the cells of the expanded element matrices turn out to be zero except those corresponding to the degrees of freedom of the relevant element. Actually, the difference between mxm and nxn forms of element matrices is not mathematical but morphological. Finally, sparse element matrices are assembled by using simple matrix addition as follows:

$$\left[M\right]_{nxn} = \sum_{k=1}^{N} \left[m_e\right]_{nxn} \tag{D.68}$$

$$\left[K\right]_{nxn} = \sum_{k=1}^{N} \left[k_e\right]_{nxn} \tag{D.69}$$

where $\left[M\right]$ and $\left[K\right]$ are global mass and stiffness matrices, and $\left[m\right]_e$ and $\left[k\right]_e$ are sparse element matrices expresses in the global coordinate frame of the structure of interest.

4. After obtaining the global mass and stiffness matrices of a finite element model, the free vibration equation is expressed as follows:

$$\left[M\right]\{\ddot{q}\} + \left[K\right]\{q\} = \{0\} \tag{D.70}$$

The solution of equation (D.70) with appropriate initial conditions gives unknown coefficients necessary to determine approximate solutions of the displacement fields u, v, ω and α for each element of the entire structure.

Table D.1. Element Stiffness Matrix of a 3 D Euler-Bernoulli Beam

$\frac{EA}{L}$	0	0	0	0	0	$\frac{-EA}{L}$	0	0	0	0	0
0	$\frac{12}{L^3}EI_1$	$\frac{12}{L^3}EI_{12}$	0	$\frac{-6}{L^2}EI_{12}$	$\frac{6}{L^2}EI_1$	0	$\frac{-12}{L^3}EI_1$	$\frac{-12}{L^3}EI_{12}$	0	$\frac{-6}{L^2}EI_{12}$	$\frac{6}{L^2}EI_1$
0	$\frac{12}{L^3}EI_{12}$	$\frac{12}{L^3}EI_2$	0	$\frac{-6}{L^2}EI_2$	$\frac{6}{L^2}EI_{12}$	0	$\frac{-12}{L^3}EI_{12}$	$\frac{-12}{L^3}EI_2$	0	$\frac{-6}{L^2}EI_2$	$\frac{6}{L^2}EI_{12}$
0	0	0	$\frac{GJ_e}{L}$	0	0	0	0	0	$\frac{-GJ_e}{L}$	0	0
0	$\frac{-6}{L^2}EI_{12}$	$\frac{-6}{L^2}EI_2$	0	$\frac{4}{L}EI_2$	$\frac{-4}{L}EI_{12}$	0	$\frac{6}{L^2}EI_{12}$	$\frac{6}{L^2}EI_2$	0	$\frac{2}{L}EI_2$	$\frac{-2}{L}EI_{12}$
0	$\frac{6}{L^2}EI_1$	$\frac{6}{L^2}EI_{12}$	0	$\frac{-4}{L}EI_{12}$	$\frac{4}{L}EI_1$	0	$\frac{-6}{L^3}EI_1$	$\frac{-6}{L^3}EI_{12}$	0	$\frac{-2}{L^2}EI_{12}$	$\frac{2}{L^2}EI_1$
$\frac{-EA}{L}$	0	0	0	0	0	$\frac{EA}{L}$	0	0	0	0	0
0	$\frac{-12}{L^3}EI_1$	$\frac{-12}{L^3}EI_{12}$	0	$\frac{6}{L^2}EI_{12}$	$\frac{-6}{L^2}EI_1$	0	$\frac{12}{L^3}EI_1$	$\frac{12}{L^3}EI_{12}$	0	$\frac{6}{L^2}EI_{12}$	$\frac{-6}{L^2}EI_1$
0	$\frac{-12}{L^3}EI_{12}$	$\frac{-12}{L^3}EI_2$	0	$\frac{6}{L^2}EI_2$	$\frac{-6}{L^2}EI_{12}$	0	$\frac{12}{L^3}EI_{12}$	$\frac{12}{L^3}EI_2$	0	$\frac{6}{L^2}EI_2$	$\frac{-6}{L^2}EI_{12}$
0	0	0	$\frac{-GJ_e}{L}$	0	0	0	0	0	$\frac{GJ_e}{L}$	0	0
0	$\frac{-6}{L^2}EI_{12}$	$\frac{-6}{L^2}EI_2$	0	$\frac{2}{L}EI_2$	$\frac{-2}{L}EI_{12}$	0	$\frac{6}{L^2}EI_{12}$	$\frac{6}{L^2}EI_2$	0	$\frac{4}{L}EI_2$	$\frac{-4}{L}EI_{12}$
0	$\frac{6}{L^2}EI_1$	$\frac{6}{L^2}EI_{12}$	0	$\frac{-2}{L}EI_{12}$	$\frac{2}{L^2}EI_1$	0	$\frac{-6}{L^2}EI_1$	$\frac{-6}{L^2}EI_{12}$	0	$\frac{-4}{L}EI_{12}$	$\frac{4}{L}EI_2$

Table D.2. Element Mass Matrix of a 3 D Euler-Bernoulli Beam

$\frac{140}{420}\rho AL$	0	0	0	0	0	$\frac{70}{420}\rho AL$	0	0	0	0	0
0	$\frac{156}{420}\rho AL$	0	0	0	$\frac{22}{420}\rho AL^2$	0	$\frac{54}{420}\rho AL$	0	0	0	$\frac{-13}{420}\rho AL^2$
0	0	$\frac{156}{420}\rho AL$	0	$\frac{-22}{420}\rho AL^2$	0	0	0	$\frac{54}{420}\rho AL$	0	$\frac{13}{420}\rho AL^2$	0
0	0	0	$\frac{140}{420}\rho AI_xL$	0	0	0	0	0	$\frac{70}{420}\rho AI_xL$	0	0
0	0	$\frac{-22}{420}\rho AL^2$	0	$\frac{4}{420}\rho AL^3$	0	0	0	$\frac{-13}{420}\rho AL^2$	0	$\frac{-3}{420}\rho AL^3$	0
0	$\frac{22}{420}\rho AL^2$	0	0	0	$\frac{4}{420}\rho AL^3$	0	$\frac{13}{420}\rho AL^2$	0	0	0	$\frac{-3}{420}\rho AL^3$
$\frac{70}{420}\rho AL$	0	0	0	0	0	$\frac{140}{420}\rho AL$	0	0	0	0	0
0	$\frac{54}{420}\rho AL$	0	0	0	$\frac{13}{420}\rho AL^2$	0	$\frac{156}{420}\rho AL$	0	0	0	$\frac{-22}{420}\rho AL^2$
0	0	$\frac{54}{420}\rho AL$	0	$\frac{-13}{420}\rho AL^2$	0	0	0	$\frac{156}{420}\rho AL$	0	$\frac{22}{420}\rho AL^2$	0
0	0	0	$\frac{70}{420}\rho AI_xL$	0	0	0	0	0	$\frac{140}{420}\rho AI_xL$	0	0
0	0	$\frac{13}{420}\rho AL^2$	0	$\frac{-3}{420}\rho AL^3$	0	0	0	$\frac{22}{420}\rho AL^2$	0	$\frac{4}{420}\rho AL^3$	0
0	$\frac{-13}{420}\rho AL^2$	0	0	0	$\frac{-3}{420}\rho AL^3$	0	$\frac{-22}{420}\rho AL^2$	0	0	0	$\frac{4}{420}\rho AL^3$